RESILIENCE LIMITATIONS AND RESISTANCE OF HYPORHEIC MICROBIAL COMMUNITIES FROM CHRONIC HEAVY METAL CONTAMINATION ENVIRONMENTS: ANALYSIS WITH THE NOVEL RESAZURIN RESORUFIN SMART TRACER

by

Daniel Joseph Stanaway

A thesis

submitted in partial fulfillment

of the requirements for the degree of

Master of Science in Hydrologic Sciences

Boise State University

August 2012

BOISE STATE UNIVERSITY GRADUATE COLLEGE

DEFENSE COMMITTEE AND FINAL READING APPROVALS

of the thesis submitted by

Daniel Joseph Stanaway

Thesis Title: Resilience Limitations and Resistance of Hyporheic Microbial Communities From Chronic Heavy Metal Contamination Environments: Analysis with the novel Resazurin Resorufin Smart Tracer

Date of Final Oral Examination: 20 April 2012

The following individuals read and discussed the thesis submitted by student Daniel Joseph Stanaway, and they evaluated his presentation and response to questions during the final oral examination. They found that the student passed the final oral examination.

Kevin P. Feris, Ph.D.	Chair, Supervisory Committee
Shawn G. Benner, Ph.D.	Member, Supervisory Committee
Alejandro N. Flores, Ph.D.	Member, Supervisory Committee

The final reading approval of the thesis was granted by Kevin P. Feris, Ph.D., Chair of the Supervisory Committee. The thesis was approved for the Graduate College by John R. Pelton, Ph.D., Dean of the Graduate College.

DEDICATION

I would like to dedicate this to my wife, Margaret, for setting off on this adventure with me and the support and encourage she has provided. Hot dinners, a warm hug, and a sympathetic ear after hard days were everything I could ask for. This work could not have been completed without Margaret's understanding of late nights, long weekends, and a preoccupied husband. This has not been easy, but this has been achieved together for the promise of our future. I would also like to express my deep appreciation to my family who has supported us in this endeavor, understanding when we couldn't be home for family celebrations and holidays and never asked anything of us except that we embrace this adventure and live our lives. This unwavering support means everything to me.

ACKNOWLEDGEMENTS

I would like to thank my major thesis advisor, Dr. Kevin Feris, for his patience and expertise throughout this thesis. Kevin's dedication to his student's success is matched only by his expectations, a combination that leads to extraordinary personal and academic growth. Kevin's willingness to try new approaches and push the envelope has resulted in a truly interdisciplinary thesis and provided me a knowledge base that spans from microbiology to hydrological processes to modeling. These frontiers could only be explored by an advisor willing to take risks and go beyond one's own expertise.

Accordingly, I would also like to thank my co-advisors, Dr. Shawn Benner and Dr. Lejo Flores both playing a critical role in the formulation of this thesis and the ideas within. This thesis required multiple advisers, each contributing their best efforts to ensure success. The thoughtful interactions I have had with my advisory committee, and the devotion of faculty to student success, is my greatest compliment to the Geosciences and Biology Departments and to Boise State University. Additionally, I would like to extend a hearty thank you to Dr. Roy Haggerty at Oregon State University. Dr. Haggerty provided the opportunity to join his group in a field release of the tracer used in this study and has provided feedback, comments, and support throughout this thesis. This is especially relevant because he is one of a handful that understands this technology. This thesis would not be what is without his involvement. I would also like to thank Dr. Paul Olin in BSU's BioTrace Laboratory for his comments and guidance in understanding the geochemical components of the thesis. Finally, I'd like to thank Diane Smith, Beth Gee,

Mary Korol in the Biology Department Administration for their help handling thesis funding. Funding sources include EPA STAR Fellowship FP917110, NSF Ecosystems Grant DEB 07174490, and the NSF Idaho EPSCoR EPS-0814387. Field training was supported by the NSF EAR 0838338.

ABSTRACT

River ecosystems are among the most threatened and rapidly altering systems in the world because of anthropogenic disturbance. Chronic heavy metal contamination of lotic environments is a global concern and a widespread environmental and human health threat. This persistent stressor can shape microbial community structure and function, often selecting for the genotypic and phenotypic characteristics that increase fitness in toxic environments and may encumber the microbial community hosting metal resistance mechanisms with additional energetic costs. This cost should be expressed in heterotrophic aerobic microbial metabolism, a primary ecological process variable and can be estimated through respiration measurements. Hyporheic respiration is a proposed functional indicator of ecosystem health and is sensitive to gradients in environmental quality. The ecological importance and contaminant retention of the hyporheic zone presents these communities as a valuable indicator of natural resource damage.

In this study, we illustrate the first documentation of the Resazurin Resorufin Smart Tracer as a functional indicator of lotic ecosystem integrity. This tool was used to quantify metabolism of hyporheic microbial communities from the chronic metal contamination gradient of the Clark Fork River, Montana, USA in column experiments. Communities from low, mid, and high contamination locations of the gradient were paired with pristine reference sites to test hypotheses regarding the use of the Resazurin Resorufin Smart Tracer to estimate ecological functional resilience and resistance to

chronic metal stress. We found that acute metal stress inhibits respiration in both communities and that the communities did not differ in metal resistance potential. This research indicates the Resazurin Resorufin Smart Tracer has potential as a functional indicator of ecological integrity and suggests that lotic heavy metal contamination represents a persistent stress from which this ecosystem was not able to recover in over 100 years.

TABLE OF CONTENTS

LIST OF TABLES

LIST OF FIGURES

LIST OF ABBREVIATIONS

Raz	Resazurin
Rru	Resorufin
RRST	Resazurin Resorufin Smart Tracer
CF	Clark Fork River, Montana
MCI	Metal Contamination Index
eMCI	Effluent Metal Contamination Index
sMCI	Sediment Metal Contamination Index
R	Retardation
k_1	Resazurin Decay Rate Coefficient
k_2	Resorufin Decay Rate Coefficient
k_{12}	Resazurin to Resorufin Reduction Rate Coefficient
KR	Clark Fork at Kohr's Ranch
LBF	Little Blackfoot River
RC	Rock Creek
PD	Posterior Distribution
MAE	Mean Absolute Error

RRADE	Resazurin Resorufin Advection Dispersion Equation
MCMC	Markov chain Monte Carlo

CHAPTER ONE: PERSISTENT METAL CONTAMINATION LIMITS LOTIC ECOSYSTEM HETEROTROPHIC METABOLISM AFTER MORE THAN 100 YEARS OF EXPOSURE: A NOVEL APPLICATION OF THE RESAZURIN RESORUFIN SMART TRACER

Abstract

Persistent stress from anthropogenic metal deposition in lotic ecosystems is a global concern. This long-term selective pressure shapes hyporheic microbial assemblages and influences ecosystem functional integrity. We hypothesized that, even after 100 years of adaptation opportunity, ecosystem function remains inhibited by sediment-associated metal stress and that the Resazurin Resorufin Smart Tracer can be used as an indicator of that impact. The Resazurin Resorufin Smart Tracer system is applied here in a novel capacity as a metric of ecosystem function by quantifying ecosystem respiration of microbial communities. Hyporheic microbial communities exposed to differing magnitudes of chronic metal stress were compared to pristine reference sites in controlled column experiments. A Markov chain Monte Carlo technique was developed to solve the inverse smart tracer transport equation to derive community respiration data. Results suggest metals inhibit respiration by 13-30% relative to reference sites and this inhibition is directly related to the level of *in situ* metal stress. We demonstrate the first application of a hydrologic smart tracer as a functional indicator of ecological integrity within anthropogenically influenced flowing water systems and

provide data suggesting resilience is limited in hyporheic ecosystems even after more than a century of microbial adaption to chronic pollutants.

Introduction

Freshwaters are the most extensively altered systems in the world, placing them amongst the most threatened ecosystems on the planet (1-3). In addition, heavy metal contamination in lotic ecosystems is a persistent and widespread environmental and human health threat (4, 5). These persistent environmental pollutants can enact selective pressures, shaping ecosystem function and community structure (6).

Key ecosystem level processes and the community structure of macro- (7, 8) and micro-organisms (9-11) respond to gradients of environmental stress, with micro-organisms being the most sensitive indicators of anthropogenic contamination (10, 12-14). In chronic metal contaminated environments, changes in the hyporheic microbial assemblage have been detected at concentrations nearly an order of magnitude less than responses in benthic macro-invertebrates can be measured (15), and microbial functional suppression has been observed in chronically metal contaminated terrestrial ecosystems (11, 16, 17). However, currently applied metrics of river health rely primarily upon macroorganism communities (e.g., aquatic invertebrates, fish and algal communities) (18-21) while often omitting microbial catalyzed functional processes (e.g., organic matter breakdown, ecosystem metabolism, sediment respiration) (22). Omission of these ecosystem level process variables is partially due to difficulties in measuring these responses in an integrated fashion across space and time on reach scales that may improve lotic ecosystem monitoring and assessment (23). Hyporheic microbial metabolic

function catalyzes a suite of ecological processes (e.g., decomposition, nutrient spiraling, etc.) (24, 25), is responsible for 40 to >90% of total stream metabolism (26), and is important to the trophic base of lotic food webs (27, 28). Also, the hyporheic zone can retain orders of magnitude greater concentrations of anthropogenic contaminants than surface waters (29). Because of this intricate role in ecosystem function and contaminant retention, measures of hyporheic community respiration may be valuable indicators of natural resource damage (23, 30).

Ecosystem respiration is a useful functional indicator for establishing changes in ecosystem properties along contamination gradients (11, 31). Commonly employed means of estimating respiration include measuring changes in dissolved oxygen (DO) concentrations in flowing systems (32) or via point measurements of DO consumption in respiration chambers (33). Although DO-based methods offer the advantage of continuous monitoring, they are subject to non-target processes (e.g., atmospheric exchange, changes in concentration via groundwater mixing, autotrophic contributions, etc.) and can be highly uncertain (34). Reach scale DO measurements in flowing water systems are unreliable in instances when reaeration $\geq$ ecosystem respiration, and estimates from respiration chambers require extrapolation to ecosystem relevant reach scales from smaller scales of measurement (32, 34, 35). Additionally, many of these methods require modification of *in situ* conditions through alteration of local hydrodynamics and/or extraction of sediment, potentially influencing the target process (20, 36, 37).

We propose the Resazurin Resorufin (Raz Rru) Smart Tracer (RRST) as a continuous and direct method of interrogating heterotrophic microbial metabolism and

collecting physical transport data as a means to quantify the influence of long-term contaminant exposure on sediment respiration in flowing water systems. The RRST has previously been proposed as a hydrological tool coupling solute transport and microbiological activity at the sediment - water interface of freshwater systems (38), potentially associating ecosystem processes with transient storage (39, 40). Resazurin is irreversibly reduced to resorufin in the presence of metabolically active aerobic heterotrophic microbial communities (41); a reduction reaction that is proportional to DO consumption (42). In addition, the RRST is suspected to be relatively insensitive to non-target processes and provide physical transport information at the reach scale while simultaneously measuring ecosystem respiration (38). Resazurin may also provide detection advantages over using naturally occurring substrates as ecosystem health metrics (i.e., leaf litter decomposition). Since they are introduced substances with low limits of detection, the RRST is easily discerned from background and is insensitive to environmental spatial and temporal variability, a concern associated with the use of naturally occurring substrates (23, 43). Collectively, these attributes are characteristic of effective environmental monitoring technologies (22, 23, 30, 36, 37) and indicate that the RRST may be useful as a lotic ecosystem quality assessment tool.

We tested the potential of the RRST as an indicator of environmental integrity by quantifying the influence of chronic heavy metal exposure (> 100 years) on hyporheic microbial community respiration. Specifically, we predicted 1) chronic exposure to heavy metals has an energetic cost that limits heterotrophic microbial respiration and 2) the RRST is able to detect this inhibition through quantifying respiration of hyporheic microbial communities in flowing water systems. To test these hypotheses, Raz to Rru

reduction was measured in column experiments with sediment collected along a contamination gradient in the Clark Fork River drainage in Montana. Lower Raz to Rru reaction rate constants correlated with higher sediment heavy metal contents. The results of these experiments suggest a legacy of impaired hyporheic microbial community function imparted by heavy metal contamination even after 100 years of adaption, characterize RRST performance as a novel ecological monitoring tool in a geochemically complex environment, and indicate the potential for the RRST to be employed for continuous interrogation of ecosystem integrity at the reach scale.

Methods

Study Location

Historic mining in the Clark Fork River has deposited elevated concentrations of As, Cd, Cu, Pb, and Zn several hundred times above background with concentrations declining from the headwaters in western Montana downstream to the confluence (5, 29). Shallow hyporheic sediment from differently contaminated locations along the Clark Fork contamination gradient and paired reference sites was collected (Figure 1.1), field sieved to a uniform grain size (1.7-2.36 mm), and shipped on wet ice to Boise, ID for analysis. Three sites were selected along the contamination gradient representing high, medium, and low metal contamination and were paired to reference sites similar in elevation, hydrogeological properties, and proximity (Table 1.1). This reference-site approach is well recognized as a means to estimate the impact of anthropogenic disturbance (23, 44). No significant environmental differences in hydraulic gradient, pH,

organic matter, dissolved oxygen, and temperature between Clark Fork sites and reference reaches were observed.

Experimental Design

Column experiments commenced within 24 hrs post collection. Sediment was packed into four replicate submerged columns per site (30 cm x 1.5 cm glass chromatography columns, Kontes Glass Company, New Jersey, USA). Influent solution consisting of 1 mM sodium phosphate buffered (pH = 6.6 ± 0.09) water from the most pristine stream and 1 µM RRST was supplied at a constant flow rate (~0.3 mL min^{-1}) and temperature (~15.4°C ± 2.6°C). Experiments lasted approximately four hours until a breakthrough plateau in electrical conductivity (EC) was observed. Effluent was collected and measured for conductivity, trace metals (Na, Mg, Al, Si, P, K, Ca, Cr, Mn, Fe, Ni, Cu, Zn, As, Se, Kr, Sr, Ag, Cd, Ba, Pb, U), and RRST. Sampling intervals varied and ranged from 10-28 min with increased frequency during breakthrough. Sample points were linearly interpolated at an interval of 0.05 hr (3 min) for modeling.

Resazurin/Resorufin Quantification

Raz and Rru samples were 0.22 µm filter sterilized and stored in the dark at 4°C for < 24 hrs prior to reading. Raz (λ_{exc} = 602 nm, λ_{emi} = 634 nm) and Rru (λ_{exc} = 530 nm, λ_{emi} = 590 nm) fluorescence measurements were performed with a Synergy Mx multi-mode microplate reader with Gen 5 software (Biotek Instruments, Inc) with bandpass set to 9 and sensitivity set to 100. Prior to quantification, pH was raised to approximately 9.5 with the addition of 15 µL of 50 mM NaOH (pH ~12.7) to 100 µL of sample in a sterile black-walled 96 well plate (Costar part # 3603). This pH adjustment was made to

maximize the fluorescent signals from both Raz and Rru (45, 46). The remaining sample volume was frozen for metal analysis. Standard curves generated with resazurin and resorufin sodium salts (Sigma Aldrich) were linear from 0 to 1 µM, bracketing the concentrations observed in column effluents.

Trace Metal Quantification

Metal concentrations of column effluent and sediment were quantified with an X-Series II Inductively Coupled Plasma Mass Spectrometer (ICP-MS) (Thermo Fisher, Bremen, Germany). Solution was filtered (0.45 µm) and treated with 0.125 mL of 10% trace metal grade HNO_3 according to EPA method 1669, then frozen until time of analysis. Discrete time point metal analysis samples were prepared from the frozen RRST samples and were brought to approximately 5 mL (4-8 fold dilution) in 2% triple distilled HNO_3 for measurement.

Sediment associated metal concentration was determined with EPA method 3051A for microwave digestion. Leachate was diluted to 2% HNO_3 for analysis. External standard verification (San Joaquin Soil, SRM 2709a, NIST) of average concentration of the five target metals are as follows of the reported range: arsenic (within reported range of 6.4-10 mg kg^{-1}), cadmium (within reported range of 0.33-0.66 mg kg^{-1}), copper (within 2.2% of 24-28 mg kg^{-1}), lead (within 4.3% of 8.1-11 mg kg^{-1}), and zinc (within 1% of 69-87 mg kg^{-1}). See Chapter 2 for additional details.

Metal Contamination Index Calculation

Metal concentrations at each site and in column effluent were used to calculate a metal contamination index (MCI) (12, 47). This index normalizes the relative degree of

contamination to the most pristine site of the dataset. The MCI assigns a composite contamination score to a sediment or effluent sample as follows,

$$MCI = \sum((\log (Me_n)/\log (\text{background } Me_n))/n$$

where Me_n is the metal species, As, Cd, Cu, Pb, or Zn, n is the number of metals included in the index, and background is the respective metal concentration of the most pristine site.

Dissolved Oxygen

To establish a relationship between DO consumption and Raz-to-Rru reduction, DO consumption was measured with non-intrusive fluorescence quenching (PreSens Precision Sensing GmbH, Regensburg, Germany) under various discharge regimes (0.1, 0.15, 0.2, 0.3 mL min^{-1}) (33). Oxygen sensor foils were adhered inside the column at the influent and effluent ends prior to packing with hyporheic sediments. DO consumption was determined as the difference between influent and effluent concentrations measured at the same time. Five DO consumption measurements and corresponding RRST levels were made during steady-state conditions on three replicate columns per discharge.

Bacterial Enumeration

Samples of sediment from each field site included in the column experiments were frozen upon receipt. DNA was isolated from five 0.5 g sub-samples from each site via the FastDNA® SPIN Kit for Soil and the FastPrep® Instrument (MP Biomedicals, Santa Ana, CA). Microbial densities per site were analyzed with real-time quantitative PCR (qPCR) amplifying the 16S rRNA gene with Bact 1369F and Prok 1492R primers and Taqman probe 1389F, using amplifications settings described previously (48).

Relative biomass density was inferred from the number of 16s gene copies per g sediment. qPCR standard curves were linear across seven orders of magnitude with a range of $2.9 \times 10^1 - 2.9 \times 10^8$ 16s gene copies μL^{-1} of extracted DNA.

Organic Carbon Quantification

Dried (85°C for >24 hrs) and sieved (<1.18 mm) column sediment was hand pulverized to <125 µm, then oven dried again (80°C for >24 hrs). Sediment associated inorganic carbon was removed by oxidation with 7 mL of 0.73 M sulfurous acid (H_2SO_3) in acid-washed vials (49). Acid-sediment solution was oven dried at 80°C for >24 hrs and the remaining organic carbon quantified on replicate (n=3) ~100 mg samples with the Flash EA 1112 Series NC Soil Analyzer (Thermo Scientific Inc., Bremen, Germany). Results were validated with internal standards (SRM 2709a) and verified with in-house external standards (CBXO Soil, BioTrace Lab, Boise, ID).

Data Analysis

Resazurin Resorufin ADE Forward Model

RRST transport in column experiments is described by two dependent 1-D reactive advection dispersion equations associated by the pseudo-first order Raz-to-Rru reduction rate coefficient k_{12} as:

$$\frac{\partial C_{Raz}}{\partial t} = \frac{\alpha_L v}{R}\frac{\partial^2 C_{Raz}}{\partial x^2} - \frac{v}{R}\frac{\partial C_{Raz}}{\partial x} - k_1 C_{Raz} - k_{12} C_{Raz}$$

$$\frac{\partial C_{Rru}}{\partial t} = \frac{\alpha_L v}{R}\frac{\partial^2 C_{Rru}}{\partial x^2} - \frac{v}{R}\frac{\partial C_{Rru}}{\partial x} - k_2 C_{Rru} - k_{12}\frac{M_{Rru}}{M_{Raz}} C_{Raz}$$

where C_{Raz} is the concentration of Raz [µmol L^{-1}]; C_{Rru} is the concentration of Rru [µmol L^{-1}]; t is time [hr]; x is distance [cm]; α_L is longitudinal dispersivity [cm]; v [cm hr^{-1}] is

the average pore water velocity; R [-] is retardation coefficient due to sorption; k_{12} [hr^{-1}] is the reaction rate coefficient of Raz to Rru; k_1 [hr^{-1}] is the reaction rate coefficient of Raz decay; k_2 [hr^{-1}] is the reaction rate coefficient of Rru decay; M_{Raz} [g mol^{-1}] is the molecular weight of Raz; and M_{Rru} [g mol^{-1}] is the molecular weight of Rru (38).

Inverse Solution to the Reactive Advection Dispersion Equation

A probabilistic Markov chain Monte Carlo data assimilation algorithm was developed to solve the inverse Raz Rru advection dispersion equation solution. Ecological respiration data is contained in k_{12} that cannot be measured directly and is inextricably linked to the chemical and physical transport parameters. This computational intensive approach was selected because it 1) is capable of providing uncertainty estimation through supplying parameter solutions as a posterior distribution, 2) ensures convergence to the global solution, 3) ensures physically appropriate parameter values, and 4) is less sensitive to initial estimation than gradient search methods (50). Parameter values and uncertainty are described as the maximum likelihood and standard deviation of the parameter distribution

This approach stochastically selects a proposal solution consisting of a value for each parameter from a constrained window and applies the solution to the forward model for determination of goodness-of-fit with respect to the interpolated breakthrough curves. This process is repeated for 1,000,000 iterations. A solution is maintained until a more probable set of parameter values is realized, based on goodness-of-fit and the physical appropriateness, as determined through a prior distribution. A more probable solution is determined by an acceptance ratio, α, that is the quotient of the probability density of the goodness-of-fit of the proposed model parameter solution, $X^{(t+1)}$, and that of the current

solution, $X^{(t)}$. The acceptance ratio is then compared to a uniform random number, r, generated between 0-1 for each proposal solution. If $\alpha > r$, the proposal solution, $X^{(t+1)}$, is accepted and becomes the current solution, if $\alpha < r$, $X^{(t+1)}$ is rejected. Acceptance ratios of more probable proposal solutions are > 1 and will always be accepted. As α approaches 1, meaning the probability density of the goodness-of-fit of solutions $X^{(t+1)}$ and $X^{(t)}$ are similar, there is a higher likelihood of acceptance. Improbable solutions may also be accepted when r approaches zero on any given proposal iteration. The frequency of this occurrence is rather low and is functionally useful to avoid local minima. All accepted simulations form a parameter's posterior distribution, from this distribution, the parameter value is the mode ± standard deviation. A more detailed discussion of this modeling application can be found in Appendix A and the code is documented in Appendix B.

Statistical Analysis

Significance of respiration differences in contamination gradient communities and reference sites as a function of the metal contamination index was measured using ANOVA. All pair wise means were contrasted post-hoc using the Tukey-Kramer test and were considered statistically significant at $P \leq 0.05$. Correlation P values of RRST parameters, environmental variables, and ecosystem process variables are significant at $P \leq 0.05$.

Results and Discussion

Based on prior observations by our group in metal contaminated floodplain soils (11, 47), we hypothesized that, even after 100 years of opportunity for adaptation,

hyporheic microbial community function remain suppressed by sediment-associated metal stress and that the RRST can be used as a functional indicator of that ecological impact. To test these hypotheses, we quantified differences in sediment respiration along a metal contamination gradient using column experiments that controlled for edaphic properties known to affect metal availability *in situ* (e.g., differences in DOC, dissolved nutrients, temperature, pH, etc).

The RRST approach demonstrated that highly contaminated sites exhibited lower metabolic respiration capacity. Specifically, the reaction rate constant of Raz reduction to Rru (k_{12}) was shown to be higher at reference sites relative to metal contaminated sites (Figure 1.2), and k_{12} normalized to bacterial density increased as metal contamination declined along the Clark Fork contamination gradient (Figure 1.3). Here k_{12} is interpreted as a measure of community level hyporheic respiration and as such is reflective of *in-situ* metabolic activity inclusive of between site variability. When k_{12} is normalized to sediment associated bacterial densities, it reflects the level of metabolic inhibition at a per cell level. Ecological interpretation and the utility of this method as a functional-based environmental quality assessment tool is presented by 1) evaluating RRST performance, 2) a discussion of hyporheic microbial adaptation to chronic metal stress, and 3) observations of the RRST in transient biogeochemical environments.

Assessing RRST Performance

Validation of the RRST was based upon reliability of Markov chain Monte Carlo to produce consistent parameter values and ensuring insensitivity of RRST to reduction by abiotic processes. Convergence to consistent and realistic parameter values in replicate model simulations provides confidence that k_{12} accurately reflects an ecosystem

metabolic response and that calculated differences in k_{12} are not relicts of model variation. We verified that the primary driver of RRST reduction was microbial respiration and not abiotic reduction, thereby supporting the applicability of this method as a functional indicator of ecosystem quality.

Markov Chain Monte Carlo Convergence

Convergence analysis was performed through analysis of the expected value and standard deviation of each Raz Rru advection dispersion equation parameter's posterior distribution across 10 Markov chain Monte Carlo optimization experiments from one column per site. Satisfactory convergence was operationally defined as when the variance in the expected value of the posterior distribution parameters across the optimization experiments was at least two orders of magnitude less than the parameter value with consistent model error variance of $< 10^{-6}$.Variance across the optimization experiments for k_{12} outperformed this criterion and was 3 to 5 orders of magnitude lower than the estimated k_{12} values across all sediment types. This low level of variation suggests that site-level k_{12} estimates reflect actual differences in respiration and not variation due to the optimization procedure. Notwithstanding dispersivity, variation of the remaining Raz Rru advection dispersion equation parameters were within that of k_{12} (Table 1.2). Posterior distributions of all parameters are realistic and within expected ranges (additional details are provided in Appendix A).

Raz-to-Rru Reaction Rate Coefficient (k_{12})

Raz-to-Rru reduction rate is described by k_{12} of the Raz Rru advection dispersion equation and is assumed to reflect only the biotic reduction of the compound (38). Raz

lost has a strong, direct linear relationship to k_{12} (R^2=0.88) and DO consumption versus Raz lost (R^2=0.93) and Rru gained (R^2=0.78) show similar behavior. Sediment associated bacterial density, inferred from 16s rRNA gene copies g^{-1} of sediment from each site, has a significant positive correlation with k_{12} ($R^2 = 0.29$, $P < 0.01$). The correlations of Raz reduction to bacterial density and DO consumption indicate k_{12} is sensitive to sediment respiration. Differences in k_{12} were detected between all sites with low standard deviation within sites (Table 1.1).

The abiotic geochemical reactivity of resazurin and resorufin is largely unknown and may affect each compound differently. Elements found in the geochemically complex Clark Fork sediments have reducing capacity (e.g., Cu, Fe, Mn, OC, sulfides, etc), however, no significant decrease in Raz concentration was observed in batch experiments with sterilized Clark Fork sediments after 24 hr (average Raz concentration (n=3): $t_0 = 70 \pm 3.8$ ppb, $t_{24} = 66 \pm 5.4$ ppb, $P = 0.45$). This data indicates the heavy metals present in Clark Fork sediments were negligibly influential on k_{12} directly. Rru gained/Raz lost ratio ranged from 0.44-0.83 and the mass balance ranged from 0.49-0.77 of the influent solution, indicating imperfect recovery. Raz/Rru mass not accounted for in the mass balance was attributed to decay of each compound (k_1, k_2) and loss due to sorption, a process encapsulated in the retardation term (R) (Table 1.1 and Appendix A for details of parameter estimation). Unique sorption characteristics of each compound was not expected, therefore a single R value was applied to both Raz and Rru (38). Additionally, the further reduction of resorufin to hydroresorufin, a non-fluorescent molecule, is also known (51); however, hydroresorufin rapidly re-oxidizes to Rru in the presence of DO and should not influence results (52, 53). This RRST assessment

indicates k_{12} is driven by sediment respiration and is insensitive to abiotic reduction although complete geochemical behavior of this tracer is not yet fully understood.

Ecological Response to Chronic Metal Contamination

The magnitude of chronic metal stress in the contamination gradient was estimated with an index of the concentrations of the most toxic metals present (12). A metal contamination index was employed because it estimates total metal stress in a composite measure, avoiding problematic analysis of single metal cause and effects (54, 55). A significant negative relationship between the sediment metal contamination index and k_{12} ($P = 0.01$) was observed and suggests that metal stress limits hyporheic sediment respiration and correspondingly ecological function continues to be inhibited along the metal contamination gradient after >100 years of chronic metal exposure. This observation corroborates prior studies of flood plain soil communities in this system and pure culture studies quantifying the metabolic costs of metal tolerance (11, 47, 56). Sites above a metal contamination index threshold of 0.7 demonstrated a substantially stronger correlation between k_{12} and metal contamination ($R^2 = 0.48$, $P = 0.003$). This may suggest a threshold at which chronic metal exposure maintains a negative impact on ecosystem function and a level at which communities are not resilient to chronic stress.

The k_{12} of the contaminated sediment columns was significantly lower than that of the reference site columns (average: 0.68 (reference), 0.53 (contaminated), $P = 0.008$). Furthermore, reference site k_{12} was significantly greater than its contaminated counterpart at each contamination level site pair ($P = 0.02$, $P < 0.001$, $P < 0.001$; low, middle, high elevation sites, respectively) (Table 1.1, Figure 1.2). The difference in k_{12} is smallest in the least contaminated-reference site pair (0.10), and increases with the more highly

contaminated mid-elevation (0.17) and high-elevation (0.18) site pairs. Assuming reference site k_{12} represents the full metabolic potential in each site pair, these differences correspond to contaminated site respiration of 87%, 70%, and 76% of their reference counterparts, respectively, calculated as contaminated k_{12} divided by reference k_{12}. When k_{12} values for the contaminated sites were compared on the reach scale and normalized to cell densities, the magnitude of chronic metal stress impeded respiration at the per cell level (Figure 1.3). There was a strong inverse linear relationship (R^2=0.98) between the sediment metal contamination index and the cell density normalized k_{12} with the contaminated sites. Further, the cell density normalized k_{12} values were significantly different among all of the contaminated sites sampled ($P < 0.05$), suggesting that the observed differences among sediment types was due to differences in sediment associated metal concentrations and not due to differences in associated microbial biomass. This data supports our hypothesis that hyporheic metabolic activity continues to be inhibited by, and directly related to, the magnitude of chronic metal concentrations in this system aligning with patterns of ecosystem functional suppression that have been observed in studies of Clark Fork floodplain soils (11, 47).

Anthropogenic deposition of heavy metals in natural ecosystems is a persistent environmental stressor that can influence the genotypic and phenotypic character of the exposed community (6).We observed that ecosystem respiration remains suppressed in the Clark Fork River. These data suggest that aerobic heterotrophic hyporheic microbial communities are not fully resilient to this chronic metal stress that imposes a legacy of impaired ecosystem function even after long periods of selection for tolerant communities have structured the hyporheic microbial community species composition

(12-15, 48). *In situ* studies of soil microfauna indicate metabolic inhibition at metal concentrations and mixtures comparable to the Clark Fork (16, 17). Soil microbial communities exposed to chronically elevated concentrations of multiple heavy metals demonstrated inhibited sulfatase and dehydrogenase activity compared to uncontaminated soils with minimum As, Cd, Cu, Pb, and Zn concentrations of (ppm) 2.8, below detection limit, 9, 67, and 91, respectively (16). Similarly, microbial basal respiration was negatively correlated with Cu (23.8-1626.75 ppm), Pb (55.9-5060 ppm), and Zn (38.6-2534) along a contamination gradient at a reclaimed mining area decommissioned for at least 20 years (17). The metabolic inhibition we and others have observed may result from the energetic cost of maintaining and expressing metal tolerance mechanisms necessary for survival in contaminated environments (56).

RRST Continuous Detection of Transient Geochemical Conditions

Raz breakthrough curves show a strong rising limb, peaking at elevated concentrations, followed by a decline to plateau concentrations, a pattern most evident in contaminated site columns (Figure 1.4). This differential temporal behavior in Raz transformation suggests respiration inhibition followed by stimulation. This response induces a systematic difference in model error between treatment groups. Error generation is primarily isolated to the Raz BTC rising limb with significantly greater error associated with contaminated site columns (average mean absolute error: Ref = 0.025, Cont = 0.049, $P < 0.001$), suggesting a mechanistic explanation for the deviation of observed data from the Raz Rru advection dispersion equation model.

Transient geochemical conditions within the columns stem from the introduction of the buffered (pH 6.6 ± 0.09) RRST influent solution as it mixes with the untreated

column pore water (i.e., river water used for column packing). This pH was chosen to represent the lower end of the *in situ* diel pH variation previously measured in Clark Fork hyporheic pore waters (57, 58). The phosphate buffer we employed imposed an increase in ionic strength relative to background (+192.0 ± 15 µs/cm) concomitant to the change in pH. These changes in column aqueous geochemistry could facilitate metal dissolution from sediment surfaces further increasing the complexity of a transient state (57, 59). Metal dissolution is evident in these experiments in discrete time point analysis of the arsenic breakthrough curve that co-varies with Raz concentrations (Figure 1.5), and by increases in effluent metal concentrations relative to the influent solution (e.g., As, Cd, Cu, Zn) (Figure 1.6) trends that are strongest in contaminated sediment column effluents. Changing ionic strength, pH, and metal concentrations generate transient column geochemistry and could all be influential drivers of the observed biotic responses. The more pronounced differential Raz behavior may be because of the increased complexity of the transient state associated with contaminated sediment and/or a stronger biotic response of metal resistant communities to transient pH and ionic strength conditions (60-62).

Raz behavior is suspected to be a biotic response to transient geochemical conditions within the column and may be evidence of the utility of this method for continuous detection of cause and effect relationships of the biotic community to environmental stimuli. If proven valid, this advocates for the use of this tool to assess dynamic community metabolic responses to changing environmental stimuli in the laboratory and potentially field studies. As such, the RRST may be useful for monitoring *in situ* ecological functional responses to environmental perturbations, alleviating bias

associated with time and space dependent assessments (63). Additionally, the RRST method could have a pertinent role for metabolic assessment of ecosystem integrity because it potentially maintains the advantages of currently applied metrics (continuous detection in flowing water systems) while reducing uncertainties associated with using naturally occurring substrates (43) and DO measurements where reaeration is a considerable confounding variable amongst additional complications (32, 34, 35).

These observations cautiously support the RRST as a hydrologic tool for quantifying effects of anthropogenic pollutants to ecosystem processes in flowing water systems. Further, our findings suggest a lack of ecosystem resilience to long-term perturbations evident in that heterotrophic hyporheic metabolic function remains suppressed in the Clark Fork despite >100 years of selection for tolerant communities. The RRST was able to detect differences in respiration along a contamination gradient with a high degree of precision, indicating that long-term exposure to metal stress inhibits metabolic function up to 30% relative to reference conditions and that inhibition is directly related to the magnitude of metal stress. Raz also responded to transient biogeochemical conditions, suggesting the RRST is capable of detecting continuous differences in biotic processes through time in response to a changing environment. Therefore, while the RRST shows promise as a functional indicator of ecosystem health, additional study is required to confirm its utility and develop quantifiable empirical relationships between Raz-to-Rru reduction rate constants (k_{12}) and tangible ecological productivity metrics such as carbon cycling rates.

Table 1.1 Site and Column Effluent Characteristics. Sites are organized in contaminated – reference pairs from the lowest contamination/elevation to the highest.

		Site Characteristics										Column Effluent Characteristics				
Site	Treatment	Elev (m)	Slope	k_{12} (hr^{-1})	Sed MCI[1]	As (µg/g)	Cd (µg/g)	Cu (µg/g)	Pb (µg/g)	Zn (µg/g)	Effl MCI[1]	As (ppb)	Cd (ppb)	Cu (ppb)	Zn (ppb)	Sed TOC (µg/g)
Bitterroot River	Ref	957	0.1%	0.80 ± 0.02	0.00	0.79 ± 0.79	0.01 ± 0	2.7 ± 0.55	1.8 ± 1.6	4.5 ± 1.6	0.05	21 ± 2.7	0.12 ± 0.03	2.2 ± 1.7	44 ± 16	0.33 ± 0.09
CF at Missoula	Cont	981	0.5%	0.70 ± 0.07	0.92	4.1 ± 1.1	0.23 ± 0.05	24 ± 7.5	4.8 ± 1.2	90 ± 18	0.70	197 ± 28	0.24 ± 0.09	35 ± 8.6	59 ± 8	7.3 ± 2.4
Rock Creek	Ref	1084	0.2%	0.55 ± 0.01	0.08	3.4 ± 0.56	0.01 ± 0.01	2.5 ± 0.5	2.0 ± 1.5	3.6 ± 1.3	0.00	25 ± 1.1	0.29 ± 0.26	0.53 ± 0.14	38 ± 7.9	7.2 ± 2.6
CF at Drummond	Cont	1220	0.3%	0.38 ± 0.04	1.15	6.8 ± 1.5	0.29 ± 0.05	42 ± 6.3	12 ± 5.3	121 ± 44	0.73	204 ± 90	0.22 ± 0.10	17 ± 6.7	169 ± 215	3.8 ± 1.4
Little Blackfoot	Ref	1363	0.5%	0.72 ± 0.01	0.69	8.6 ± 1.4	0.10 ± 0.03	4.7 ± 1.2	5.9 ± 0.84	27 ± 5.4	0.43	197 ± 4.2	1.25 ± 0.00	0.90 ± 0.21	46 ± 13	4.4 ± 2.9
CF at Kohrs Ranch	Cont	1369	0.4%	0.54 ± 0.02	1.34	26.6 ± 48	0.30 ± 0.08	143 ± 143	10 ± 2.9	102 ± 47	0.56	195 ± 8.2	0.12 ± 0.01	20 ± 2.4	54 ± 22	1.7 ± 0.3

[1]Metal Contamination Index, Sed is sediment associated metal content, Effl is column effluent metal concentration

CF is Clark Fork. Sites are listed in order of elevation with low contaminated site, CF at Missoula, associated with its reference pair, Bitterroot River. CF at Kohrs Ranch is the highest contaminated site

Table 1.2 Parameter Value Range and Convergence Diagnostics of the Resazurin Resorufin Advection Dispersion Equation

Parameter	Velocity (v)[b]	Retardation (R)[b]	Dispersivity (α_L)[b]	Raz Decay Coefficient (k_1)[b]	Rru Decay Coefficient (k_2)[b]	Raz to Rru Coefficient (k_{12})[b]	Mean Absolute Error
Parameter Values	23.8 - 27.4	1.7 - 2.3	0.40 - 1.4	0.03 - 0.09	0.10 - 0.27	0.35 - 0.91	0.02 - 0.07
Variation of 10 optimization experiments	6.9e-4 - 3.5e-3	1.5e-5 - 8.1e-4	4.9e-5 - 1.8e-2	4.9e-6 - 2.3e-5	1.7e-5 - 3.0e-4	6.9e-6 - 4.5e-4	1.1e-7 - 2.3e-6
Variation - Value difference	10^{-4} - 10^{-5}	10^{-4} - 10^{-5}	10^{-2} - 10^{-4}	10^{-3} - 10^{-4}	10^{-3} - 10^{-5}	10^{-3} - 10^{-5}	10^{-4} - 10^{-6}

[a] Range of parameter values and variation represents min and max values of the 24 columns of the dataset

[b] units: v (cm hr^{-1}), R (-), α_L (cm), $k_{1,2,12}$ (hr^{-1})

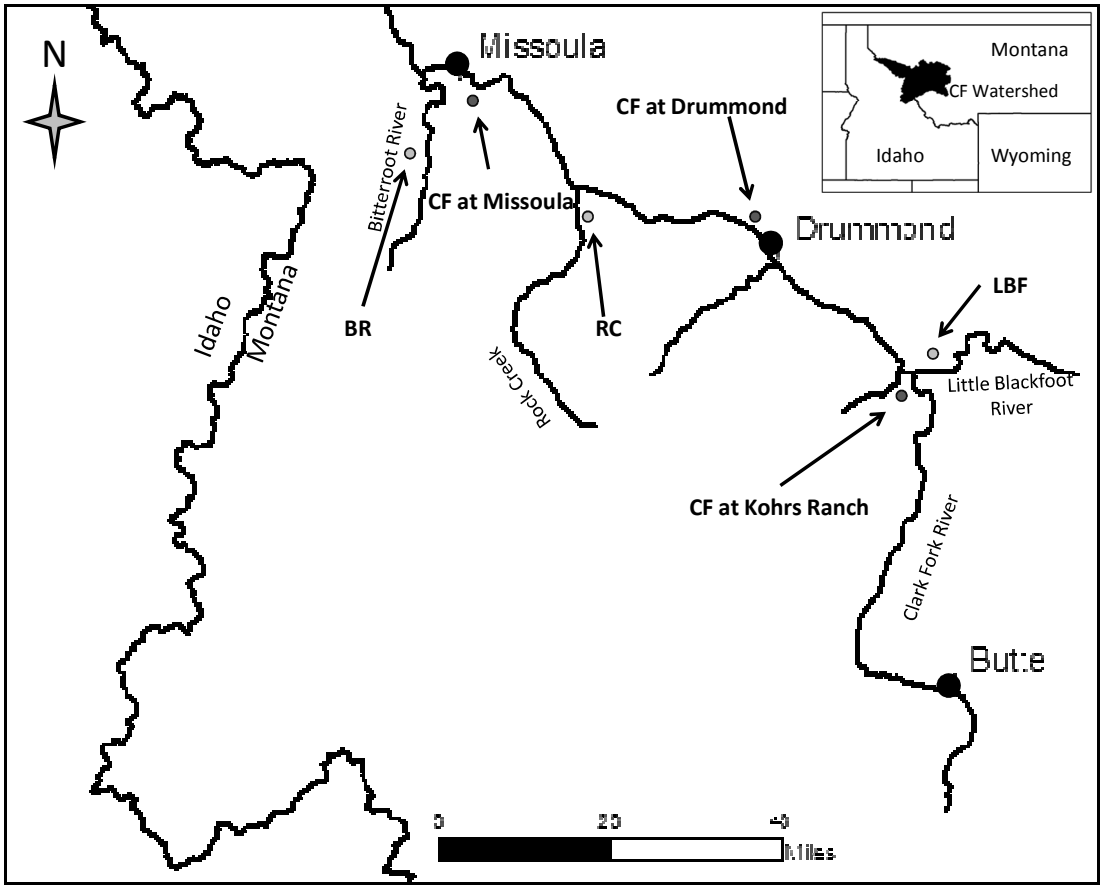

Figure 1.1 Site Map Showing Regional and Local Scales with Site Locations. Bitterroot River (BR), Rock Creek (RC), and Little Blackfoot River (LBF) are the low, middle, and high-elevation reference sites, respectively, shown as light grey circles. Contaminated sites along the Clark Fork River are shown with dark grey circles and in order of lowest to highest elevation/contamination are Missoula, Drummond, and Kohrs Ranch.

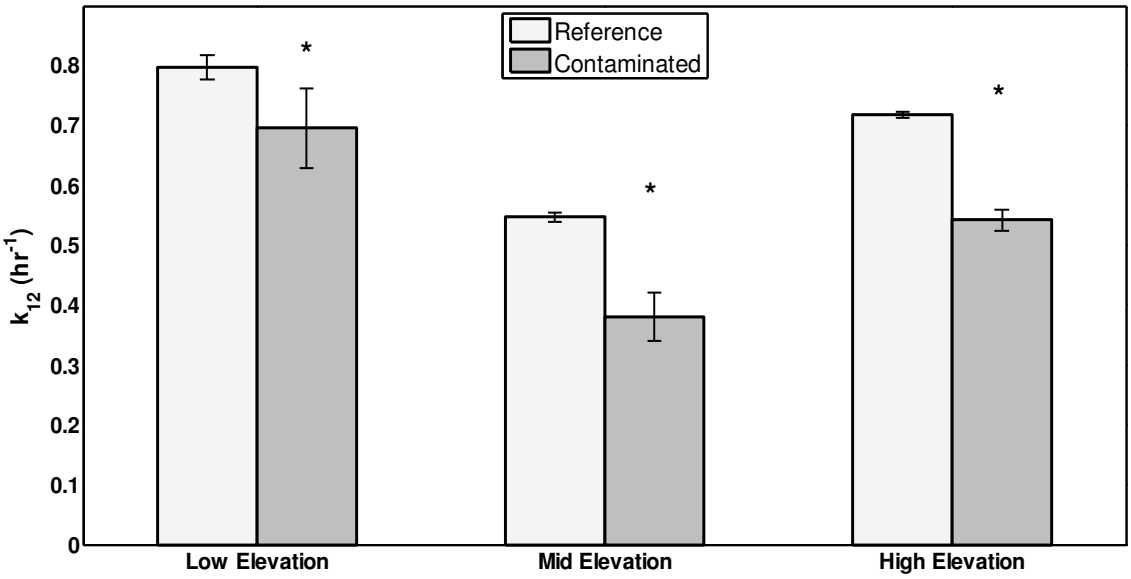

Figure 1.2 Raz-to-Rru Transformation Rate Constants (k_{12}) of Reference-Contaminated Site Pairs (means ± std. err.). * denotes significant differences among site pairs (ANOVA, $P \leq 0.05$). Low elevation = low contamination level, Mid-elevation = mid-contamination level, and High elevation = high contamination level.

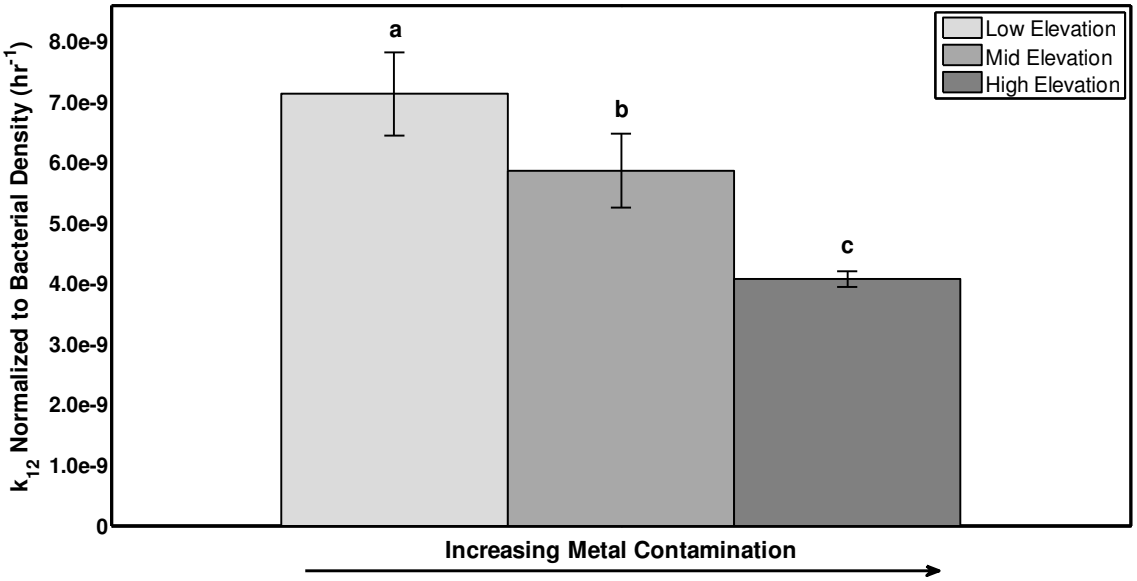

Figure 1.3 Bacterial Density Normalized k_{12} Values for Sediments Collected along the Clark Fork River Contamination Gradient (means ± std. err.). Mean normalized k_{12} values are significantly different from each other at P < 0.001 (ANOVA); letters denote significant differences among means as determined by a Tukey-Kramer Test (P ≤ 0.05 level).

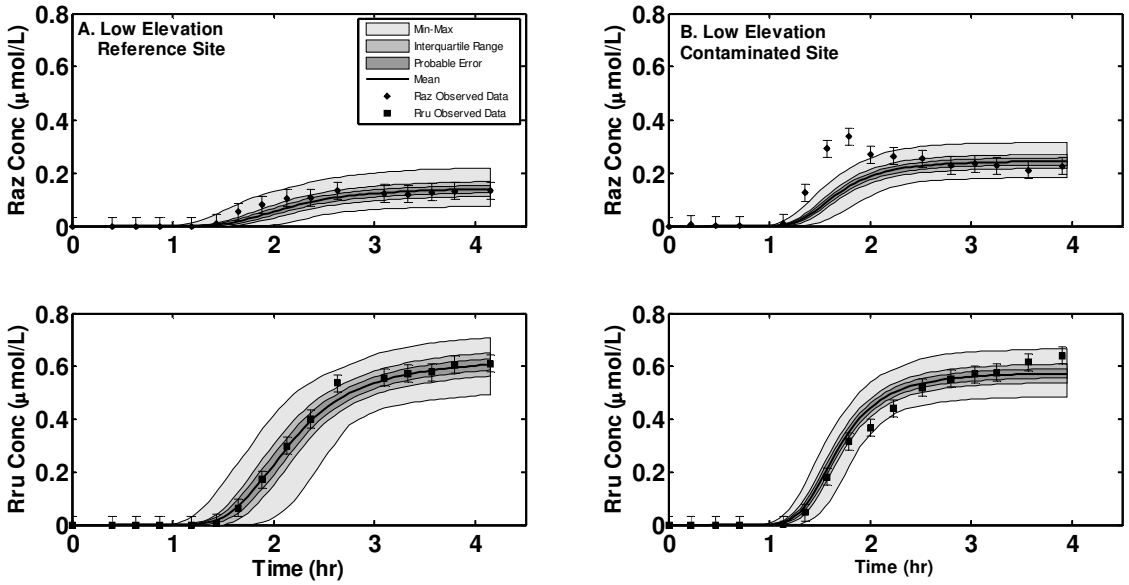

Figure 1.4 Plot of Decoupled Raz and Rru Breakthrough Curves with Uncertainty Estimation. Breakthrough curves are expressed as concentration versus time. A) Low elevation reference site: Bitterroot River sediment columns. These were the best performing model simulations with an overall average model error of 0.022. B) Low elevation contaminated Clark Fork at Missoula sediment columns. These were the worst performing model simulations with a site average error of 0.056. Error generation is primarily isolated to the rising limb of the Raz breakthrough curve.

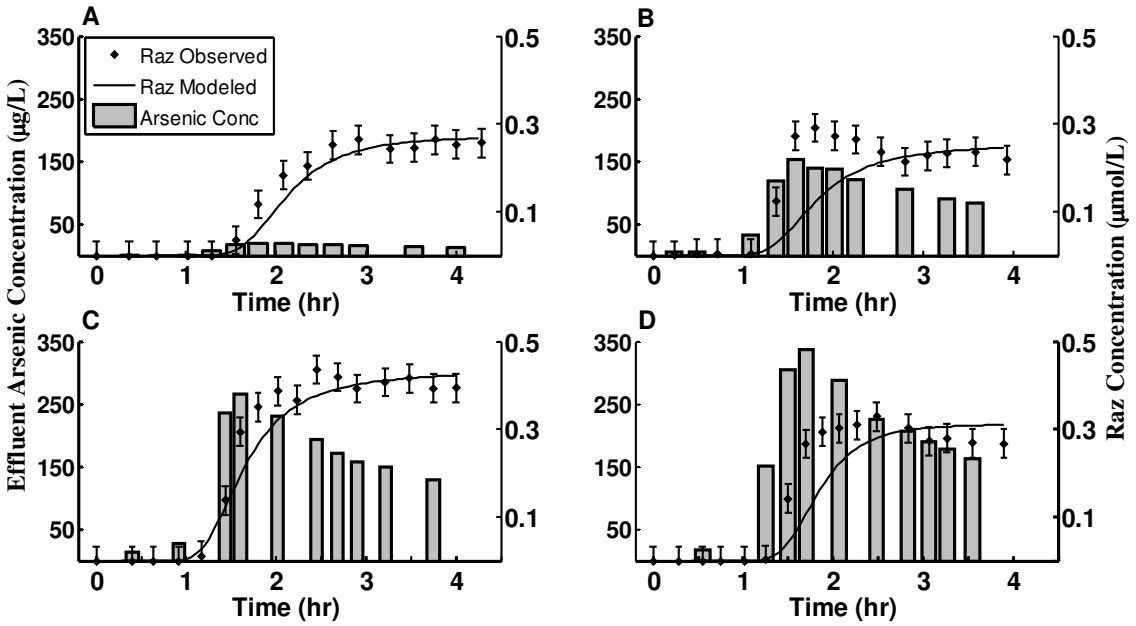

Figure 1.5 Plot of Arsenic and Raz Breakthrough Curves for Four Different Sediment Types: A) Mid elevation reference site (Rock Creek), B) Low elevation contaminated site (CF at Missoula), C) mid elevation contaminated site (CF at Drummond), D) high elevation contaminated site (CF at Kohrs Ranch).

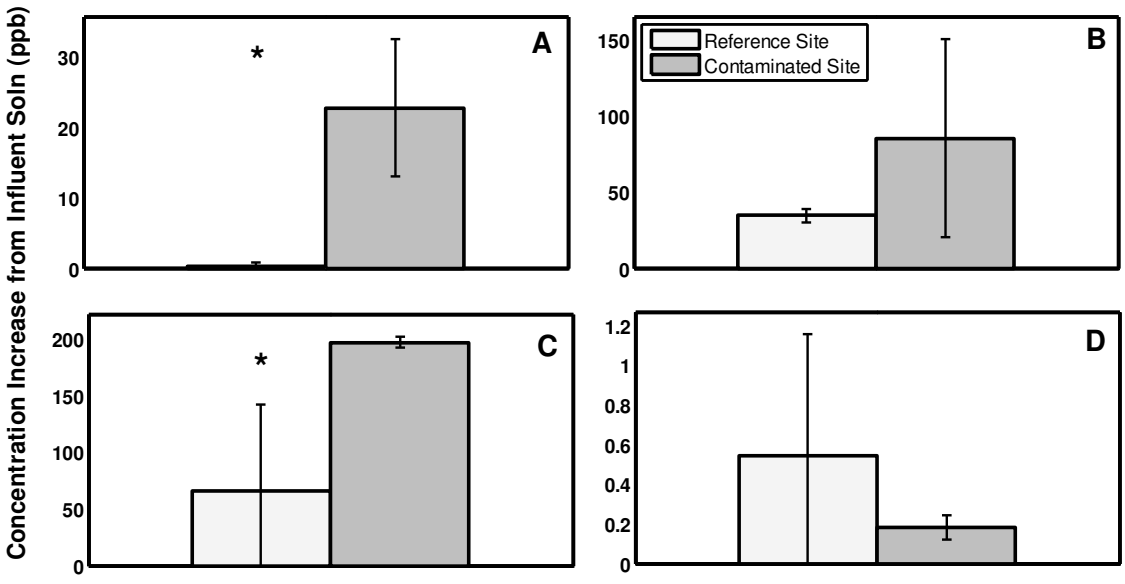

Figure 1.6 Reference and Contaminated Site Averaged Increases in Effluent Metal Concentration from Influent Solution (means ± std. err.). A) Copper, B) Zinc, C) Arsenic, D) Cadmium. Contaminated sites have significantly greater increasing in copper and arsenic concentrations. * denotes significant differences among site pairs (ANOVA, $P < 0.05$).

CHAPTER 2: DIFFERENT CHRONIC METAL CONTAMINATION REGIMES SELECT FOR SIMILAR HYPORHEIC MICROBIAL COMMUNITY METAL RESISTANCE POTENTIALS: ANALYSIS WITH THE RESAZURIN RESORUFIN SMART TRACER

Abstract

Chronic heavy metal contamination in lotic ecosystems can impose long-term metabolic inhibition in hyporheic microbial communities, reflecting the energetic cost of metal resistance. This selective stress influences the genotypic and phenotypic character of the exposed community. Pollution-induced community tolerance is expected to equip communities originating in chronic metal contaminated environments with a greater capacity to mitigate the toxic effects of an acute metal exposure. We tested this hypothesis by measuring the metabolic inhibition of two hyporheic microbial communities induced by an acute metal exposure. One community was from a metal contaminated site along the Clark Fork River, Montana and the other from a relatively uncontaminated reference site. Metabolic inhibition was estimated with the Resazurin Resorufin Smart Tracer (RRST) in column experiments. We predict that the community from the metal contaminated site should demonstrate less metabolic inhibition when exposed to an acute cadmium stress than the reference community. Contrary to this expectation, both the reference and contaminated community demonstrated similar metabolic responses to the Cd treatment characterized by consistent respiration below a

contamination threshold above which respiration declined. These results suggest that either a common metal resistance potential has evolved in response to the different metal contamination regimes of our two test sites or that the Cd-treatments we applied represent a relatively novel metal stress to both of the tested communities resulting in a similar inhibition profile.

Introduction

Heavy metal contamination of freshwater ecosystems is a persistent problem worldwide (1, 2). This chronic stress shapes the genotypic and phenotypic character of the exposed hyporheic microbial community by selecting for tolerant organisms that survive in otherwise toxic environments and encumbering the tolerant community with the metabolic cost of maintaining and expressing metal tolerance genes (6, 56). The cost of metal tolerance can manifest as inhibited basal metabolic potential during times of minimal metal exposure (47) (Chapter 1) in exchange for survival in times of higher metal stress (56). Therefore, communities that develop in chronically metal stressed environments and possess metal resistant genotypic traits to cope with acute metal exposures should have a different functional response to additional, acute metal stress than communities without these traits (60).

In stream environments, elevated concentrations of sediment associated metals are persistent and the bioavailable and mobile fraction of these contaminants oscillates on diel (57) and/or seasonal (64-66) timeframes, with daily fluctuations as much as 500% in streams impacted by heavy metal deposition (57, 58, 67-69). We hypothesized that acute metal exposure responses are representative of *in situ* ecological behavior during peak bioavailable metal concentrations, and that differences in acute responses between

communities that have developed under low and high levels of metal stress should follow the predictions of the pollution-induced community tolerance hypothesis (70, 71). The pollution-induced metal tolerance paradigm suggests metal tolerant communities should demonstrate less pronounced metabolic responses to additional metal stresses relative to communities developed under lower levels of, or in the absence of, metal stress (56, 71-74). The expression of metal tolerance traits enables tolerant communities to more rapidly acclimate to conditions of acute metal exposure than naïve communities that lack such tolerance mechanisms (56). Alternatively, communities adapted to survive under a single stress regime may be more vulnerable to additional stressors because of loss of resistance and/or resiliency (60, 62), and as such these vulnerable communities may demonstrate a more robust response to an additional acute stress (60, 75).

The cost of pollution-induced community tolerance of metal stressed communities to novel and/or other stressors has been documented (61, 76, 77). On the other hand, co-tolerances are often developed in natural systems faced with multiple stressors and/or additional stressors; a reduced negative response would be expected when resistance mechanisms have similar modes of action (73, 78, 79). However, less is known about how hyporheic microbial communities adapted to chronic metal contamination will respond to acute metal exposures. The cost of maintaining cadmium efflux genes in *Psuedomonas putida* KT440 under varying levels of Cd exposure has been quantified with the wildtype *P. putida* strains able to out compete strains with deletions of one of two Cd resistant genes in the presence of > 0.1 mM Cd because of a shortened lag phase (56). Here, we attempt to quantify the ability of metal-adapted hyporheic microbial

communities to cope with an additional acute metal exposure using the metabolically reactive Resazurin Resorufin Smart Tracer.

The Resazurin Resorufin Smart Tracer was recently proposed as a metabolically reactive hydrologic tracer capable of coupling solute transport and estimates of benthic/hyporheic microbiological activity in freshwater systems (38). In a controlled laboratory column experiment, this tracer showed promise in its initial deployment as a functional indicator of hyporheic ecological integrity (Chapter 1). RRST estimates of sediment-associated metabolic potential showed inhibition of sediment from the contamination gradient relative to reference communities with this inhibition varying linearly with metal contamination levels. The RRST also detected cause and effect relationships of community respiration to changing environmental conditions (Chapter 1).

The metabolic resistance of hyporheic microbial communities inhabiting chronically metal contaminated sediments (> 100 y) when exposed to an acute cadmium exposure was tested and compared to the resistance of a reference stream's hyporheic microbial community in column experiments using the Resazurin Resorufin Smart Tracer. We hypothesized that a hyporheic microbial community present in the chronically metal contaminated Clark Fork River, Montana would possess the metal tolerance mechanisms necessary to withstand periodic increases in metal stress and therefore would demonstrate less respiratory inhibition (i.e., greater resistance) in the presence of an experimentally applied acute cadmium (Cd) stress than communities from a reference site. Cadmium is one of the toxic metals found in the environment in which the metal-adapted community originates. Contrary to our hypothesis, our results show similar metal resistance in both communities with respiration inhibition occurring above a Cd

concentration threshold (Figure 2.1). This suggests that both communities may possess metal tolerance mechanisms and these traits are not able to overcome all levels of acute metal stress. This may indicate a mechanism for prolonged ecosystem suppression in systems chronically contaminated with heavy metals.

Methods

We tested the metabolic effects of an acute Cd stress exposure on hyporheic microbial communities exposed to differing histories of fluvially deposited heavy metals. Changes in net heterotrophic hyporheic metabolism in response to the acute Cd stress were measured in column experiments using the Resazurin Resorufin Smart Tracer, a metabolically reactive hydrologic tracer. The Clark Fork River is a sixth-order river draining 66,870 km^2 of western Montana and northern Idaho (80). Historic mining has deposited elevated concentrations of arsenic, cadmium, copper, lead, and zinc several hundred times above background with concentrations declining from the headwaters near Butte, MT to the outlet at Lake Pend Oreille in N. Idaho. Hyporheic sediment from a highly contaminated site, Clark Fork at Kohrs Bend (4^{th} order; lat. 46°28’22.38”, long. 112°43’41.59”; elevation 1350 m) was paired to a reference tributary stream, Little Blackfoot (LBF) (3^{rd} order; lat. 46°32’13.23”, long. 112°42’57.90”; elevation 1363 m). This reference stream was chosen because of its similarity in physical fluvial geomorphological characteristics to the contaminated stream with the primary difference being the level of heavy metal present. Shallow (5-15 cm) hyporheic sediment was sieved in the field to a uniform grain size (1.7-2.36 mm), packed into coolers with wet ice and shipped overnight to Boise, ID for analysis.

Within 24 hrs post collection, sediment was packed into four replicate columns per site. The columns consisted of low-pressure 30 cm x 1.5 cm glass chromatography columns (FlexColumn, Kontes Glass Company, New Jersey, USA). Of each set of four columns, two received a Cd-amendment and two did not. The two Cd-treated columns per site were fed a pH buffered (6.7 ± 0.055) solution of stream water collected from a pristine reference stream within the Clark Fork drainage (Rock Creek). The common water source normalized dissolved organic carbon availability and other pore water characteristics for each treatment combination. The Cd-treated columns received an influent solution of 200 µM PIPES buffer, 0.1 mM Cadmium Chloride, and 0.1 mM chloride (Cl) delivered at a constant discharge (~0.3 mL/min) and temperature (~15.4°C ± 2.6°C). In the control columns, the 200 µM PIPES buffer was amended with 0.2 mM NaCl instead of the 0.1 mM CdCl and 0.1 mM Cl to normalize ionic strength between treatments. Columns from each site were fed the treated pore water for 19 hrs to acclimate the sediment to the column environment and avoid measurement of transient responses. After incubation, 200 ppb resazurin was added to the treatment and control solutions and measurements of resazurin, resorufin, and Cl^- (as a conservative tracer) were taken every 10-28 minutes for the following four hours until resazurin/resorufin concentrations reached plateau, resulting in a total acute Cd exposure of 23 hours. Cd was employed because it is a potent bacterial toxicant and it does not react with the resazurin/resorufin tracer.

Influent solution was pumped from the feed reservoir to the columns with Masterflex® L/S 13 tubing (06424-13, ID 1.6 mm) using a Masterflex® peristaltic pump (L/S 7523-40 digital standard drive, Cole Parmer Instrument Co., Chicago, IL) with an

attached 12 channel, 8 roller cartridge pump head (Masterflex L/S® 7519-25) loaded with 4 Easy Load small cartridges (Masterflex L/S® 7519-85). Easy load cartridges were fitted with Masterflex® L/S Microbore 2 stop PVC tubing (06416-10, ID 0.19 mm). Microbore and L/S 13 tubing were attached using Ominfit (Cambridge, England) two-way connectors (Cole Parmer Instruments 06473-00). Luer locks connected the L/S tubing to the column via a 4-way stopcock male lock. Peristaltic pump discharge rate was gravimetrically calibrated to 0.3±0.01 mL min^{-1} at the start of each experiment.

Effluent samples were collected by fitting a luer lock connection at the effluent end of the column to a short piece of L/S 13 tubing and directing the column effluent to sterile 17 x 100 mm polypropylene culture test tubes (Fisherbrand 14-956-1J). Electrical conductivity measurements were made on these time-averaged volumes at each sampling point with an Orion 031610MD conductivity cell attached to the Orion 3 Star Portable Conductivity Meter (Thermo Scientific Inc., Bremen, Germany). Column effluent was pulled from the collection tube using a 1 mL plastic syringe and then filtered through a 0.22 µm sterile filter (25 mm Durapore membrane filters and Millipore Swinnex-25 filter holders). Each sampling time point required multiple 1 mL pulls. The first pull evacuated the filter housing of residual effluent from the previous sampling time point. Sample collection for quantification (~500 µL) was then collected from a second filtered volume. To prevent cross contamination between sampling points, filters were then cleared with 1-2 mL of air. Sterile filtered samples were measured for resazurin and resorufin concentrations at each discrete time point to establish breakthrough curves. Remaining effluent not used for resazurin/resorufin quantification was preserved and used for trace metal analysis. Volume averaged sample intervals varied and ranged from 10 to 28

minutes with higher frequency sampling occurring during breakthrough and fewer samples at plateau. Sample points were linearly interpolated at an interval of 0.05 hr (3 min) prior to data processing.

Resazurin/Resorufin Quantification

Resazurin and resorufin sodium salts were purchased from Sigma Aldrich. Initial fluorometric analysis of stock resazurin indicates an average of 1.05% resorufin contamination. Resazurin and resorufin are fluorescent compounds uniquely detectable with individual fluorometric settings (resazurin: λ_{exc} = 602 nm, λ_{emi} = 634 nm; resorufin: λ_{exc} = 530 nm, λ_{emi} = 590 nm). Fluorescence of both compounds is pH dependent with optimal fluorescence (constant and maxima) observed at pH > 8 (45, 46). Prior to measuring fluorescence, the pH of samples and standards were raised to approximately 9.5 with the addition of 2.5 µL 25 mM NaOH (control) or 2.5 µL 125 mM NaOH to 100 µL sample in 96 well flat bottom, black-walled plates (Costar part # 3603). Fluorescence measurements were performed on a Synergy Mx multi-mode microplate reader with Gen 5 software (Biotek Instruments, Inc) with bandpass set to 9 and sensitivity set to 100. All fluorescence measures were made within 24 hrs post experiment. Samples were stored in the dark at 4°C prior to reading.

Resazurin standard fluorescence remained consistent during the experimental period. The resorufin standard fluorescence showed a strong decay through time in preliminary assays under refrigeration; however, fluorescence was preserved when Rru standards were frozen. At the start of the experimental period, fresh resazurin and resorufin standards were prepared, aliquots of resorufin standards were frozen until used.

Trace Metal Quantification

Metal concentrations of column effluent (Mg, Al, Si, P, K, Ca, Cr, Mn, Fe, Ni, Cu, Zn, As, Sr, Cd, Ba, Pb, U) and sediment (Na, Mg, Al, Si, P, K, Ca, Cr, Mn, Fe, Ni, Cu, Zn, As, Se, Kr, Sr, Ag, Cd, Ba, Pb, U) were quantified with an X-Series II Inductively Coupled Plasma Mass Spectrometer (ICP-MS) (Thermo Fisher, Bremen, Germany). Effluent metal concentrations were measured on composite samples of column effluent collected over the duration of each experiment. At the completion of the experiment, 25 mL of this solution was sterile filtered with 0.45 µm Millipore Durapore Membrane Filters and treated with 0.125 mL of 10% trace metal grade HNO_3, according to EPA method 1669, and then frozen until analyzed.

Total extractable metal analysis of sediment samples followed EPA method 3051A for microwave digestion. Briefly, five 0.5 g (± 0.005) replicates per site of thawed and dried (four days at 50°C) sediment (not used in column experiments) were placed into fluorocarbon polymer microwave vessels. 10 mL of triple distilled concentrated HNO_3 was added and then the vessels were sealed according to the manufacturer's directions and digested in a microwave digester (CEM Mars Xpress, CEM Corporation, Matthews, NC) using the pre-loaded EPA 3051A program as follows: temperature ramped to 175±5°C in 5.5±0.25 min and maintained for 4.5±0.25 min. Vessels were allowed to cool in the microwave. Leachate was removed and diluted to 2% HNO_3 for ICP-MS analysis. External standard verification (San Joaquin Soil, SRM 2709a, NIST) of the average concentration of the five target metals were as follows: arsenic (within reported range), cadmium (within reported range), copper (within 2.2%), lead (within 4.3%), and zinc (within 1%).

MCI Calculation

The magnitude of metal contamination for each site and in the column effluents was expressed as a metal contamination index (MCI) (12, 81). This index normalizes the relative degree of contamination to the most pristine site within the dataset. MCI values for each sample were calculated as follows,

$$MCI=\Sigma((\log (Me_n)/\log (\text{background } Me_n))/n$$

where Me_n is the metal species (i.e., As, Cd, Cu, Pb, or Zn), n is the number of metals included in the index, and background is the respective metal concentration of the most pristine site. In this study, the measurement of chronic stress is normalized to the metal concentrations of the Bitterroot River, MT the most pristine site surveyed during the summer of 2010 with the following metal concentrations (ppm): arsenic (0.79), cadmium (0.013), copper (2.66), lead (1.83), and zinc (4.45).

Sediment MCI (sMCI) values, derived from sediment digestions, describe the magnitude of metal stress the tested hyporheic microbial community experienced *in situ*, and provides a relative measure of the environmental contamination gradient that exists within the Clark Fork River watershed. Effluent MCI (eMCI) values were calculated from the soluble metals present in the column effluents and describe the magnitude of acute metal stress. Effluent from a LBF control column was used to formulate column eMCI of the acute metal stress experiment: As (2.05), Cd (0.75), Cu (0.37), Zn (8.56), and the average of both LBF control columns were used as the baseline for the eMCI site analysis with the following concentrations (ppb): As (2.12), Cd (2.04), Cu (0.32), Zn (7.01).

Dissolved Oxygen

The relationship between resazurin/resorufin measures of sediment respiration and DO consumption was established in independent column experiments operated under various discharge regimes (0.1, 0.15, 0.2, 0.3 mL/min). Five replicate columns were measured at each discharge. Resazurin/resorufin were measured as described above. DO consumption was measured with non-intrusive fluorescence quenching (PreSens Precision Sensing GmbH, Regensburg, Germany). Oxygen sensor foils were adhered inside the column prior to packing with Boise River sediment at the influent and effluent ends. Sediment respiration measurements were made at steady state with DO consumed measured as the difference between DO concentration as the pore water entered the column and as it exited the column. González-Pinzón et al., (2012) has demonstrated the relative consistency of the relationship between sediment respiration, DO consumption, and resorufin production (82).

Bacterial Enumeration

Bacterial densities were measured on Clark Fork and Little Blackfoot sediments pre-experiment via quantitative PCR. Total community DNA was extracted from sediments using the FastDNA® SPIN Kit for Soil and the FastPrep® Instrument (MP Biomedicals, Santa Ana, CA). Using amplification setting previously described (48), five replicate DNA extractions per site were analyzed with real-time quantitative PCR (qPCR), amplifying the 16S rRNA gene with Bact 1369F and Prok 1492R primers and Taqman probe 1389F. The relative density of bacterial biomass in each sample was expressed as a function of the number of 16s gene copies g^{-1} sediment. A plasmid-based

qPCR standard curve was linear across seven orders of magnitude in the 2.9×10^{1} – 2.9×10^{8} 16s gene copies mL^{-1} range (48).

Organic Carbon Quantification

Sediment associated organic carbon (OC) was quantified using the <1.18 mm grain size fraction from each column. Column sediment was thawed and dried at 85°C for 24 hrs then sieved through a 2 mm mesh followed by a 1.18 mm mesh, coarse sediment was discarded. Sediment smaller than 1.18 mm was hand pulverized to <125 µm, collected and dried for at least 24 hrs at 80°C. Inorganic carbon was oxidized with the addition of 7 mL of 0.73 M sulfurous acid (H_2SO_3) in acid-washed vials (83). This represents at a minimum a 1:10 mixing ratio of g sediment: mL acid for all columns. The acid-sediment solution was then dried at 80°C for >24 hrs and replicate (n=3) ~100 mg samples were measured into tin discs (CD Elantech, Inc., Lakewood, NJ) for carbon quantification by the Flash EA 1112 Series NC Soil Analyzer (Thermo Scientific Inc., Bremen, Germany). A low concentration calibration curve (0.1-0.005 mg C mg^{-1} sample) was generated with San Joaquin Soil (NIST SRM 2709a) for accurate quantification of the carbon content of the Clark Fork sediments. Results were validated with internal standards (SRM 2709a) and verified with in-house external standards (CBXO Soil, BioTrace Lab, Boise, ID).

Data Analysis

Resazurin and resorufin breakthrough curves were deconstructed into constituent biological and physical parameters with the application of a Markov chain Monte Carlo data assimilation technique solving the inverse resazurin/resorufin advection dispersion

equation with a Metropolis Hastings algorithm developed to provide a probabilistic solution. This forward model is a suite of reactive advection dispersion equations describing resazurin and resorufin transport through porous media. These transport equations are associated through the k_{12} term that quantifies resazurin to resorufin reduction as (38)

$$\frac{\partial C_{Raz}}{\partial t} = \frac{\alpha_L v}{R}\frac{\partial^2 C_{Raz}}{\partial x^2} - \frac{v}{R}\frac{\partial C_{Raz}}{\partial x} - k_1 C_{Raz} - k_{12} C_{Raz}$$

$$\frac{\partial C_{Rru}}{\partial t} = \frac{\alpha_L v}{R}\frac{\partial^2 C_{Rru}}{\partial x^2} - \frac{v}{R}\frac{\partial C_{Rru}}{\partial x} - k_2 C_{Rru} - k_{12}\frac{M_{Rru}}{M_{Raz}} C_{Raz}$$

where C_{Raz} is the concentration of Raz [µmol L^{-1}]; C_{Rru} is the concentration of Rru [µmol L^{-1}]; t is time [hr]; x is distance [cm]; α_L is longitudinal dispersivity [cm]; v [cm hr^{-1}] is the average pore water velocity; R [-] is retardation coefficient due to sorption; k_{12} [hr^{-1}] is the reaction rate coefficient of Raz to Rru; k_1 [hr^{-1}] is the reaction rate coefficient of Raz decay; k_2 [hr^{-1}] is the reaction rate coefficient of Rru decay; M_{Raz} [g mol^{-1}] is the molecular weight of Raz; and M_{Rru} [g mol^{-1}] is the molecular weight of Rru (38). The forward RRADE model developed in Haggerty et al., (2008) (38) was provided and translated into Matlab® R2011a. Accuracy of the Matlab formulation was verified through comparison of resazurin/resorufin concentrations at discrete time points in simulations of initial conditions and variable values found in Haggerty et al., (2008) (38). The Markov chain Monte Carlo resazurin resorufin advection dispersion equation optimization accurately fit the model to the observed data with model error ranging from 0.0122-0.0207, significantly less model error than that generated in prior experiments (Chapter 1), most likely attributable to the long incubation time allowing for steady-state conditions. This modeling approach is previous detailed (Chapter 1).

Results and Discussion

We investigated the metal resistance capability of hyporheic microbial communities selected for under different chronic metal stress regimes by measuring the extent to which respiration was suppressed or not by an acute exposure to a toxic metal and expected chronic toxic metal exposed communities would demonstrate a greater resistance to an additional acute metal exposure than communities from lesser contaminated environments. Based on predictions of the pollution-induced community tolerance, we hypothesized that respiration of communities from chronically metal contaminated environments would be inhibited in the presence of an acute metal exposure and that this inhibition would be inversely correlated to the magnitude of long-term stress (71) (Figure 2.1). Accordingly, we predicted that the highly contaminated Kohrs Bend (KB, sMCI = 1.15) site would exhibit a smaller difference in k_{12} between treatment and control columns than that of Little Blackfoot (LBF, sMCI = 0.71). Respiration rate responses were quantified with the Resazurin Resorufin Smart Tracer by comparing the rate coefficient of resazurin to resorufin reduction by each community (k_{12}).

Resazurin to Resorufin Reduction Rate Constant

Direct correlations of cellular density to k_{12} (R^2 = 0.51) and DO consumption resazurin lost (R^2 = 093) suggest k_{12} is an accurate estimation of sediment-associated respiration (Chapter 1). In this study, k_{12} was normalized to bacterial density to provide an interpretation of the per cell metabolic response to acute metal exposure. Heterotrophic respiration in the hyporheic zone is often influenced by the availability of organic carbon (84); however, in this study, sediment associated organic carbon was not correlated to

normalized k_{12} (P =0.6) and is not a suspected driver of the differential respiration responses observed, in part because the DOC quantity and quality was normalized across communities and treatments by utilizing a common water source for all experiments. Similarly, other water chemistry constituents known to affect metabolic activity (e.g., nutrients, pH, ionic strength, etc) were normalized with same source influent solution. Therefore, metabolic differences are attributed primarily to metal toxicity.

Ecological Response to Acute Metal Exposures

We measured the level of dissolved metals in the column effluents and expressed them in terms of effluent MCI to assess the level of applied acute metal stress (Table 2.1). This metal contamination index assumes that all metals are equally toxic and ameliorates differences in concentrations and toxicity of metals in favor of a lower resolution environmentally relevant composite score (12). There was a comparable increase in effluent MCI of 0.9 and 0.8 between treatment and control for columns containing hyporheic sediments from the reference Little Blackfoot River and the contaminated Clark Fork at Kohrs Bend, respectively. However, columns amended with Cd and containing the contaminated sediments experienced a stronger overall metal exposure (average effluent MCI: Little Blackfoot control = 0.04 ± 0.06, Little Blackfoot treatment = 0.94 ± 0.06, Clark Fork at Kohrs Bend control = 1.1 ± 0.28, Clark Fork at Little Blackfoot control = 1.9 ± 0.05). k_{12} declined in the treatment columns of both sites relative to the control. The greatest inhibition was associated with a more pronounced difference in k_{12} between the control – treatment columns of the contaminated community (P = 0.005). Acute Cd exposure reduced respiration by this community by 6.9×10^{-10} hr^{-1} compared to 3.6×10^{-10} hr^{-1} of the reference community (Figure 2.2). This suggests that

the magnitude of acute stress that was greatest in the contaminated sediment Cd-treatment columns inhibits respiration even in communities developed in highly metal contaminated environments. Further categorical conclusions about relative levels of community metal resistance from this plot are inappropriate because of the unequal effluent MCI values between community types. However, a systematic metabolic inhibition corresponding to acute metal exposure was observed for both hyporheic communities (i.e., an inverse relationship of cell density normalized k_{12} versus effluent MCI) (Figure 2.3). With the exception of one reference site treatment column, normalized k_{12} shows a slight and nearly equal decline in both communities within the effluent MCI range of 0 - 1.4, above an MCI of 1.4 k_{12} is markedly depressed, suggesting a continuous response of both communities up to a stress threshold. Although we applied a single metal stress (Cd), the metal content of the sediments themselves contributed to the net contaminant stress experienced by the sediment associated microbial communities. Owing to the natural heterogeneity in sediment metal contents among sites, there was a large discrepancy across columns and treatments in the metal concentrations in the effluent pore water contributing to the overall MCI score. To understand the relative impact of each of these metals, a more highly resolved analysis of individual metals is necessary.

The level of acute metal stress present as Cd in the influent solution was constant across sediment/hyporheic community types, however, the actual level and type of acute metal stress experienced by the communities in each column varied. Effluent Cd concentrations spanned a gradient of more than 3 orders of magnitude from 2 - > 3500 ppb with nearly a 500x increase between Little Blackfoot control and treatment columns

and a 30x increase in Clark Fork at Kohrs Bend (Table 2.1). The lowest Cd concentrations are associated with control columns from both sites followed by a marked increase in the treatment columns. Cd-treated reference site columns were exposed to nearly an order of magnitude greater Cd concentration than the contaminated site control columns. Effluent copper concentrations ranged from 0.3 to 18 ppb and the contaminated site columns had greater concentrations than the reference. The Cd-treated columns of both sites had greater Cu concentrations than control columns with the reference site having a 4 fold increase to 1.3 ± 0.8 ppb and a doubling of the contaminated site columns to 18.3 ± 0.7 ppb. Zinc concentrations ranged from 7.0 ± 2.2 ppb in the reference control columns to 505 ± 45 ppb in the contaminated site treatment. Cd-treated reference site columns were similar to the contaminated site control columns with 50 ± 5.7 ppb and 32 ± 9.3 ppb Zn, respectively. Arsenic concentrations were much lower ranging from 1.2 ± 0.38 to 9.0 ± 0.25 with control columns of each site having higher As concentrations than the treatment columns, reflecting the differential sorption characteristics of As vs. Cd, Cu, and Zn (57). We analyzed individual metal-k_{12} relationships to develop a more highly resolved depiction of degree and type of metal stress than possible with the MCI calculation (Figure 2.4). This analysis shows the reference site columns received a correspondingly high Cd stress relative to the Cd-treated contaminated site columns. Cd-treated Clark Fork at Kohrs Bend columns experienced the highest overall stress and the highest concentrations of Cd, Cu, and Zn.

Cadmium is one of the most toxic metals incorporated into the MCI (85-87). It is also the highest concentration dissolved metal of the dataset, although its concentration was highly variable, which was unexpected given the consistent concentration of Cd

applied with the column influent. Effluent from cadmium-amended columns from Little Blackfoot and Clark Fork at Kohrs Bend contained 98%, 84%, 75%, 62%, less than the amount of Cd applied with the influent solution, respectively, with large within site variability of dissolved Cd concentrations of 191 and 1755 ppb, and 2792 and 4319 ppb for the Little Blackfoot and Clark Fork at Kohrs Bend, respectively. Cadmium retention in the columns is likely due to the presence of iron and manganese oxyhydroxides sediment coatings that are prevalent in the CF system (88) and sediment associated organic carbon, two factors that exhibit strong Cd adsorption potentials (89, 90). Reference site sediments had significantly higher organic carbon content relative to the contaminated site sediments ($P = 0.01$) and more than two times the amount of sediment associated Fe of 8237 mg g^{-1} sediment compared to 3524 mg g^{-1} sediment with similar Mn concentrations between sites of 210 mg g^{-1} sediment (reference) and 285 mg g^{-1} sediment (contaminated). The higher effluent Cd concentrations observed for the contaminated site may be a function of the elevated concentrations of cationic metals sorbet to these sediments at the time of collection in addition to lower sediment associated OC and Mn contents. Presence of such metal captions may have limited the availability of action binding sites on surface associated Fe/Mn-oxyhydroxides relative to the Little Blackfoot sediments (91, 92). The increase of pore water Cu and Zn from both sets of Cd-treated columns likely is due to pH and ionic strength influenced desorption driven by the application of the influent solution poised at a $pH = 6.7 \pm 0.06$ and an average increase in ionic strength of 232 ± 74 µs cm^{-1} (55, 92).

The biomass-normalized k_{12} shows Cd dependence (Figure 2.4). Normalized k_{12} for both communities remained near 3.5×10^{-9} for Cd concentrations of 1 – 200 ppb,

followed by a rapid decline associated with Cd concentrations greater than 1750 ppb that incorporates one Little Blackfoot and both Clark Fork at KB Cd-treated columns (Figure 2.4a). A clear breakpoint in ecological function exists in both the contaminated and reference communities in the Cd concentration range of >225 and <1755 ppb. This suggests both communities have similar Cd resistance at low end concentrations (< 225 ppb) and a continuous decline at high end concentrations (>1755 ppb); however, highly resolved definition of each community's ecological threshold is indistinguishable because of the absence of data in the threshold range. A definitive breakpoint in function is not as clear in the copper and zinc plots because in one Cd-treated reference site column k_{12} is inhibited at the lower end of the measured metal concentration range (0.7 ppb Cu and 18 ppb Zn) and the other reference site treatment column, although experiencing increased Cu and Zn concentrations, is not inhibited. These observations suggest metabolic inhibition of the low k_{12} column is not attributable to either of these individual metals (Figures 2.4b and 2.3c). Conversely, this column was exposed to a Cd concentration beyond the functional breakpoint potentially pointing to Cd as the primary driver of the metabolic suppression. There are no distinguishable patterns in the arsenic range of 1 – 9 ppb, indicating As did not influence community respiration.

The concentration range of metals shown to cause a definitive effect on biotic processes can vary by orders of magnitude in the literature primary due to assay conditions and varying environmental/geochemical interactions (93). Further, the relationship of k_{12} inhibition to more commonly used metabolic measurements (e.g., enzyme activity, carbon substrate utilization) is currently unavailable. However, inhibition of non-metal and metal exposed communities has been observed at the acute

Cd concentrations levels applied in this study. Cadmium concentrations required to inhibit dehydrogenase activity by 10%, 50% and 75% in metal naïve soil communities is 0.004, 0.14, and 1.12 ppm, respectively (85). A similar Cd concentration range (0.98 – 1.7 ppm) was found to inhibit thymidine uptake by 50% relative to the control in periphyton communities (94). Average effluent Cd concentration for the reference site control columns was below these minimum values while treatment columns are in the range of required to inhibit thymidine uptake by 50% and for 50 - 75% inhibition of dehydrogenase activity. Cadmium concentrations required to inhibit thymidine uptake by 50% in periphyton communities from chronically contaminated environments has been observed with Cd concentrations of 17.3 – 24.5 ppm (94). Cadmium decreased bacterial glucose uptake by 10% and 50% in metal contaminated sediments with 0.73 ppm and 50.6 ppm, respectively. (86). The contaminated site control column Cd stress was below these values while the treatment columns are within the Cd range that decreased glucose consumption by 10 – 50%. Copper induced a 10% inhibition of dehydrogenase activity of non-metal contaminated soil communities at 0.019 ppm (85). This concentration was only observed in the effluent of the highest Cu containing column of the contaminated site sediment. Likewise, Zn concentrations of 0.06 ppm induced a 10% inhibition of dehydrogenase activity and a range of 0.44 – 3.7 ppm Zn reduced thymidine incorporation by 50% in communities not previously exposed to metals (85). For communities previously exposed to Zn, 29.2 ppm Zn reduced glucose consumption by 10% (86) and reduced thymidine uptake by 50% with 39.3 ppm (94). The Zn concentrations observed in the reference site (0.01-0.02 ppm) and contaminated site (0.03-0.54 ppm) here are below the concentrations noted in other studies that inhibited

metabolic processes in non-metal exposed and metal exposed communities, suggesting that Zn is not the primary driver of normalized k_{12} inhibition. Cadmium concentrations applied in these other studies are similar to those employed here while the Zn and Cu concentrations previously demonstrated to inhibit metabolic variables are higher than observed here, supporting Cd as a primary driver of metabolic inhibition in our column experiments. However, it is noted that the multiplicative effects metals has been documented in other studies (95).

Combined, this data supports our hypothesis in that acute metal exposure inhibits respiration by hyporheic communities from chronically metal contaminated environments and reference communities. However, the more highly contaminated community did not demonstrate greater resistance to additional metal stress than the reference community that originated from a more pristine environment, contrary to our initial prediction and the pollution-induced community tolerance hypothesis (71). We present two possible explanations for these observations. The reference and contaminated community may possess different metal resistance potential that is not observed here because of the use of an acute cadmium stress. Both communities experience similar chronic Cd contamination whereas differential tolerance to metals more prevalent *in situ* may exist (e.g., Cu concentrations increase from 4.6 to 67 mg g^{-1} sediment between reference and contaminated sites whereas Cd concentrations are 0.1 and 0.2 mg g^{-1} sediment, respectively). Cu was not used in this study due to its ability to abiotically reduce resazurin (data not shown). Alternatively, both communities may possess similar metal resistance capacities because even though the metal contamination regimes differ in time and magnitude, both communities have experienced anthropogenic metal deposition.

Cd-specific metal resistance may not have developed in these communities and with metabolic inhibition primarily driven by Cd in these experiments neither community may have tolerance to the applied acute stress. Microorganisms employ four classes of metal resistance strategies: production of extracellular polysaccharides, metal efflux pumps, intra and extra-cellular chelation mechanisms, and enzyme catalyzed redox modification of toxic metals. Each strategy varies in its degree of metal specificity. Highly charged exopolysaccharides are non-specific and bind metals prior to importation into the cell (96). Metal efflux pumps vary in specificity from non-specific to exportation of similar metal families (97). Manufacturing of chelation molecules such as glutathione, polysaccharides, and chaperone proteins for intra or extra binding of metals rendering them non-reactive is metal species and/or metal-class specific (87). The most specific resistance mechanism is intra-cellular redox reaction, resulting in the formation of less toxic metal redox states, a mechanism specific to a given metal species and redox state (87, 97). Specific metal resistance mechanisms are coded for by specific genes and may provide the host with co-tolerances to multiple metals, such as *czcA1* and *cadA2* that encode the Cd/Zn and Cd/Pb efflux transporter (56) or the *copA* and *cusCFBA* Cu efflux pumps and the *cueO* for Cu oxidation (97). While metal co-tolerances exist, such as the tolerance to Pb and Zn in Cu contaminated communities (73, 78) or Cd, Zn, and Co (97), Cd co-tolerance may only develop in mainly Cu contaminated environments via the more non-specific metal resistance strategies (e.g. exopolysaccharide production (96)). Therefore, specific Cd tolerance may not have been selected for in the tested communities, leaving both equally vulnerable to the experimental acute Cd stress.

Secondly, similar metal resistance potential could exist in both communities. Our reference community is not strictly metal naïve, having experienced a less intensive historic metal contamination regime, but still sufficient to drive the sediment MCI value to 0.71, whereas our contaminated site sediment MCI is 1.15. A previous investigation found basal metabolic inhibition to be correlated to sediment MCI above a threshold of 0.7 (Chapter 1). The log scale MCI suggests a difference in contamination nearly a half order of magnitude between the two sites tested here. However, this range of environmental contamination may have selected for similar metal resistance capacities. Indeed, respiration inhibition was similar in two communities after five years of differing levels of soil Cu contamination (e.g., 10 and 82 µg g^{-1}) in the range of acute Cu exposures of 40 – 500 µg Cu g^{-1} soil (70). Perhaps, similar metal resistance potential develops within a range of concentrations of prior metal exposure. For example, a pristine community may be the most vulnerable to an acute stress, with communities developed under mid and high range contaminant exposures exhibiting greater resistance than the pristine community but similar capacities to each other. One potential explanation for the similar response of the reference and contaminated communities employed here is that both communities originated in a contamination range that equally equips for metal resistance. This explanation would suggest that similar metal resistance potential is developed in the sediment MCI range of 0.71-1.15, and may provide insight into which specific metal resistance traits have evolved in this system.

We found that both communities, from reference and contaminated streams, demonstrated a consistent response to increasing acute Cd stress until an ecological threshold was surpassed, where after strong metabolic inhibition was observed in both

communities, differing from the predictions of the pollution-induced community tolerance hypothesis. We postulated two explanations for the deviation of the observed response from the pollution-induced community tolerance model predictions, one relating to the genotypic structure of the communities and the other related to the level of community tolerance as a function of chronic metal contamination thresholds. These two explanations may be related by the level of community metal resistance being a function of which metal tolerance genes have been selected for. Perhaps, stronger selective pressure specialize the tolerant community to more specific metal resistance strategies. Our communities may have either developed specialized metal resistance genes not specific to the Cd that drove metabolic inhibition leaving both equally vulnerable to the applied stress or perhaps the level of chronic stress at each site encoded for general metal resistance and both are equally resistant.

Table 2.1 Average Sediment and Effluent Metal Contamination Index Values, k_{12} (hr^{-1}), Sediment Associated Bacterial Densities, and Effluent Metal Concentrations (means ± std. err.)

	Sediment MCI	Effluent MCI	k_{12} (hr^{-1})	Cell Density (10^8 16s rRNA gene copies g^{-1})	Cd (ppb)	Cu (ppb)	As (ppb)	Zn (ppb)
LBF Control	0.71	0.04 ± 0.06	0.39 ± 0.0003	1.09 ± 0.3	2.0 ± 1.83	0.32 ± 0.07	2.1 ± 0.10	7.0 ± 2.2
LBF Treatment	0.71	0.94 ± 0.06	0.35 ± 0.04	1.09 ± 0.3	973 ± 1106	1.3 ± 0.81	1.2 ± 0.38	50 ± 5.7
KR Control	1.15	1.1 ± 0.28	0.88 ±0.01	2.5 ± 0.8	118 ± 152	9.7 ± 0.49	9.0 ± 0.25	32 ± 9.3
KR Treatment	1.15	1.9 ± 0.05	0.71 ± 0.01	2.5 ± 0.8	3556 ± 1080	18.3 ± 0.71	5.2 ± 0.02	505 ± 45

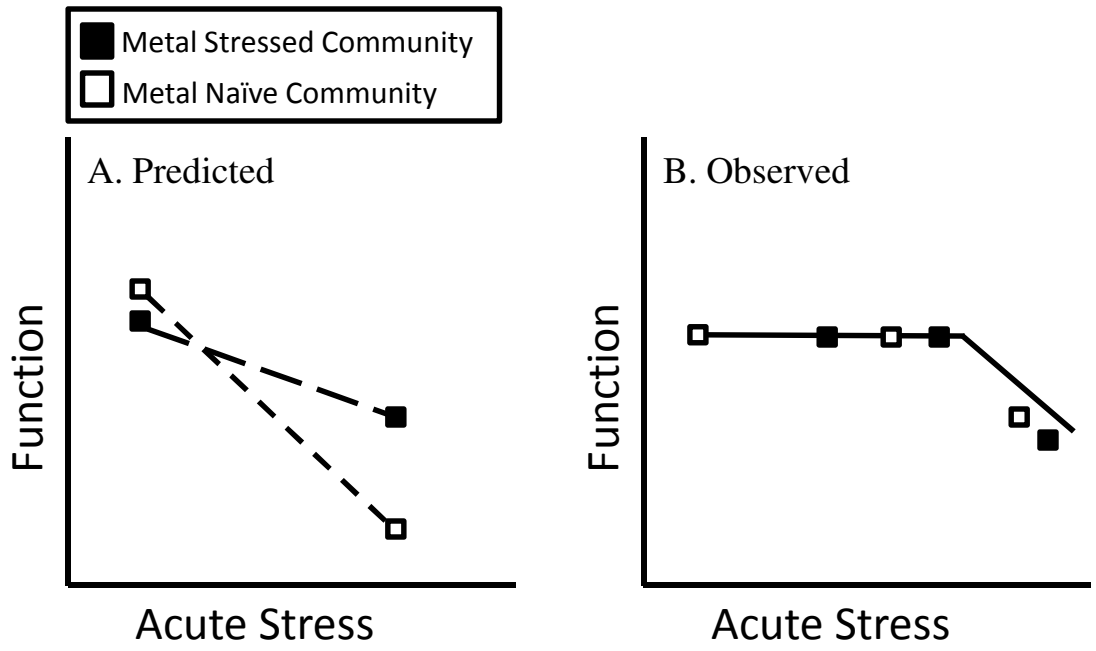

Figure 2.1 A Conceptual Model of Pollution Induced Community Tolerance (A) and the Pattern Observed in our Experiments (B). The pollution-induced community tolerance hypothesis predicts communities that have developed stress resistance via prolonged exposure to a pollutant or toxic stressor will exhibit greater resilience to related acute stresses relative to communities developed in lesser magnitudes or the absence of the pollutant or stress. Contrary to this hypothesis, respiration of hyporheic microbial communities with different metal contamination histories in this data set shows a threshold response to increasing acute metal stress.

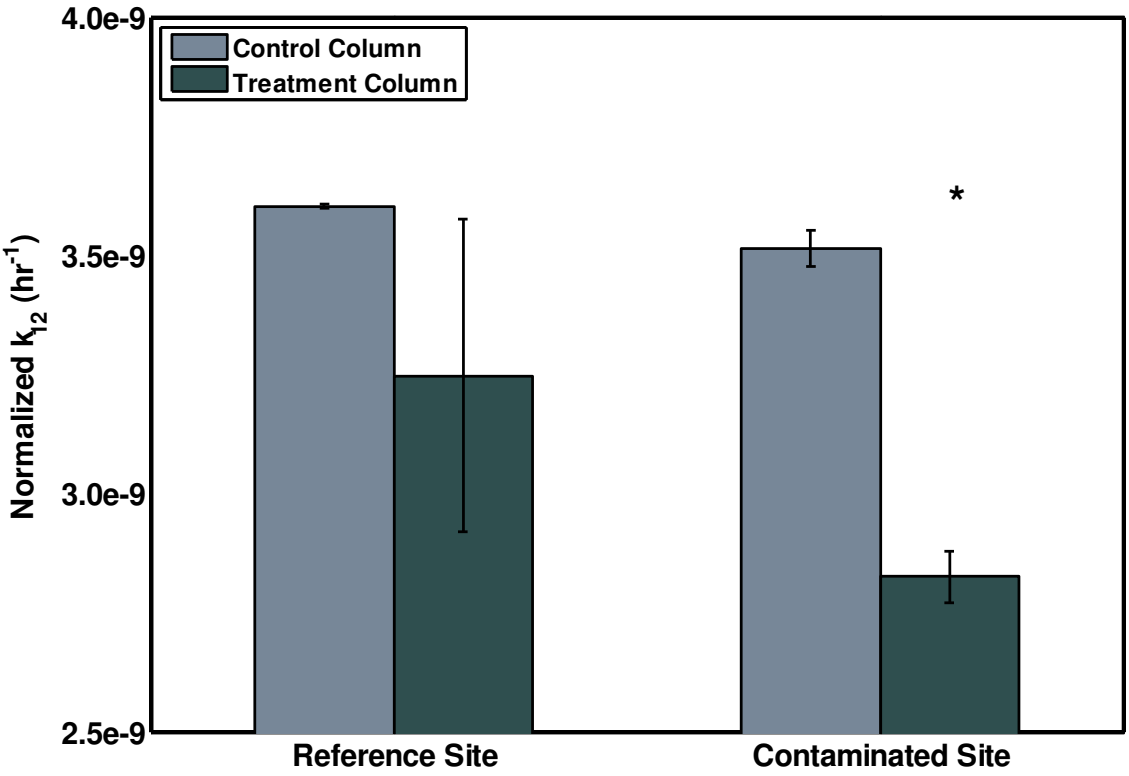

Figure 2.2 Average Cell Density-Normalized k_{12} of Reference and Contaminated Sites for Control and Cd-Treated Columns. * denotes significant differences between treatment and control columns (ANOVA, P < 0.05).

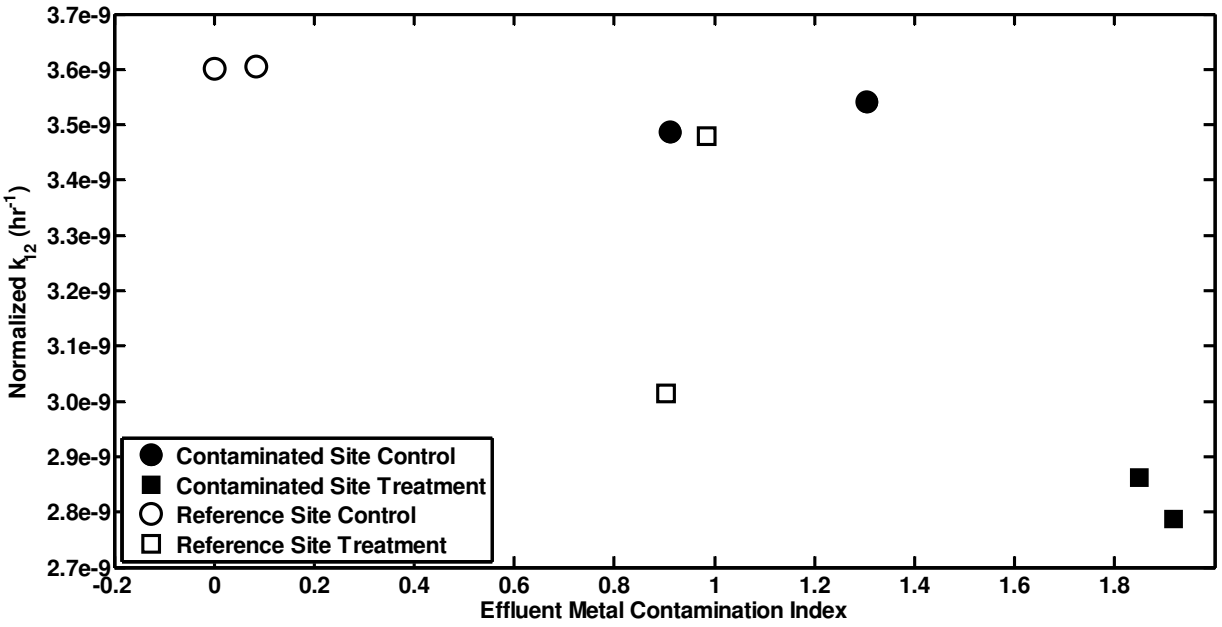

Figure 2.3 Effluent Metal Contamination Index vs. Cell Density-Normalized k_{12}. Data points are individual responses measured for each experimental treatment.

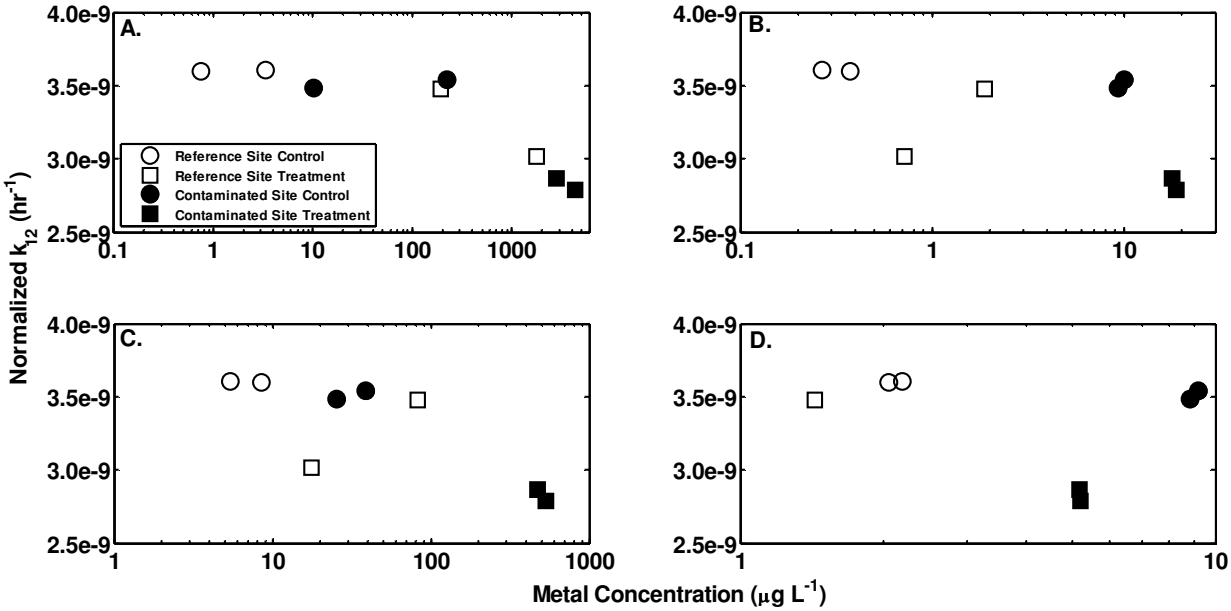

Figure 2.4 Individual Effluent Metal Concentrations vs. Cell Density-Normalized k_{12}. A) Cadmium, B) Copper, C) Zinc, D) Arsenic

CONCLUSIONS

This study documents our investigation of a lotic ecosystem exposed to more than 100 years of anthropogenic metal contamination with the experimental Resazurin Resorufin Smart Tracer. The Clark Fork River, Montana, USA with its extensive mining history provided the environmental setting to examine the resilience of differently contaminated hyporheic microbial communities (i.e., to return to the level of function observed in their corresponding paired pristine reference sites) and the metabolic capability of the communities from metal contaminated environments to resist an additional acute metal exposure. Our results show than even with more than 100 years of adaption opportunity to this metal stress, hyporheic microbial communities continue to be inhibited and have not regained pre-contaminated metabolic function, suggesting this community has not become resilient to this chronic stress. Additionally, metabolic inhibition was observed in the presence of an acute metal stress in two communities with different historic metal contamination regimes. No increase in the ability to resist additional metal stressors was observed between the two communities. This latter observation was not expected and does not adhere to the predictions of the well-accepted, pollution-induced community tolerance hypothesis. We postulate two possible explanations. The first is that these two communities have not had the opportunity to develop resistance to the metal species applied (i.e. cadmium) and therefore we would not expect tolerance. Secondly, both communities may possess equal cadmium resistance because even though their metal contamination histories differ, both communities

experience some level of metal stress and other work suggests some limited cross-over between tolerance mechanisms selected under the metal stresses present in our field sites and cadmium. These explanations require further study into the genomic structure of the metal resistant communities and detailed study of metal contamination thresholds in relation to the degree of resistance this stress endows.

The Resazurin Resorufin Smart Tracer showed promise as a functional indicator of ecosystem quality, detecting differences between contaminated sites and their paired reference sites and along the contaminated gradient. Reduced k_{12} was associated with greater anthropogenic stress (i.e., increased chronic and acute metal exposures) as our hypotheses predicted. The Resazurin Resorufin Smart Tracer also displayed the capability to detect cause and effect relationships between a changing environment and microbial metabolism. In this primary documentation, the use of the Resazurin Resorufin Smart Tracer as a functional indicator of ecosystem integrity is supported in the laboratory. However, continuing to develop the relationships of k_{12} as a metric of ecological currency is of upmost importance. Specifically, future work may want to focus on relating this reaction rate coefficient to carbon and nutrient spiraling. Also, this system should be tested with other anthropogenic contaminants (e.g., phosphate and nitrogen, thermal pollution, organic pollutants, etc). Efforts should be directed to *in situ* application of this tracer in this capacity.

REFERENCES

1. Sala, O. E.; Chapin, F. S.; Armesto, J. J.; Berlow, E.; Bloomfield, J.; Dirzo, R.; Huber-Sanwald, E.; Huenneke, L. F.; Jackson, R. B.; Kinzig, A.; Leemans, R.; Lodge, D. M.; Mooney, H. A.; Oesterheld, M. n.; Poff, N. L.; Sykes, M. T.; Walker, B. H.; Walker, M.; Wall, D. H., Global Biodiversity Scenarios for the Year 2100. *Science* **2000,** *287*, (5459), 1770-1774.

2. Carpenter, S. R.; Stanley, E. H.; Vander Zanden, M. J., State of the World s Freshwater Ecosystems: Physical, Chemical, and Biological Changes. *Ann. Rev. Environ. Resour.* **2011,** *36*, (1).

3. Vörösmarty, C. J.; McIntyre, P.; Gessner, M. O.; Dudgeon, D.; Prusevich, A.; Green, P.; Glidden, S.; Bunn, S. E.; Sullivan, C. A.; Liermann, C. R., Global threats to human water security and river biodiversity. *Nature* **2010,** *467*, (7315), 555-561.

4. Apitz, S. E.; Davis, J. W.; Finkelstein, K.; Hohreiter, D. W.; Hoke, R.; Jensen, R. H.; Jersak, J.; Kirtay, V. J.; Mack, E. E.; Magar, V. S., Assessing and managing contaminated sediments: Part II, evaluating risk and monitoring sediment remedy effectiveness. *Integr. Environ. Assess. Manage.* **2005,** *1*, (1), e1-e14.

5. Moore, J. N.; Luoma, S. N., Hazardous wastes from large-scale metal extraction. A case study. *Environ. Sci. Technol.* **1990,** *24*, (9), 1278-1285.

6. Hoffmann, A. A.; Hercus, M. J., Environmental Stress as an Evolutionary Force. *Bioscience* **2000,** *50*, (3), 217-226.

7. Hooper, D.; Chapin Iii, F.; Ewel, J.; Hector, A.; Inchausti, P.; Lavorel, S.; Lawton, J.; Lodge, D.; Loreau, M.; Naeem, S., Effects of biodiversity on ecosystem functioning: a consensus of current knowledge. *Ecol. Monogr.* **2005,** *75*, (1), 3-35.

8. Hughes, A. R.; Byrnes, J. E.; Kimbro, D. L.; Stachowicz, J. J., Reciprocal relationships and potential feedbacks between biodiversity and disturbance. *Ecol. Lett.* **2007,** *10*, (9), 849-864.

9. Schimel, J.; Balser, T. C.; Wallenstein, M., Microbial stress-response physiology and its implications for ecosystem function. *Ecology* **2007,** *88*, (6), 1386-1394.

10. Rousk, J.; Bååth, E.; Brookes, P. C.; Lauber, C. L.; Lozupone, C.; Caporaso, J. G.; Knight, R.; Fierer, N., Soil bacterial and fungal communities across a pH gradient in an arable soil. *ISME J.* **2010,** *4*, (10), 1340-1351.

11. Ramsey, P. W.; Rillig, M. C.; Feris, K. P.; Gordon, N. S.; Moore, J. N.; Holben, W. E.; Gannon, J. E., Relationship between communities and processes; new insights from a field study of a contaminated ecosystem. *Ecol. Lett.* **2005,** *8*, (11), 1201-1210.

12. Feris, K.; Ramsey, P.; Frazar, C.; Moore, J. N.; Gannon, J. E.; Holben, W. E., Differences in Hyporheic-Zone Microbial Community Structure along a Heavy-Metal Contamination Gradient. *Appl. Environ. Microbiol.* **2003,** *69*, (9), 5563-5573.

13. Feris, K. P.; Ramsey, P. W.; Frazar, C.; Rillig, M.; Moore, J. N.; Gannon, J. E.; Holben, W. E., Seasonal dynamics of shallow-hyporheic-zone microbial community structure along a heavy-metal contamination gradient. *Appl. Environ. Microbiol.* **2004,** *70*, (4), 2323-2331.

14. Feris, K. P.; Ramsey, P. W.; Rillig, M.; Moore, J. N.; Gannon, J. E.; Holben, W. E., Determining rates of change and evaluating group-level resiliency differences in hyporheic microbial communities in response to fluvial heavy-metal deposition. *Appl. Environ. Microbiol.* **2004,** *70*, (8), 4756-4765.

15. Feris, K. P.; Ramsey, P. W.; Gibbons, S. M.; Frazar, C.; Rillig, M. C.; Moore, J. N.; Gannon, J. E.; Holben, W. E., Hyporheic microbial community development is a sensitive indicator of metal contamination. *Environ. Sci. Technol.* **2009,** *43*, (16), 6158-6163.

16. Płaza, G. A.; Nałęcz-Jawecki, G.; Pinyakong, O.; Illmer, P.; Margesin, R., Ecotoxicological and microbiological characterization of soils from heavy-metal- and hydrocarbon-contaminated sites. *Environ. Monit. Assess.* **2010,** *163*, (1), 477-488.

17. Liao, M.; Xie, X. M., Effect of heavy metals on substrate utilization pattern, biomass, and activity of microbial communities in a reclaimed mining wasteland of red soil area. *Ecotoxicol. Environ. Saf.* **2007,** *66*, (2), 217-223.

18. Courtney, L. A.; Clements, W. H., Assessing the influence of water and substratum quality on benthic macroinvertebrate communities in a metal-polluted stream: an experimental approach. *Freshwat. Biol.* **2002,** *47*, (9), 1766-1778.

19. Davies, S. P.; Jackson, S. K., The Biological Condition Gradient: A Descriptive Model for Interpreting Change in Aquatic Ecosystems. *Ecol. Appl.* **2006,** *16*, (4), 1251-1266.

20. Mayer-Pinto, M.; Underwood, A. J.; Tolhurst, T.; Coleman, R. A., Effects of metals on aquatic assemblages: What do we really know? *J. Exp. Mar. Biol. Ecol.* **2010,** *391*, (1–2), 1-9.

21. Pérez, P.; Beiras, R.; Fernández, E., Monitoring copper toxicity in natural phytoplankton assemblages: application of Fast Repetition Rate fluorometry. *Ecotoxicol. Environ. Saf.* **2010,** *73*, (6), 1292-1303.

22. Gessner, M. O.; Chauvet, E., A case for using litter breakdown to assess functional stream integrity. *Ecol. Appl.* **2002,** *12*, (2), 498-510.

23. Young, R. G.; Matthaei, C. D.; Townsend, C. R., Organic matter breakdown and ecosystem metabolism: functional indicators for assessing river ecosystem health. *J. N. Am. Benthol. Soc.* **2008,** *27*, (3), 605-625.

24. Battin, T.; Kaplan, L.; Newbold, J.; Hansen, C., Contributions of microbial biofilms to ecosystem processes in stream mesocosms. *Nature* **2003,** *426*, (6965), 439-442.

25. Mulholland, P. J.; Webster, J. R., Nutrient dynamics in streams and the role of J-NABS. *J. N. Am. Benthol. Soc.* **2010,** *29*, (1), 100-117.

26. Boulton, A. J.; Datry, T.; Kasahara, T.; Mutz, M.; Stanford, J. A., Ecology and management of the hyporheic zone: stream-groundwater interactions of running waters and their floodplains. *J. N. Am. Benthol. Soc.* **2010,** *29*, (1), 26-40.

27. Hall Jr, R. O.; Meyer, J. L., The trophic significance of bacteria in a detritus-based stream food web. *Ecology* **1998,** *79*, (6), 1995-2012.

28. Wright, M. S.; Covich, A. P., Relative Importance of Bacteria and Fungi in a Tropical Headwater Stream: Leaf Decomposition and Invertebrate Feeding Preference. *Microb. Ecol.* **2005,** *49*, (4), 536-546.

29. Benner, S. G.; Smart, E. W.; Moore, J. N., Metal Behavior during Surface-Groundwater Interaction, Silver Bow Creek, Montana. *Environ. Sci. Technol.* **1995,** *29*, (7), 1789-1795.

30. Dolédec, S.; Statzner, B., Responses of freshwater biota to human disturbances: contribution of J-NABS to developments in ecological integrity assessments. *J. N. Am. Benthol. Soc.* **2010,** *29*, (1).

31. Feio, M. J.; Alves, T.; Boavida, M.; Medeiros, A.; GraÇA, M. A. S., Functional indicators of stream health: a river-basin approach. *Freshwat. Biol.* **2010,** *55*, (5), 1050-1065.

32. Venkiteswaran, J. J.; Schiff, S. L.; Wassenaar, L., Aquatic Metabolism and Ecosystem Health Assessment Using Dissolved O_2 Stable Isotope Diel Curves. *Ecol. Appl.* **2008,** *18*, (4), 965-982.

33. Warkentin, M.; Freese, H. M.; Karsten, U.; Schumann, R., New and fast method to quantify respiration rates of bacterial and plankton communities in freshwater ecosystems by using optical oxygen sensor spots. *Appl. Environ. Microbiol.* **2007,** *73*, (21), 6722.

34. Aristegi, L.; Izagirre, O.; Elosegi, A., Comparison of several methods to calculate reaeration in streams, and their effects on estimation of metabolism. *Hydrobiologia* **2009,** *635*, (1), 113-124.

35. McCutchan Jr, J. H.; Saunders III, J. F.; Lewis Jr, W. M.; Hayden, M. G., Effects of groundwater flux on open-channel estimates of stream metabolism. *Limnol. Oceanogr.* **2002**, 321-324.

36. Crane, M.; Burton, G. A.; Culp, J. M.; Greenberg, M. S.; Munkittrick, K. R.; Ribeiro, R.; Salazar, M. H.; St-Jean, S. D., Review of aquatic in situ approaches for stressor and effect diagnosis. *Integr. Environ. Assess. Manage.* **2007,** *3*, (2), 234-245.

37. Liber, K.; Goodfellow, W.; Den Besten, P.; Clements, W.; Galloway, T.; Gerhardt, A.; Green, A.; Simpson, S., In situ-based effects measures: Considerations for improving methods and approaches. *Integr. Environ. Assess. Manage.* **2007,** *3*, (2), 246-258.

38. Haggerty, R.; Argerich, A.; Martí, E., Development of a "smart" tracer for the assessment of microbiological activity and sediment-water interaction in natural waters: The resazurin-resorufin system. *Water Resour. Res.* **2008,** *44*.

39. Haggerty, R.; Martí, E.; Argerich, A.; von Schiller, D.; Grimm, N. B., Resazurin as a "smart" tracer for quantifying metabolically active transient storage in stream ecosystems. *J. Geophys. Res.* **2009,** *114*, (G3), G03014.

40. Argerich, A.; Haggerty, R.; Martí, E.; Sabater, F.; Zarnetske, J., Quantification of metabolically active transient storage (MATS) in two reaches with contrasting transient storage and ecosystem respiration. *J. Geophys. Res.* **2011,** *116*, (G3), G03034.

41. Karakashev, D.; Galabova, D.; Simeonov, I., A simple and rapid test for differentiation of aerobic from anaerobic bacteria. *World J. Microbiol. Biotechnol.* **2003,** *19*, (3), 233-238.

42. McNicholl, B. P.; McGrath, J. W.; Quinn, J. P., Development and application of a resazurin-based biomass activity test for activated sludge plant management. *Water Res.* **2007,** *41*, (1), 127-133.

43. Tiegs, S.; Langhans, S.; Tockner, K.; Gessner, M., Cotton strips as a leaf surrogate to measure decomposition in river floodplain habitats. *J. N. Am. Benthol. Soc.* **2007,** *26*, (1), 70-77.

44. Stoddard, J. L.; Larsen, D. P.; Hawkins, C. P.; Johnson, R. K.; Norris, R. H., Setting Expectations for the Ecological Condition of Streams: The Concept of Reference Condition. *Ecol. Appl.* **2006,** *16*, (4), 1267-1276.

45. Bueno, C.; Villegas, M.; Bertolotti, S.; Previtali, C.; Neumann, M.; Encinas, M., The Excited State Interaction of Resazurin and Resorufin with Aminesin Aqueous Solutions. Photophysics and Photochemical Reaction¶. *Photochem. Photobiol.* **2002,** *76*, (4), 385-390.

46. Kangasniemi, K. H. Fluorescent diagnostics for imaging dissolved oxygen. The University of Texas at Dallas, 2005.

47. Ramsey, P. W.; Rillig, M. C.; Feris, K. P.; Moore, J. N.; Gannon, J. E., Mine waste contamination limits soil respiration rates: a case study using quantile regression. *Soil Biol. Biochem.* **2005,** *37*, (6), 1177-1183.

48. Feris, K. P.; Ramsey, P. W.; Frazar, C.; Rillig, M. C.; Gannon, J. E.; Holben, W. E., Structure and Seasonal Dynamics of Hyporheic Zone Microbial Communities in Free-Stone Rivers of the Western United States. *Microb. Ecol.* **2003,** *46*, (2), 200-215.

49. Heron, G.; Barcelona, M. J.; Andersen, M. L.; Christensen, T. H., Determination of Nonvolatile Organic Carbon in Aquifer Solids After Carbonate Removal by Sulfurous Acid. *Ground Water* **1997,** *35*, (1), 6-11.

50. Gilks, W. R.; Richardson, S.; Spiegelhalter, D. J., *Markov chain Monte Carlo in practice*. Chapman & Hall/CRC: 1996.

51. Porcal, G. V.; Altamirano, M. S.; Glusko, C. A.; Bertolotti, S. G.; Previtali, C. M., Photophysical properties of the phenoxazin dyes resazurin and resorufin in soybean lecithin microemulsions. *Dyes Pigm.* **2011,** *88*, (3), 240-246.

52. O'Brien, J.; Wilson, I.; Orton, T.; Pognan, F., Investigation of the Alamar Blue (resazurin) fluorescent dye for the assessment of mammalian cell cytotoxicity. *Eur. J. Biochem.* **2000,** *267*, (17), 5421-5426.

53. Guerin, T.; Mondido, M.; McClenn, B.; Peasley, B., Application of resazurin for estimating abundance of contaminant degrading micro organisms. *Lett. Appl. Microbiol.* **2001,** *32*, (5), 340-345.

54. Peijnenburg, W. J. G. M.; Vijver, M. G., Metal-specific interactions at the interface of chemistry and biology. *Pure Appl. Chem.* **2007,** *79*, (12), 2351.

55. Gadd, G. M., Metals, minerals and microbes: geomicrobiology and bioremediation. *Microbiol.* **2010,** *156*, (3), 609.

56. Gibbons, S. M.; Morales, S. E.; Gannon, J. E.; Feris, K.; McGuirl, M. A.; Ramsey, P. W.; Hynninen, A., Use of microcalorimetry to determine the costs and

benefits to Pseudomonas putida strain KT2440 of harboring cadmium efflux genes. *Appl. Environ. Microbiol.* **2011,** *77*, (1), 108-113.

57. Nimick, D. A.; Gammons, C. H.; Cleasby, T. E.; Madison, J. P.; Skaar, D.; Brick, C. M., Diel cycles in dissolved metal concentrations in streams: occurrence and possible causes. *Water Resour. Res* **2003,** *39*, (9), 1247.

58. Brick, C.; Moore, J., Diel variation of trace metals in the upper Clark Fork River, Montana. *Environ. Sci. Technol* **1996,** *30*, (6), 1953-1960.

59. Stachowicz, M.; Hiemstra, T.; van Riemsdijk, W. H., Multi-competitive interaction of As(III) and As(V) oxyanions with Ca2+, Mg2+, PO3−4, and CO2−3 ions on goethite. *J. Colloid Interface Sci.* **2008,** *320*, (2), 400-414.

60. Clements, W. H.; Rohr, J. R., Community Responses to Contaminants: Using Basic Ecologicl Principles to Predict Exotoxicological Effects *Environ. Toxicol. Chem.* **2009,** *28*, (9), 1789-1800.

61. Courtney, L. A.; Clements, W. H., Sensitivity to Acidic pH in Benthic Invertebrate Assemblages with Different Histories of Exposure to Metals. *J. N. Am. Benthol. Soc.* **2000,** *19*, (1), 112-127.

62. Tobor-Kaplon, M. A.; Bloem, J.; Römkens, P. F. A. M.; Ruiter, P. C. d., Functional stability of microbial communities in contaminated soils. *Oikos* **2005,** *111*, (1), 119-129.

63. Gammons, C. H.; Milodragovich, L.; Belanger-Woods, J., Influence of diurnal cycles on metal concentrations and loads in streams draining abandoned mine lands: an example from High Ore Creek, Montana. *Environ. Geol.* **2007,** *53*, (3), 611-622.

64. Sarmiento, A. M.; Nieto, J. M.; Olías, M.; Cánovas, C. R., Hydrochemical characteristics and seasonal influence on the pollution by acid mine drainage in the Odiel river Basin (SW Spain). *Appl. Geochem.* **2009,** *24*, (4), 697-714.

65. Bourg, A. C. M.; Kedziorek, M. A. M.; Crouzet, C., Seasonal cycles of dissolved Cd, Mn and Zn in river water caused by variations in pH induced by biological activity. *Aquatic Geochemistry* **2000,** *6*, (4), 461-471.

66. Nimick, D. A.; Cleasby, T. E.; McCleskey, R. B., Seasonality of diel cycles of dissolved trace-metal concentrations in a Rocky Mountain stream. *Environmental Geology* **2005,** *47*, (5), 603-614.

67. Munk, L. A.; Faure, G., Effects of pH fluctuations on potentially toxic metals in the water and sediment of the Dillon Reservoir, Summit County, Colorado. *Appl. Geochem.* **2004,** *19*, (7), 1065-1074.

68. Gammons, C. H.; Milodragovich, L.; Belanger-Woods, J., Influence of diurnal cycles on metal concentrations and loads in streams draining abandoned mine lands: an example from High Ore Creek, Montana. *Environmental Geology* **2007,** *53*, (3), 611-622.

69. Jones, C. A.; Nimick, D. A.; McCleskey, R. B., Relative effect of temperature and pH on diel cycling of dissolved trace elements in Prickly Pear Creek, Montana. *Water, Air, Soil Pollut.* **2004,** *153*, (1), 95-113.

70. Brandt, K. K.; Frandsen, R. J. N.; Holm, P. E.; Nybroe, O., Development of pollution-induced community tolerance is linked to structural and functional resilience of a soil bacterial community following a five-year field exposure to copper. *Soil Biol. Biochem.* **2010,** *42*, (5), 748-757.

71. Blanck, H.; Wängberg, S. Å., Induced community tolerance in marine periphyton established under arsenate stress. *Can. J. Fish. Aquat. Sci.* **1988,** *45*, (10), 1816-1819.

72. Vinebrooke, R. D.; Cottingham, K. L.; Norberg, J.; Scheffer, M.; Dodson, S. I.; Maberly, S. C.; Sommer, U., Impacts of multiple stressors on biodiversity and ecosystem functioning: the role of species co-tolerance. *Oikos* **2004,** *104*, (3), 451-457.

73. Tlili, A.; Marechal, M.; Berard, A.; Volat, B.; Montuelle, B., Enhanced co-tolerance and co-sensitivity from long-term metal exposures of heterotrophic and autotrophic components of fluvial biofilms. *Sci. Total Environ.* **2011,** *409*, (20), 4335-4343.

74. Deng, H.; Li, X. F.; Cheng, W. D.; Zhu, Y. G., Resistance and resilience of Cu-polluted soil after Cu perturbation, tested by a wide range of soil microbial parameters. *FEMS Microbiol. Ecol.* **2009,** *70*, (2), 293-304.

75. Gunderson, L. H., Ecological Resilience--In Theory and Application. *Annu. Rev. Ecol. Syst.* **2000,** *31*, (ArticleType: research-article / Full publication date: 2000 / Copyright © 2000 Annual Reviews), 425-439.

76. Tobor-Kaplon, M. A.; Bloem, J.; De Ruiter, P. C., Functional stability of microbial communities from long-term stressed soils to additional disturbance. *Environ. Toxicol. Chem.* **2006,** *25*, (8), 1993-1999.

77. Clements, W. H.; Brooks, M. L.; Kashian, D. R.; Zuellig, R. E., Changes in dissolved organic material determine exposure of stream benthic communities to UV-B radiation and heavy metals: implications for climate change. *Global Change Biol.* **2008,** *14*, (9), 2201-2214.

78. Diaz-Ravina, M.; Baath, E.; Frostegard, A., Multiple heavy metal tolerance of soil bacterial communities and its measurement by a thymidine incorporation technique. *Appl. Environ. Microbiol.* **1994,** *60*, (7), 2238.

79. Wright, M. S.; Peltier, G. L.; Stepanauskas, R.; McArthur, J. V., Bacterial tolerances to metals and antibiotics in metal-contaminated and reference streams. *FEMS Microbiol. Ecol.* **2006,** *58*, (2), 293-302.

80. Laidlaw, T. In *Montana's Large River Monitoring Program*, Great Rivers Reference Condition Workshop, Cincinnati, OH, 1996; Cincinnati, OH, 1996.

81. Ramsey, P. W.; Rillig, M. C.; Feris, K. P.; Moore, J. N.; Gannon, J. E., Mine waste contamination limits soil respiration rates: a case study using quantile regression. *Soil Biology and Biochemistry* **2005,** *37*, (6), 1177-1183.

82. Gonzalez-Pinzon, R.; Haggerty, R.; Argerich, A.; Acker, S.; Myrold, D. In *Quantitative Relationship between Resazurin and Respiration in Stream Ecosystems*, 2011; The Oregon Water Conference: 2011.

83. Heron, G.; Barcelona, M. J.; Andersen, M. L.; Christensen, T. H., Determination of Nonvolatile Organic Carbon in Aquifer Solids After Carbonate Removal by Sulfurous Acid. *GROUND WATER -WORTHINGTON THEN DUBLIN OHIO-* **1997,** *35*, (1), 6-11.

84. Battin, T. J.; Kaplan, L. A.; Findlay, S.; Hopkinson, C. S.; Marti, E.; Packman, A. I.; Newbold, J. D.; Sabater, F., Biophysical controls on organic carbon fluxes in fluvial networks. *Nature Geoscience* **2008,** *1*, (2), 95-100.

85. Welp, G., Inhibitory effects of the total and water-soluble concentrations of nine different metals on the dehydrogenase activity of a loess soil. *Biol. Fertility Soils* **1999,** *30*, (1), 132-139.

86. Romero, M. C.; Gatti, E. M.; Bruno, D. E., Effects of heavy metals on microbial activity of water and sediment communities. *World Journal of Microbiology and Biotechnology* **1999,** *15*, (2), 179-184.

87. Nies, D. H., Microbial heavy-metal resistance. *Appl. Microbiol. Biotechnol.* **1999,** *51*, (6), 730-750.

88. Hochella Jr, M. F.; Moore, J. N.; Putnis, C. V.; Putnis, A.; Kasama, T.; Eberl, D. D., Direct observation of heavy metal-mineral association from the Clark Fork River Superfund Complex: Implications for metal transport and bioavailability. *Geochim. Cosmochim. Acta* **2005,** *69*, (7), 1651-1663.

89. Dong, D.; Hua, X.; Li, Y.; Zhang, J.; Yan, D., Cd adsorption properties of components in different freshwater surface coatings: the important role of ferromanganese oxides. *Environ. Sci. Technol.* **2003,** *37*, (18), 4106-4112.

90. Mahony, J. D.; Di Toro, D. M.; Gonzalez, A. M.; Curto, M.; Dilg, M.; De Rosa, L. D.; Sparrow, L. A., Partitioning of metals to sediment organic carbon. *Environ. Toxicol. Chem.* **1996,** *15*, (12), 2187-2197.

91. Langmuir, D., Aqueous environmental geochemistry. In Upper Saddle River, NJ: Prentice Hall: 1997.

92. Warren, L. A.; Haack, E. A., Biogeochemical controls on metal behaviour in freshwater environments. *Earth-Sci. Rev.* **2001,** *54*, (4), 261-320.

93. Wardle, D.; Giller, K., The quest for a contemporary ecological dimension to soil biology. *Soil Biol Biochem* **1996,** *28*, (12), 1549.

94. Lehmann, V.; Tubbing, G.; Admiraal, W., Induced metal tolerance in microbenthic communities from three lowland rivers with different metal loads. *Arch. Environ. Contam. Toxicol.* **1999,** *36*, (4), 384-391.

95. Preston, S.; Coad, N.; Townend, J.; Killham, K.; Paton, G. I., Biosensing the acute toxicity of metal interactions: Are they additive, synergistic, or antagonistic? *Environ. Toxicol. Chem.* **2000,** *19*, (3), 775-780.

96. Harrison, J. J.; Ceri, H.; Turner, R. J., Multimetal resistance and tolerance in microbial biofilms. *Nat. Rev. Microbiol.* **2007,** *5*, (12), 928-938.

97. Silver, S.; Phung, L. T., A bacterial view of the periodic table: genes and proteins for toxic inorganic ions. *J. Ind. Microbiol. Biotechnol.* **2005,** *32*, (11), 587-605.

APPENDIX A

Resazurin Resorufin Smart Tracer Advection Dispersion Equation: Markov Chain Monte Carlo Data Assimilation

This appendix provides a description of the Resazurin Resorufin Smart Tracer advection dispersion equation Markov chain Monte Carlo (RRADE-MCMC) optimization algorithm with figures and tables addressing the tuning parameters and corresponding influence on model performance (Table A1); model progression (Figure A1); model behavior through time and expected value convergence (Figure A2), and Resazurin Resorufin advection dispersion equation parameter and joint distributions (Figure A3). Also included is the correlation matrix of all measured variables (Table A2).

Description of RRADE-MCMC

RRADE-MCMC Initial Conditions, Variable Parameterization, and Heuristic Rules

Constants must be explicitly defined for input into the RRADE forward model. The initial concentration of Raz (µmol/L), initial Rru contamination of Raz solution (µmol/L), and time (hr) must all be individually input into the model for each column as well as the RRADE model parameters: C_{Raz} is the concentration of Raz [µmol L^{-1}]; C_{Rru} is the concentration of Rru [µmol L^{-1}]; t is time [hr]; x is distance [cm]; α_L is longitudinal dispersivity [cm]; v [cm hr^{-2}] is the average pore water velocity; R [-] is retardation coefficient due to sorption; k_{12} [hr^{-1}] is the reaction rate coefficient of Raz to Rru; k_1 [hr^{-1}] is the reaction rate coefficient of Raz decay; k_2 [hr^{-1}] is the reaction rate coefficient of Rru decay; M_{Raz} [g mol^{-1}] is the molecular weight of Raz; M_{Rru} [g mol^{-1}] is the molecular weight of Rru (1). Other input variables, length of column (30 cm) and the molecular weight of Raz (251.2 g/mol) and Rru (235.2 g/mol) are universal constants in these experiments and defined within the forward model. The following variables require an imposed restriction on parameter values to be physically representative of their process;

$R \geq 1$, $\alpha_L \geq 0$, and the rate coefficients k_1, k_2, and k_{12} must all be □ 0. One heuristic rule, defining the Raz decay rate coefficient, k_1, as less than the Rru decay rate coefficient, k_2 is also imposed and supported by laboratory data, preliminary modeling and previously published values (1).

Execution of the RRADE-MCMC

This data assimilation method consists of a sensitivity analysis and a Markov chain Monte Carlo (MCMC). MCMC conditions uncertain model states and parameters on imperfect observations. MCMC constrains potential parameter values by stochastically sampling and accepting values in a two-stage design. The first stage, referred to as the "burn-in," is designed to identify informed prior parameter distributions by conditioning model simulations on the observations using relatively permissive criteria for acceptance of parameter sets. The informed prior distributions derived from the burn-in phase constitute the distributions from which parameters are subsequently sampled and conditioned on observations with more restrictive acceptance criteria to obtain the posterior distribution (PD). We refer to this as the optimization phase. Building from the burn-in, informed prior sampling refines parameter estimation with increasing confidence. Statistical moments of the PD contain the expected value and associated uncertainty. The prior distribution is loosely defined and contains all possible realizations of the parameter values. The PD is a refined estimation of the parameter value with confidence intervals. The informed prior (i.e., post burn-in) and PDs are assumed to have a Gaussian distribution. In this way, RRADE-MCMC parameter estimation grows more exact as the model progresses from the initial sensitivity analysis to the posterior distribution (Figure A1).

Sensitivity Analysis

The RRADE-MCMC requires an initial estimation of each RRADE parameter constrained by the prior distribution for PD sampling. Because initial estimations of parameter values are unknown, a sensitivity analysis (SA) was employed to constrain the unknown state space for each parameter requiring optimization (v, α_L, R, k_1, k_2, k_{12}). The SA was run for 3,000,000 iterations to stochastically assign each parameter a value from a window constrained by an exaggerated range sufficiently sized to encompass all possible values, and runs the forward model generating Raz and Rru concentration profiles. Each iteration is independent and parameter values are selected using uniform random number (URN) generation. Parameter values from an iteration are accepted and stored if the mean absolute error (MAE) of the modeled simulation is less than a threshold error (determined as the plate reader variation of replicate reads of Raz and Rru for known concentrations of each compound (0.0323 µmol/L)). Stored values are then transformed into Gaussian prior distributions and input to the MCMC. The Gaussian distribution is defined by the mean and standard deviation of the 95% range of the accepted values. The 95% range was selected to exclude outlying values. This process is repeated for every column.

RRADE-MCMC: Metropolis-Hastings Decision

To condition uncertain RRADE model states and parameters, the RRADE-MCMC solves Bayes theorem (eq. S1). Bayes formula,

$$p(\Theta|Y) = \frac{p(Y|\Theta)p(\Theta)}{p(Y)} \quad \text{(A1)}$$

computes a continuous distribution for unknown parameters (the PD), $p(\Theta|Y)$, based on the likelihood of proposed parameter values, $p(Y|\Theta)$, multiplied by a prior

distribution, $p(\theta)$, divided by the probability of realizing current parameter values, $p(Y)$,, a normalization constant that is often omitted. Bayes theorem poses the inverse problem in stochastic space returning PDs that are interpreted as the probability that a parameter will assume a certain value given the forward model, observed (experimental) data, and the constrained state space (2, 3).

Proposal solutions of the MCMC are accepted or declined according to the Metropolis Hastings (MH) acceptance-rejection decision based on goodness of fit (mean absolute error (MAE)), and the physical appropriateness of the solution, determined by comparison to the prior distribution. The MH acceptance-rejection decision is based on the product of the probability density of the error associated with $X^{(t+1)}$, the proposal vector of parameters, and the likelihood of occurrence of $X^{(t+1)}$, normalized by the corresponding error density-parameter likelihood product of X^t, the currently accepted parameter solution in the Markov chain. This ratio is expressed as the probability ratio α where,

$$\alpha = \frac{f(X^{(t+1)}) * \pi(X^{(t+1)})}{f(X^t) * \pi(X^t)}. \quad \text{(A2)}$$

This formulation includes information about the goodness of fit of the proposed and current solution vectors, as well as their likelihood of occurrence. The probability ratio is then compared to a URN distributed between 0-1, r, and the proposed parameters accepted if α > r as

$$X^t = \begin{cases} X^{(t+1)} & \text{if } \alpha > r \\ X^t & \text{if } \alpha < r \end{cases}. \quad \text{(A3)}$$

If $X^{(t+1)}$ is a more probable solution than X^t, α > 1 and is automatically accepted. If α > r, the proposal is accepted. Accepted solutions transition the chain and become the current step. If α < r the proposal is discarded and the chain is stationary with X^t

remaining the current step. One of the strengths of the MH criteria is that a proposed solution vector associated with a lower estimation error may not be accepted if the parameters are highly unlikely based on the informed priors.

The following formulas are used to compute α. The likelihood, $p(Y|\theta)$, of a given vector of model values satisfying the measured observations is determined according to

$$f(X^{(t+1)}) = \exp^{-\frac{1}{2}} * \sum \frac{(\phi - \phi(X^{(t+1)}))2}{\sigma_x^2} \quad \text{(A4)}$$

and

$$f(X^{t}) = \exp^{-\frac{1}{2}} * \sum \frac{(\phi - \phi(X^{t}))^2}{\sigma_x^2} \quad \text{(A5)}$$

where ϕ is the vector of observed Raz and Rru concentrations, $\phi(X^{(t+1)})$ is the vector of concentrations of the proposed solution, $\phi(X^{t})$ is the vector of concentrations of the current step in the Markov chain, and σ_x is observation error.

Prior distribution evaluation of $X^{(t+1)}$, $\pi(X^{(t+1)})$ and $\pi(X^{t})$, determines if the proposal vector is within the state space and is calculated as

$$\pi(X^{(t+1)}) = \exp^{-\frac{1}{2}} * \sum \frac{(X^{(t+1)} - \theta))^2}{\sigma^2} \quad \text{(A6)}$$

and

$$\pi(X^{t}) = \exp^{-\frac{1}{2}} * \sum \frac{(X^{t} - \theta))^2}{\sigma^2}. \quad \text{(A7)}$$

In this equation, $X^{(t+1)}$ is the proposed vector of parameters, X^{t} is the accepted vector of parameters in the current step of the Markov chain, □ is the vector of median values from the SA and σ is a vector of standard deviation values from the SA.

Both σ and σ_x are MH decision acceptance-rejection criteria. Larger values are less stringent and allow less probable simulations to be accepted, increasing the acceptance rate. Decreasing these values increases selectivity and decreases acceptance

rate. This is the primary difference between a burn-in period where larger values of σ and σ_x are allowed in order to determine an "informed prior" distribution from which parameters will subsequently be sampled to determine the parameter PDs.

RRADE-MCMC: Tuning

Multiple MCMC MH decision and acceptance criteria were tested to drive the algorithm to optimal performance. MCMC performance is based primarily on convergence, secondarily on acceptance rate and thirdly on computation time and resources. To increase performance, acceptance criteria (σ, σ_x) and MH decision criteria were manipulated (Table A1).

Convergence: Convergence is judged upon the variance of the PD expected value and standard deviation across replicate RRADE-MCMC experiments being at least 2 orders of magnitude less than the parameter value, MCMC-replicate parameters values being within the probable error for that parameter, and the variance of the MAE. Probable error is a statement of certainty around the central tendency that one half of the distribution lies within this range (4), therefore the true mean.

Acceptance Rate: Algorithm efficiency is a measure of how completely the PD is sampled on a given timeframe, quantified by the acceptance rate (5). Metropolis-Hastings MCMC algorithms have been empirically found to be at least 80% efficient with an acceptance rate of 0.15-0.5 (6).

Acceptance rate is increased with accurate and adequately constrained prior distributions that guide the algorithm in selecting a prudent starting point and sampling space, random walk step size, and the shape of the Gaussian distribution contained within the MH decision (equations A4-A7). Because of the assumption of Gaussianity, the

algorithm efficiency of the RRADE-MCMC experiments are predominantly controlled by the variance of the parameter sampling distribution during the burn-in and optimization phases of the experiment; σ_{prior} and $\sigma_{burn\text{-}in}$, respectively, as well as the corresponding variance of the observation error distribution during the burn-in and optimization phases; $\sigma_{x\ prior}$ and $\sigma_{x\ burn\text{-}in}$, respectively.

Random walk step size during the MCMC experiment is proportional to σ_{prior} and $\sigma_{burn\text{-}in}$, which are calibrated from the SA and burn-in respectively. "Good" σ_{prior} and $\sigma_{burn\text{-}in}$ values compromise between being too large, which has the effect of stepping the proposed parameter vector to low probability regions of the sample space and reducing the acceptance rate, or too small, which discouraging complete exploration of the sampling space and potentially making convergence sensitive to local minima (6). In this study, step size was decreased after the SA and burn-in phases to increase acceptance rate. Small step size increase acceptance frequency because the probability ratio, α, will be near 1 due to the similarity in the likelihood of the current and proposed solutions. Tuning step size in this manner must be done judiciously as to not over constrain movement through sampling space.

Transitions in the chain and the magnitude of step size are shown in Figure A2b. Stationary behavior (no movement along y axis) between transitions (change in y axis value) is due to maintenance of the current step in the chain through numerous iterations because of rejection of less probable solutions. The longer a stationary period, the more weight these highly probable parameter values impose upon the shape of the PDs, justifying the distribution's mode as the expected parameter value. Transition step size is the magnitude of change in parameter value between successive iterations. The

magnitude of transitions in the demonstration plot range from 9.9957E-5 to 0.2870, oscillating around the mode value of 0.7571. This range and variability of step size avoids local minima and explores the entire state space, ultimately converging to the most probable solution.

RRADE-MCMC: Burn-in

The first 5% of the total iterations were discarded as the burn-in (50,000 burn-in iterations, 1,000,000 optimization iterations). At this point, the initial starting point asserts negligible influence on populating the PD and this transient stage has shifted posterior sampling to a more favorable sampling position.

For each column, the burn-in period begins by initializing a vector of median parameter values, □, and standard deviations, σ_{prior}, from the ignorant prior distribution generated through the SA and corresponding to [v, α_L, R, k_1, k_2, k_{12}]. RRADE-MCMC initiates at a randomly selected starting point from the prior distribution for each parameter, creating the X^t vector. A random walk from X^t generates $X^{(t+1)}$ and the acceptance ratio, α, is calculated. Burn-in is designed for greater leniency in the acceptance criteria allowing for higher acceptance frequency. Accepted simulations are stored and passed as the informed prior distribution for the optimization phase.

RRADE-MCMC: Posterior Distribution Sampling

PD sampling initiates by resetting the sampling state space, newly defined by the accepted simulations of the burn-in (i.e., the informed priors) and imposing a stricter acceptance criteria. PD sampling also elaborates on the MH decision with three additional procedures; a Metropolis jump dynamic, a single parameter optimization, and

the building of a global PD. Together, updating the sampling state space, resetting the MH decision to more selective criteria, and imposing additional acceptance protocols ensures convergence to the most probable inverse solution with a highly refined estimate of the PD.

The jump diffusion uses a Metropolis jump dynamic to avoid local minima in the algorithm. At a frequency of 0.5%, preceding the MH decision, the jump component creates a transition in the Markov chain accepting the $X^{(t+1)}$ solution without regard to α. This transition is a random walk from X^t and is designed to unconditionally accept a less probable solution. This forces the algorithm to re-build to the globally most probable solution from an improbable state in the chain. During the 99.5% of time when the jump diffusion is not activated, the MH decision is engaged as normal.

Iterations not subjected to the Metropolis jump dynamic and accepted by the MH decision ($\alpha > r$) are then routed to a single parameter optimization intending to maintain highly accurate parameter values. At this point, there is the current step in the chain from the previous iteration, $X^{(t)}$, and the current accepted proposal vector, $X^{(t+1)}$, that will become the current step in the chain. The MAE of $X^{(t+1)}$ is calculated and is the baseline for subsequent comparison. The algorithm generates a vector populated by a random combination of the X^t and $X^{(t-1)}$ vectors with lowest error, maintaining the parameter sequence (i.e. v is position 1, α_L is position 2, R is position 3, k_1 is position 4, k_2 is position 5, k_{12} is position 6). This vector is then applied to the forward model and the MAE calculated. If MAE of the combined vector is reduced from the previous, this vector is stored and the associated MAE becomes the baseline for subsequent comparison, if the MAE is greater than the previous, the vector is discarded. A new

vector is generated from $X^{(t)}$ and $X^{(t-1)}$ and the process recurs for 10 iterations. The vector minimizing the MAE then becomes the current step in the chain. This re-combination of high scoring simulations attempts to optimize individual parameters that may be bulkily discarded with the previous $X^{(t)}$.

In addition to a more rigorous MH decision, the global PD for each column of one RRADE-MCMC experiment is developed through concatenation of five local 1,000,000 iteration PDs from independent model runs, deemed local runs. Each local run is a complete cycle of the MCMC (burn-in and PD sampling). The global PD is then populated with the 5,000,000 accepted parameter vectors in the concatenated Markov chains. The RRADE solution is derived from the mode and standard deviation of the global PD. RRADE-MCMC temporal behavior is shown in Figure A2. The algorithm successfully navigates the state space with successive iterations fluctuating around the mode value. Mode value variability of a local run exemplifies the need for concatenation of local runs into a global simulation (Figure A2a).

Prior, Posterior and Joint Distribution

The RRADE-MCMC algorithm generates a PD containing the expected value of the parameter (mode) and a standard deviation. PDs for all six RRADE parameters are unimodal and treated as normal distributions (Figure A3a). The PD for velocity most closely matches its prior, indicating agreement between initial estimation and model output, whereas the remaining parameters show a marked migration from the prior. This was expected given the paucity of prior knowledge of these unknown parameters, whereas velocity was estimated prior to RRADE-MCMC using a Cl^- tracer and by setting σ to 0.20, three orders of magnitude less than the actual value. This restricts the random

walk to converge to values near the estimated velocity and imposes stringent acceptance criterion. In contrast, for the remaining five parameters we were not able to apply an accurate estimation using ancillary information and thus the σ is on the same, or within an, order of magnitude of the parameter value explaining the marked migration towards more probable state space from the prior distribution during model execution. The PDs of k_1 and k_2 reflect the heuristic rule $k_1 < k_2$.

The joint distribution, shown as the RRST BTC bracketed by confidence intervals representing the min max values, the 95% range, and the interquartile range (IQR) provides uncertainty estimation (Figure A3b). The expected value of each parameter value distribution populates the forward model to derive the average BTC. Statistical quantiles are developed using Monte Carlo randomly sampling the PD for each parameter and running the forward model. This is repeated 2500 times resulting in an ensemble of concentrations for a given interpolated time point. The demonstration plot depicts results for a 2500 member ensemble for 84 interpolated time points. For each of these time points, the concentration distribution is described by the confidence intervals surrounding the mean BTC. The high reproducibility accompanied with narrow IQR assures confidence in the optimized parameter values.

Table A.1 Tuning Parameters of the RRADE MCMC. Table shows successive tuning parameters attempted and increase model performance. Model performance is judged based upon minimization of variation of RRADE parameters, acceptance frequency, and computational resources. Parameter values associated with tune number 15 were selected for optimal performance.

Tune #	Acceptance Criteria				MH Decision Criteria			Selected Column Parameter Modal Variation							Average Acceptance Rate	
	$\sigma_{Burn\text{-}in}$	$\sigma_{posterior}$	$\sigma_{x\ burn\text{-}in}$	$\sigma_{x\ posterior}$	$c_{auto\ accept}$	$N_{parameter\ optim}$	$S_{sims\ concatenated}$	v	R	α_L	k1	k2	k12	MAE	burn in	posterior
1	σprior	0.75*σburn	0.1	0.03	-	-	-	9.61E-01	8.07E-03	1.11E-01	1.43E-03	1.32E-03	3.81E-03	-	0.1086	0.0591
2	2*σprior	0.75*σburn	0.1	0.03	-	-	-	9.44E-03	1.84E-03	1.02E-02	2.59E-05	1.34E-05	1.63E-04	7.59E-06	0.1854	0.0274
3	2*σprior	0.5*σburn	0.1	0.03	-	-	-	1.78E-03	1.38E-03	1.01E-02	1.30E-05	3.44E-05	1.30E-04	6.12E-06	0.1858	0.0617
4	2*σprior	0.5*σburn	0.1	0.04	-	-	-	2.84E-03	5.33E-04	1.41E-02	1.57E-05	3.59E-05	5.95E-05	5.10E-06	0.1852	0.1007
5	2*σprior	0.5*σburn	0.11	0.035	-	-	-	4.11E-03	2.97E-03	4.86E-03	4.83E-05	1.16E-04	9.62E-05	2.18E-06	0.2097	0.0776
6	2*σprior	0.5*σburn	0.11	0.035	0.995	-	-	9.49E-03	1.63E-03	2.74E-02	3.27E-04	3.01E-04	5.44E-04	6.75E-05	0.2102	0.097
7	2*σprior	0.5*σburn	0.11	0.04	0.995	-	-	5.69E-03	1.05E-03	1.14E-02	1.54E-05	4.01E-05	9.62E-05	3.34E-06	0.2104	0.1104
8	2*σprior	0.5*σburn	0.11	0.035	0.99	-	-	1.22E-03	1.14E-03	1.57E-02	2.88E-05	1.61E-05	2.84E-04	8.10E-06	0.2112	0.1126
9	2*σprior	0.5*σburn	0.11	0.035	0.99	10	-	6.88E-03	4.95E-04	4.86E-03	1.08E-04	4.56E-04	1.08E-04	5.00E-06	0.2212	0.1126
10	2*σprior	0.5*σburn	0.11	0.035	0.995	10	-	6.85E-03	3.31E-04	4.65E-03	3.94E-05	3.55E-05	9.57E-05	1.37E-06	0.2096	0.0965
11	2*σprior	1.0*σburn	0.11	0.035	0.995	10	-	8.25E-02	5.18E-03	2.41E-01	2.72E-04	1.81E-04	4.95E-04	9.53E-05	0.2108	0.0295
12	2*σprior	0.5*σburn	0.11	0.035	0.995	15	-	3.47E-03	8.09E-04	1.97E-03	8.22E-06	1.70E-05	4.06E-05	1.98E-06	0.2104	0.0693
13	2*σprior	0.5*σburn	0.11	0.035	0.995	10	4	1.11E-03	1.87E-04	1.44E-03	8.77E-06	9.61E-06	2.90E-05	3.90E-07	0.2102	0.097
14	2*σprior	0.5*σburn	0.11	0.035	0.995	20	4	7.79E-04	2.29E-04	7.96E-04	2.60E-05	4.37E-05	4.84E-05	2.47E-07	0.2102	0.097
15	2*σprior	0.5*σburn	0.11	0.035	0.995	10	5	1.15E-03	2.71E-04	5.95E-03	2.61E-05	1.11E-05	7.88E-06	7.22E-07	0.2109	0.0685
16	2*σprior	0.5*σburn	0.11	0.035	0.995	10	6	3.16E-03	9.17E-04	7.46E-03	1.11E-05	8.64E-06	1.27E-04	4.18E-06	0.2114	0.0689

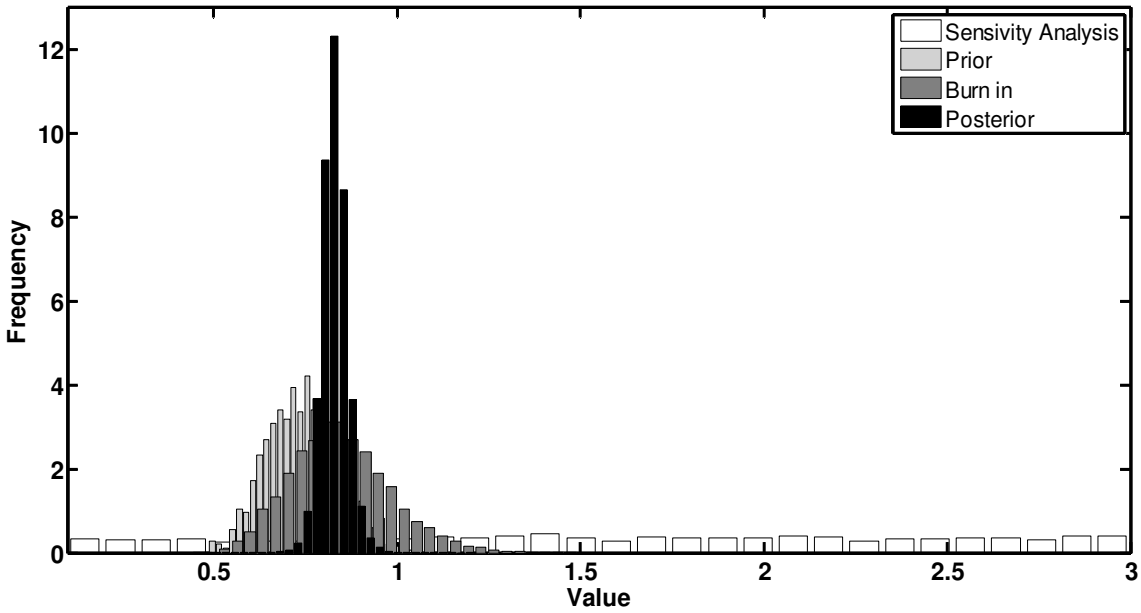

Figure A.1 Progression of RRADE-MCMC from Sensitivity Analysis to Ensemble Statistical Distribution, Parameter Values vs. Frequency. Subsequent stages of the RRADE-MCMC are shown in progressively darker shades. The x-axis shows initial sensitivity analysis (SA) window estimation of parameter value range.

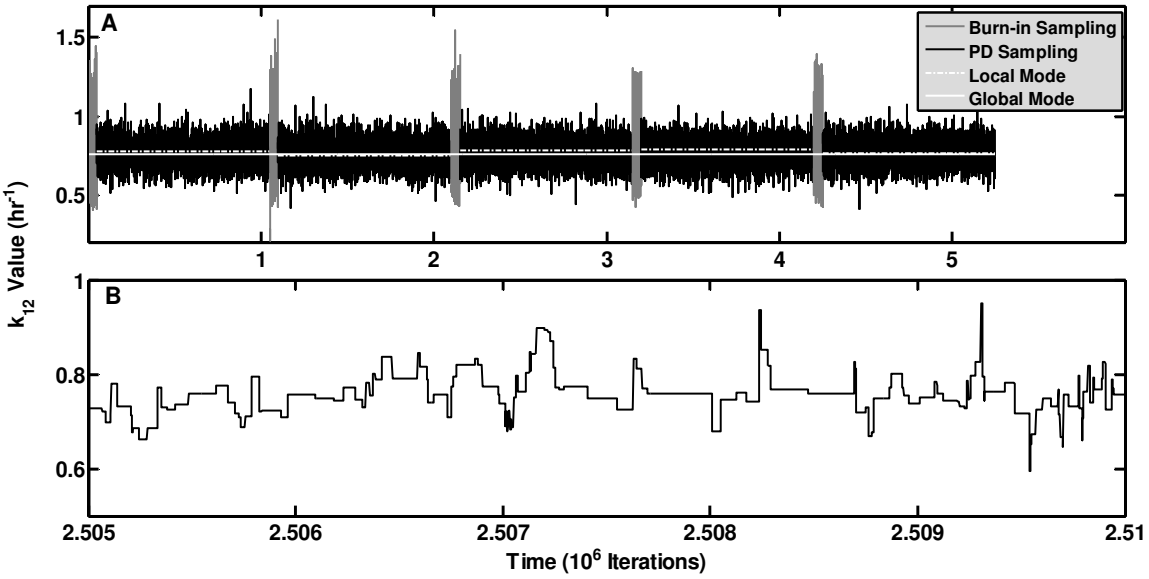

Figure A.2 RRADE-MCMC Model Behavior through Time with Mode Value, k_{12} vs. Iteration. A) One complete model simulation showing mode variation during a local 1,000,000 iteration run, contrasted by the consistent global mode, with accepted simulations fluctuating around this central tendency. B) Panel A in a highly resolved view showing stationary behavior between transitions in the chain with variable step size.

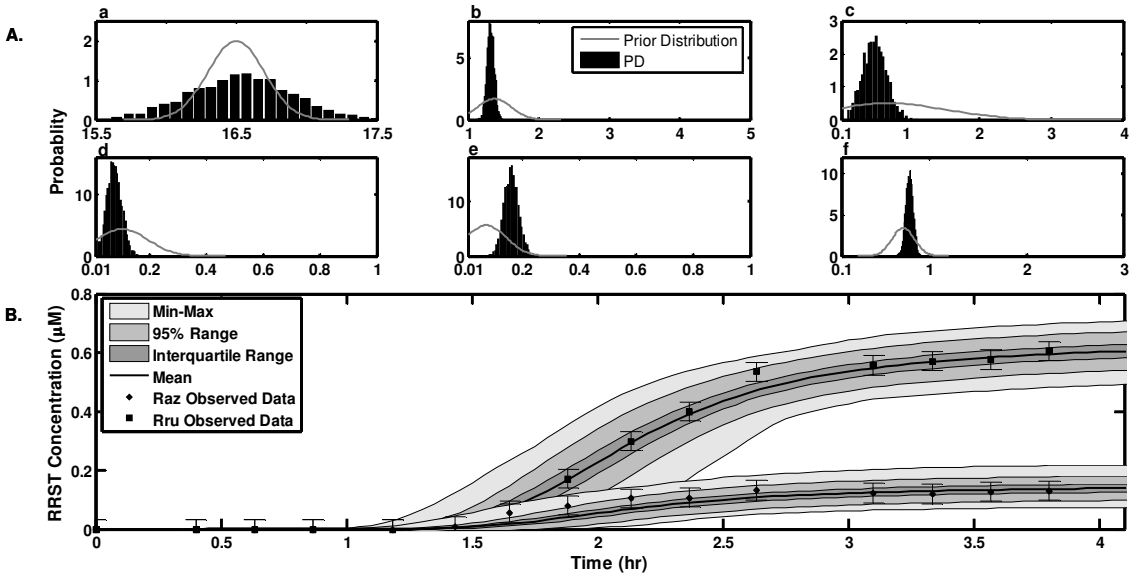

Figure A.3 RRADE Parameter Distributions and Joint Distribution. A) The constrained prior distribution and the posterior distribution of the six RRADE parameters, parameter value versus frequency with x axis showing initial window constrains of the SA, a is velocity (cm/hr), b is *R* (-), c is dispersivity (cm), d is k_2 (hr^{-1}), e is k_1 (hr^{-1}), is k_{12} (hr^{-1}). B) Joint distribution of the RRADE BTC showing observed data points and modeled BTC bracketed with confidence intervals.

References

1. Haggerty, R.; Argerich, A.; Martí, E., Development of a "smart" tracer for the assessment of microbiological activity and sediment-water interaction in natural waters: The resazurin-resorufin system. *Water Resour. Res.* **2008,** *44*.

2. Martin, C.; Ayesa, E., An Integrated Monte Carlo Methodology for the calibration of water quality models. *Ecol. Model.* **2010,** *221*, (22), 2656-2667.

3. Wang, J.; Zabaras, N., A Markov random field model of contamination source identification in porous media flow. *Int. J. Heat Mass Transfer* **2006,** *49*, (5-6), 939-950.

4. Dodge, Y.; Marriott, F. H. C.; International Statistical, I., *The Oxford dictionary of statistical terms*. Oxford University Press: Oxford; New York, 2003.

5. Roberts, G.; Tweedie, R., *Understanding MCMC*. Springer: Berlin, 2003.

6. Roberts, G. O.; Rosenthal, J. S., Optimal Scaling for Various Metropolis-Hastings Algorithms. *Statistical Science* **2001,** *16*, (4), 351-367.

APPENDIX B

Correlation Matrix of RRADE Parameters, Model Variables and Environmental Characteristics

Table B.1 Correlation Matrix of RRADE Parameters, Modeling Variables and Environmental Characteristics. Significant correlations are shown in grey. Table continued on page 89.

	R	alpha	k1	k2	k12	norm k12	Raz Lost	Rru Gained	Raz Lost:Rru Gained	Bacterial Density	Model Error (MAE)	Mass Recovery
R	1.00	0.01	0.13	0.97	0.01	0.00	0.00	0.47	0.01	0.00	0.00	0.00
alpha		1.00	0.08	0.06	0.54	0.01	0.24	0.02	0.00	0.01	0.39	0.00
k1			1.00	0.00	0.49	0.00	0.02	0.05	0.00	0.00	0.10	0.00
k2				1.00	0.33	0.02	0.68	0.00	0.00	0.08	0.89	0.01
k12					1.00	0.54	0.00	0.00	0.98	0.01	0.12	0.06
norm k12						1.00	0.00	0.09	0.00	0.00	0.01	0.00
Raz Lost							1.00	0.06	0.02	0.00	0.01	0.00
Rru Gained								1.00	0.00	0.99	0.78	0.27
Raz Lost:Rru Gained									1.00	0.00	0.02	0.00
Bacterial Density										1.00	0.01	0.00
Model Error (MAE)											1.00	0.00
Mass Recovery												1.00

	Elevation	OC	eMCI	plateau EC	Change in EC	sMCI	Mg_Eff (ppb)	Al_Eff (ppb)	P_Eff (ppb)	K_Eff (ppb)	Ca_Eff (ppb)	Cr_Eff(ppb)
R	0.45	0.77	0.71	0.81	0.03	0.10	0.00	0.14	0.01	0.01	0.00	0.42
alpha	0.03	0.78	0.00	0.08	0.49	0.10	0.06	0.22	0.40	0.01	0.00	0.00
k1	0.00	0.10	0.52	0.58	0.15	0.38	0.62	0.10	0.25	0.29	0.30	0.93
k2	0.00	0.23	0.10	0.19	0.01	0.02	0.19	0.15	0.03	0.75	0.96	0.50
k12	0.06	0.30	0.16	0.58	0.00	0.01	0.02	0.56	0.00	0.08	0.00	0.34
norm k12	0.00	0.10	0.49	0.48	0.36	0.48	0.60	0.51	0.62	0.02	0.04	0.55
Raz Lost	0.85	0.09	0.49	0.93	0.06	0.10	0.03	0.45	0.04	0.01	0.00	0.73
Rru Gained	0.00	0.82	0.16	0.70	0.00	0.03	0.09	0.89	0.01	0.67	0.27	0.14
Raz Lost:Rru Gained	0.00	0.17	0.32	0.61	0.21	0.40	0.78	0.63	0.58	0.10	0.07	0.20
Bacterial Density	0.02	0.41	0.72	0.55	0.49	0.70	0.02	0.97	0.30	0.02	0.00	0.60
Model Error (MAE)	0.88	0.22	0.00	0.00	0.10	0.00	0.18	0.25	0.04	0.03	0.01	0.73
Mass Recovery	0.01	0.07	0.64	0.63	0.92	0.98	0.26	0.47	0.63	0.01	0.00	0.51

	Mn_Eff (ppb)	Fe_Eff (ppb)	Ni_Eff (ppb)	Cu_Eff (ppb)	Zn_Eff (ppb)	As_Eff (ppb)	Sr_Eff (ppb)	Cd_Eff (ppb)	Ba_Eff (ppb)	Pb_Eff (ppb)	Na_Sed (ug/g)	Mg_Sed (ug/g)
R	0.01	0.01	0.64	0.04	0.17	0.49	0.00	0.000	0.649	0.088	0.115	0.087
alpha	0.00	0.90	0.04	0.86	0.20	0.00	0.00	0.018	0.066	0.148	0.000	0.068
k1	0.24	0.06	0.72	0.09	0.78	0.67	0.02	0.055	0.000	0.164	0.000	0.547
k2	0.52	0.01	0.71	0.52	0.72	0.09	0.18	0.212	0.000	0.799	0.000	0.670
k12	0.05	0.27	0.72	0.36	0.04	0.05	0.01	0.259	0.386	0.022	0.158	0.650
norm k12	0.44	0.79	0.75	0.04	0.83	0.47	0.00	0.002	0.010	0.181	0.000	0.768
Raz Lost	0.02	0.52	0.88	0.07	0.10	0.27	0.00	0.013	0.522	0.012	0.527	0.798
Rru Gained	0.54	0.10	0.90	0.47	0.06	0.07	0.89	0.639	0.007	0.331	0.000	0.517
Raz Lost:Rru Gained	0.13	0.31	0.65	0.04	0.63	0.35	0.00	0.009	0.001	0.423	0.000	0.928
Bacterial Density	0.04	0.35	0.53	0.04	0.32	0.97	0.00	0.000	0.221	0.068	0.007	0.233
Model Error (MAE)	0.55	0.16	0.63	0.00	0.56	0.00	0.03	0.064	0.700	0.003	0.339	0.192
Mass Recovery	0.03	0.68	0.78	0.03	0.63	0.81	0.00	0.001	0.009	0.079	0.000	0.980

	Al_Sed (ug/g)	Si_Sed (ug/g)	P_Sed (ug/g)	K_Sed (ug/g)	Ca_Sed (ug/g)	Cr_Sed (ug/g)	Mn_Sed (ug/g)	Fe_Sed (ug/g)	Ni_Sed (ug/g)	Cu_Sed (ug/g)	Zn_Sed (ug/g)	As_Sed (ug/g)
R	0.000	0.000	0.004	0.577	0.278	0.009	0.653	0.000	0.071	0.015	0.004	0.249
alpha	0.000	0.340	0.001	0.042	0.041	0.012	0.005	0.007	0.009	0.592	0.253	0.997
k1	0.015	0.049	0.027	0.021	0.771	0.192	0.156	0.115	0.768	0.675	0.956	0.254
k2	0.025	0.772	0.022	0.049	0.985	0.157	0.011	0.218	0.454	0.214	0.081	0.096
k12	0.941	0.002	0.605	0.102	0.437	0.358	0.212	0.824	0.428	0.048	0.002	0.122
norm k12	0.003	0.004	0.001	0.510	0.723	0.029	0.361	0.012	0.592	0.403	0.422	0.029
Raz Lost	0.121	0.000	0.313	0.032	0.586	0.792	0.692	0.170	0.769	0.170	0.005	0.627
Rru Gained	0.075	0.507	0.043	0.851	0.364	0.048	0.095	0.245	0.263	0.218	0.034	0.159
Raz Lost:Rru Gained	0.000	0.016	0.001	0.033	0.959	0.022	0.128	0.011	0.272	0.946	0.970	0.420
Bacterial Density	0.000	0.000	0.000	0.315	0.319	0.009	0.552	0.000	0.144	0.366	0.059	0.659
Model Error (MAE)	0.145	0.000	0.469	0.700	0.014	0.203	0.002	0.076	0.681	0.010	0.000	0.102
Mass Recovery	0.001	0.000	0.007	0.017	0.877	0.093	0.363	0.016	0.583	0.664	0.236	0.541

	Se_Sed (ug/g)	Se_Sed (ug/g)	Sr_Sed (ug/g)	Cd_Sed (ug/g)	In_Sed (ug/g)	Ba_Sed (ug/g)	Pb_Sed (ug/g)	Bi_Sed (ug/g)	U_Sed (ug/g)	Raz Uncertainty Est	Rru Uncertainty Est
R	0.000	0.001	0.594	0.012	0.027	0.666	0.057	0.453	0.822	0.609	0.000
alpha	0.000	0.000	0.000	0.235	0.333	0.033	0.046	0.248	0.003	0.003	0.000
k1	0.001	0.000	0.002	0.740	0.408	0.752	0.111	0.133	0.169	0.039	0.001
k2	0.004	0.001	0.000	0.056	0.059	0.332	0.000	0.103	0.068	0.001	0.020
k12	0.559	0.633	0.033	0.004	0.192	0.029	0.000	0.373	0.594	0.003	0.067
norm k12	0.000	0.000	0.040	0.801	0.975	0.579	0.367	0.601	0.872	0.048	0.000
Raz Lost	0.012	0.012	0.720	0.021	0.359	0.052	0.026	0.231	0.431	0.351	0.000
Rru Gained	0.105	0.071	0.000	0.041	0.257	0.138	0.000	0.894	0.630	0.000	0.395
Raz Lost:Rru Gained	0.000	0.000	0.000	0.839	0.670	0.891	0.080	0.326	0.143	0.003	0.000
Bacterial Density	0.000	0.000	0.170	0.169	0.345	0.734	0.509	0.788	0.619	0.669	0.000
Model Error (MAE)	0.168	0.294	0.882	0.000	0.000	0.001	0.020	0.075	0.128	0.222	0.045
Mass Recovery	0.000	0.000	0.022	0.432	0.968	0.424	0.772	0.202	0.213	0.117	0.000

APPENDIX C

RRADE – MCMC Code in MATLAB®

Resazurin Resorufin Advection Dispersion Equation Forward Model

```
%This is the Resazurin Resorufin Advection Dispersion Forward Model.

%1. User must explicitly define the following variables. The length of column (30 cm)
here must also be explicitly defined.

%   Craz0 (umol/L) initial concentration of raz

%   t (hr)

%   Frru (dimonsionless) fraction of rru contam in raz

%   var(1) = v (cm/hr)

%   var(2) = R (dimonsionless)

%   var(3) = alpha (cm) sorbing dispersivity

%   var(4) = k1 (hr^-1) rate coeffiecient of raz decay

%   var(5) = k2 (hr^-1) rate coefficient of rru decay

%   var(6) = k12 (hr^-1) rate coefficient of biological raz reduction

function [t,Craz,Crru] = RRADE_MCMC(var,Frru,Craz0,t)

% var is vector of all six variables that need to be optimized

Mrru = 235.2; %this is the molecular weight of resorufin (g/mol)

Mraz = 251.17; %this is the molecular weight of resazurin (g/mol)

x = 30; %length of column (cm)

%2. Equation building

%2a. These equations are inputs into the model
```

```
k1tot = var(4)+var(6);  % (hr^-1)

beta1_v1 = sqrt(1./(4.*var(3).*var(3))+k1tot./(var(1).*var(3)./var(2)));

beta2_v1 = sqrt(1./(4.*var(3).*var(3))+var(5)./(var(1).*var(3)./var(2)));

y12 = (var(6)./k1tot)*(Mrru./Mraz);

%Raz Model

D=(1-Frru).*Craz0./2*exp(x./(2*var(3)));

E=(x-
sqrt(var(1)*var(1)/var(2)/var(2)+4*k1tot*var(1)/var(2)*var(3)).*t)./((2*sqrt(var(1)./var(2
)*var(3)).*t));

f = length(E);

if(-10<f<0)

F=exp(-beta1_v1*x)*(1+erf(abs(E)));

elseif(f>=0);

F=exp(-beta1_v1*x)*erfc(E);

else(f<=-10);

F=exp(-beta1_v1*x)*(1+erf(10));

end

G =
exp(beta1_v1*x)*erfc((x+sqrt(var(1)*var(1)./var(2)./var(2)+4.*k1tot*var(1)/var(2)*var(3
)).*t)./(2*sqrt(var(1)/var(2)*var(3).*t)));
```

```
        Craz=D*(F+G);
%Rru Model
        J = Craz0*(((1-Frru)*y12*k1tot)/(k1tot-
var(5))+Frru)/2*exp(var(1)/var(2)*x/(2*var(1)/var(2)*var(3)));
        K = (x-
sqrt(var(1)/var(2)/var(2)+4*var(5)*var(1)/var(2)*var(3)).*t)./(2*sqrt(var(1)*var(2)*var(3
).*t));
        l = length(K);
        if(-10<l<0)
            L=exp(-beta2_v1*x)*(1+erf(abs(E)));
          elseif(l>=0);
            L=exp(-beta2_v1*x)*erfc(E);
        else(l<=-10);
            L=exp(-beta2_v1*x)*(1+erf(10));
        end
        m = length(K);
        if(m<-20)
          0;
        else
```

```
M =
exp(beta2_v1*x).*erfc((x+sqrt(var(1)*var(1)/var(2)/var(2)+4*var(5)*var(1)./var(2)*var(3
)).*t)./(2*sqrt(var(1)/var(2)*var(3).*t)));
end
N = J.*(L+M);
Crru = N-((Craz.*y12*k1tot)/(k1tot-var(5)));
Crru = Crru';
Craz = Craz';
End
```

Sensitivity Analysis Code

```
%This wrapper combines all columns from all experiments and is intended to run without
interruption.  The range used here for parameter estimation operate on ignorant prior
knowledge of the distribution and are the same for each column- ignorance of prior
distribution is an assumption of MCMC and setting the ranges the same for each column
asserts objectivity for each simulation, except for velocity, which uses CXTFIT
estimation.   As these are large windows, the simulation will need be run a million or
more times per columns.
%The 6 columns of the resulting ascii file correspond to R, alpha, k1, k2, k12
%The windows for each parameter are as follows with justification for
%selection of the range:
%   V: Column Dependant- values from CXTFIT
```

```
%   D: 0.1-10 cm, The LB of this rangerepresents if the solute mass was a wall moving
through the column and
    %   arriving at the measurement point instanteously, the UB would be if
    %   only dispersion were responsible for the solute transfer in the column
%   R: 1-10, The LB represents if no retardation occurred, which mass
    %   recovered in each column rejects this possbility.  This value cannot go
    %   below 1 as this would indicate mass accumulation (see equation for
    %   proof).  The UB was selected arbitrarily and may need modification
    %   depending upon the simulation results
%   K values: .01-5 hr^-1, first guess as to encompassing range.  This may need
    %   modification depending upon the posterior distribution
    % Daniel Stanaway 11.20.2010
%%%%%%%%%%%%%%%%%%%%%%%%%%%%%%%%%%%%%%%%%%%%%%%%%%%%%%%%%%%%%%%%%%%%%%%%%%%%
%This wrapper uses the RADD function to model the Bitterroot, Column 1 data
%set path to interpolated data
path(path,'E:\Thesis\LAB\RRADE-MATLAB\Interpolated Data')
% Read in observed and interpolated profile and timestep
load('BR1_Raz'); Craz_obs = single(BR1_Raz');
load('BR1_Rru'); Crru_obs = single(BR1_Rru');
load('BR1_xi');
%These are the variables that need explicit defintion
```

```
Craz0 = 1.103;  %(umol/L) initial concentration of raz+rru - noted as total concentration
because Frru is in function so rru contamination will be accounted for
%RC = 0.011; %(umol/L) initial rru concentration, rru contamination of raz
Frru = 0.01; % percent rru contamination (Craz0/RC)
% create variable for number of MC runs
N = 3000000;
% Variables describing observational error
std_pr = .0323; %the Synergy Mx documentation says sensitivity is 6-12 ppb,
%the St Dev from the standards of all experiments averaged for all concentrations is
approximately .014 umol/L for both Raz and Rru (see STD_Standards.xlsx)
%this is less than that published by Biotek.  This value may need to be
%modfified depending on results.  A value of 0.049 value here represents the
%average umol/L concentration of the upper end sensitivity (12 ppb).  The
%value shown here is from experimental data see file (SynergyMXerror.xlsx),
%using the value found for rru, that is the higher of the two. When the raz
%and rru stdev values are averaged, 100000 runs returned only 12 accepted runs.  The rru
value returned 37 for the same number of runs.
% Declare MCMC vector for acceptance and for iterative variables
Accept = single(zeros(N,1));
R = single(zeros(N,1));
alpha = single(zeros(N,1));
k1 = single(zeros(N,1));
k2 = single(zeros(N,1));
```

```
k12 = single(zeros(N,1));
%This for loop will iterate to find the best combination of the variables
%within
parfor i=1:N
    t = BR1_xi; %(hr) time vector
    %parameter estimation
    v(i) = single(18.6-16.6)*rand(1)+16.6;
    %v(i) = single((25.10-12.60)*rand(1)+12.6); %the CXTFIT estimated velocity is 17.6
cm/hr, this represents a +/- half cm/hr
    R(i) = single((5.000-1.000)*rand(1)+1.000); %I am unsure of the range of the R value,
so I selected a large range to start
    alpha(i) = single((4.000-0.1)*rand(1)+0.1); %CXTFIT estimation of dispersivity of Cl
is 10.6 cm, Haggerty and others predict
    %dispersivity of sorptive solutes to increase.  Upper bound may need to be amended
    k1(i) = single((1.000-0.0100)*rand(1)+0.0100); %raz decay, unsure of this value as
well, Haggerty notes 0.141, but trying a larger range here to start
    k2(i) = single((1.000-0.0100)*rand(1)+0.0100); %rru decay, Haggerty notes 0.514 but
trying a large range
    k12(i)= single((3.000-0.100)*rand(1)+0.1000); %raz reduction to rru, Haggerty notes
1.41, not sure of range
    %call RRADE function
    [t,Craz(:,i),Crru(:,i)] = RRADE(v(i),R(i),alpha(i),k1(i),k2(i),k12(i),Frru,Craz0,t);
    %distance of each point from the modeled and true data for Raz and Rru
```

```
    dist_raz = Craz(:,i) - Craz_obs;
    dist_rru = Crru(:,i) - Crru_obs;
    %absolute average distance between modeled run and true data- this can
    %become more stringent if the max distance is used
    zraz = mean(abs(dist_raz));
    zrru = mean(abs(dist_rru));
    praz = 1 - normcdf(zraz,0,std_pr); % probability that profile i was drawn from a
gaussian
    % distribution with 0 mean standard deviation std_pr
    prru = 1- normcdf(zrru,0,std_pr); %probability that profile i was drawn from a
gaussian
    % distribution with 0 mean standard deviation std_pr
    %automatic acceptance rule - if zraz/zrru has a higher value than the
    %probability of the variance of the plate reader accept this run
    %(praz>praz_accept)
    %coin flip acceptance fills the tails of the pdf - if a random number
    %(0-1)< praz accept this run.  This has a lower probability of
    %acceptance
    %Acceptance conditions must be met for both raz and rru breakthrough
    %curves
    praz_accpt = 1 - normcdf(std_pr,0,std_pr);
    prru_accpt = 1 - normcdf(std_pr,0,std_pr);
    %random number generation
```

```
    razrand = rand;
    rrurand = rand;
    if((praz>praz_accpt)&&(prru>prru_accpt))
      Accept(i) = 1;   %store all accepted runs in this vector (1 accept 0 discard)
    end
end
%store all variables of the accepted runs - these will populate each %the pdf
R_accpt = single(R(Accept==1));
alpha_accpt = single(alpha(Accept==1));
k1_accpt = single(k1(Accept==1));
k2_accpt = single(k2(Accept==1));
k12_accpt = single(k12(Accept==1));

BR1_OUT = double([R_accpt alpha_accpt k1_accpt k2_accpt k12_accpt]);
save('BR1_OUT','BR1_OUT','-ASCII');
close all; clear all;
```

RRADE-MCMC Code

```
%RRADE MCMC
%D. Stanaway 3/26/2011
%%%%%%%%%%%%%%%%%%%%%%%%%%%%%%%%%%%%%%%%%%%%%%%%%%%%%%%%%%%%%%%%%%%%%%%
%This script iterates through the Clark Fork Breakthrough curves,         %
%organized by elevation (Bitterroot, CFFB, Rock Creek, Drummond, Kohrs Cd,%
```

```
%LBF Cd,LBF, Kohrs Ranch) fitting each observed breakthrough curve with
%the RRADE model converging to the best simulation through Markov Chain
%Monte Carlo
%%%%%%%%%%%%%%%%%%%%%%%%%%%%%%%%%%%%%%%%%%%%%%%%%%%%%%%%%%%%%%%%%%%%%%%
%%%%%%%%%%%%%%%%%%%%%%%%%%%%%%%%%%%%%%%%%%%%%%%%%%%%%%%%%%%%%%%%%%%%%%%
%set path
%path(path,'E:\RRADE MCMC Practice')
%load CF data
load('CF_MCMC_data')
CF = CF_MCMC_data;
[nrows,ncol] = size(CF);
for u = 1:32
    %output progress
    overall_progress = u/ncol
    %generate Location as current file - used to save each column
    outputbasename = char(CF(1,u).Location);
    %declare # of simulations
    N_reps = 1000000;
    N_burnin = 50000;
    %declare iteration numbers for repeated simulations and generate
    %variable to direct each 'r'
    r = 5; %this needs to be noted in the OutputError and OutputMode empty containers
    replicate = [0 N_reps 2*N_reps 3*N_reps 4*N_reps 5*N_reps];
```

```
%1. Declare input data and variables
%identify observed and interpolated data
Craz0 = single(CF(1,u).Craz0);
Frru = single(CF(1,u).Frru);
t = single(CF(1,u).Time_Interpolated);
Craz_obs = single(CF(1,u).Raz_Interpolated);
Crru_obs = single(CF(1,u).Rru_Interpolated);
%place Raz and Rru data into a column vector
x_obs = single([Craz_obs';Crru_obs']);
%declare empty containers to store the values from 4 independent
%runs
Phi_np1_ALL  = zeros(6,r*N_reps,'single'); %six is number of parameters to be
optimized, amend if more parameters are optimized
X_np1_ALL    = zeros(length(x_obs),r*N_reps,'single');
Craz_np1_ALL = zeros(length(Craz_obs),r*N_reps,'single');
Crru_np1_ALL = zeros(length(Crru_obs),r*N_reps,'single');
for o = 1: r %this for loop is for multiple runs of the same column
   %Declare observational error
   sig_obs = 0.11;
   %Perform Burnin
   [phi_np1_store,n_a] = BURNIN(CF,Craz0,Frru,t,x_obs,N_burnin,sig_obs,u);
   %Calculate frequency of acceptance
   f_a_burn = n_a./N_burnin
```

```
        while(f_a_burn<0.001)
            [phi_np1_store,n_a] = BURNIN(CF,Craz0,Frru,t,x_obs,N_burnin,sig_obs,u);
            f_a_burn = n_a./N_burnin
        end
        %run posterior distribution
        [Phi_np1_all,X_np1_all,Craz_np1_all,Crru_np1_all,f_a_post] =
POSTDIST(phi_np1_store,N_reps,x_obs,Craz_obs,Crru_obs,Frru,Craz0,t);
        %compile the accepted values from all five runs to create mode
        %values and ensembles
        Phi_np1_ALL(:,replicate(o)+1:replicate(o+1)) = round(Phi_np1_all*10000)/10000;
        X_np1_ALL(:,replicate(o)+1:replicate(o+1))    = X_np1_all;
        Craz_np1_ALL(:,replicate(o)+1:replicate(o+1)) = Craz_np1_all;
        Crru_np1_ALL(:,replicate(o)+1:replicate(o+1)) = Crru_np1_all;
    end
    %compute error and mode values from simulation
    [ME,mode] = RunStatsandError(Phi_np1_ALL,t,Craz_obs,Crru_obs,Frru,Craz0);
    OutputError = ME;
    OutputMode(:,1) = mode;
%     %4. Compute posterior statistics to save
%     [t,ensmean_Craz,ensmean_Crru] = RRADE_MCMC(OutputMode,Frru,Craz0,t);
%     %ensmean_Crru = mode(Crru_np1_ALL,2);
%     ensstd_Crru = std(Crru_np1_ALL,[],2);
%     ensmax_Crru  = max(Crru_np1_ALL,[],2);
```

```
%     ensmin_Crru  = min(Crru_np1_ALL,[],2);
%     %ensmean_Craz = mode(Craz_np1_ALL,2); given an error becuase of
%     %zeros, so using the mode values from Phi_np1_ALL, the mode values
%     %of the accepted simulation is used here
%     ensstd_Craz = std(Craz_np1_ALL,[],2);
%     ensmax_Craz  = max(Craz_np1_ALL,[],2);
%     ensmin_Craz  = min(Craz_np1_ALL,[],2);
     denseoutput = [outputbasename,'_dense.mat'];
     save(denseoutput,'Phi_np1_ALL','OutputError','OutputMode','f_a_burn','f_a_post');
    close all; clear all
    load('CF_MCMC_data')
    CF = CF_MCMC_data;
    [nrows,ncol] = size(CF);
End
```

MCMC Burn-in Code

```
function [phi_np1_store,n_a] = BURNIN(CF,Craz0,Frru,t,x_obs,N_burnin,sig_obs,u)
%declare container
phi_np1_store = zeros(6,N_burnin,'single');
%Declare Prior Distribution
%mean value
vprior     = single(CF(1,u).Vave_prior);
Rprior     = single(CF(1,u).Rave_prior);
alphaprior = single(CF(1,u).alphaave_prior);
```

```
k1prior    = single(CF(1,u).k1ave_prior);
k2prior    = single(CF(1,u).k2ave_prior);
k12prior   = single(CF(1,u).k12ave_prior);
%place in means in a vector
MuPhi = [vprior Rprior alphaprior k1prior k2prior k12prior]';
%Standard Deviation
sig_v     = single(CF(1,u).Vstd_prior);
sig_R     = single(CF(1,u).Rstd_prior);
sig_alpha = single(CF(1,u).alphastd_prior);
sig_k1    = single(CF(1,u).k1std_prior);
sig_k2    = single(CF(1,u).k2std_prior);
sig_k12   = single(CF(1,u).k12std_prior);
%Place STD in a vector
SigPhi = 2*[sig_v sig_R sig_alpha sig_k1 sig_k2 sig_k12]';
%Initialize the vector of parameters currently in the Markov chain
vstart     = single(CF(1,u).Vave_prior + CF(1,u).Vstd_prior*randn(1,1));
Rstart     = single(CF(1,u).Rave_prior + CF(1,u).Rstd_prior*randn(1,1));
while(Rstart<=0)
   Rstart     = single(CF(1,u).Rave_prior + CF(1,u).Rstd_prior*randn(1,1));
end
alphastart = single(CF(1,u).alphaave_prior + CF(1,u).alphastd_prior*randn(1,1));
while(alphastart<=0)
   alphastart = single(CF(1,u).alphaave_prior + CF(1,u).alphastd_prior*randn(1,1));
```

```
end
k1start    = single(CF(1,u).k1ave_prior + CF(1,u).k1std_prior*randn(1,1));
while(k1start<=0)
   k1start    = single(CF(1,u).k1ave_prior + CF(1,u).k1std_prior*randn(1,1));
end
k2start    = single(CF(1,u).k2ave_prior + CF(1,u).k2std_prior*randn(1,1));
while(k2start<=0)
   k2start    = single(CF(1,u).k2ave_prior + CF(1,u).k2std_prior*randn(1,1));
end
k12start   = single(CF(1,u).k12ave_prior + CF(1,u).k12std_prior*randn(1,1));
while(k12start<=0)
   k12start   = single(CF(1,u).k12ave_prior + CF(1,u).k12std_prior*randn(1,1));
end
phi_np1 = [vstart Rstart alphastart k1start k2start k12start];
%set accepted to zero
n_a = 0;
%2. Perform the burn-in and keep the initial state
for i=1:N_burnin
   % 2a. Generate a candidate parameter set using a random walk
   v_p     = phi_np1(1) + sig_v*randn;
   while(v_p<=0)
      v_p = phi_np1(1) + sig_v*randn;
   end
```

```
R_p     = phi_np1(2) + sig_R*randn;
while(R_p<=1)
   R_p     = phi_np1(2) + sig_R*randn;
end
alpha_p = phi_np1(3) + sig_alpha*randn;
while((alpha_p<=0)||(alpha_p>5))
   alpha_p = phi_np1(3) + sig_alpha*randn;
end
k1_p    = phi_np1(4) + sig_k1*randn;
while(k1_p<=0)
   k1_p    = phi_np1(4) + sig_k1*randn;
end
k2_p    = phi_np1(5) + sig_k2*randn;
while(k2_p<k1_p) %set k2 > k1
   k2_p    = phi_np1(5) + sig_k2*randn;
end
k12_p   = phi_np1(6) + sig_k12*randn;
while(k12_p<=0)
   k12_p   = phi_np1(6) + sig_k12*randn;
end
phi_p = [v_p; R_p; alpha_p; k1_p; k2_p; k12_p];
% 2b. Run the advection-dispersion model
Craz0_i = Craz0 + 0.01*randn;
```

```
    Frru_i = Frru + 0.002*randn;
    [t,Craz_p,Crru_p] = RRADE_MCMC(phi_p,Frru_i,Craz0_i,t);
    x_p = [Craz_p; Crru_p];
    % 2c. Perform the Metropolis-Hastings decision
    if(i==1)
       keep = 1;
    else
       [keep,phi_p] =
MH_Decision(x_obs,sig_obs,x_p,phi_p,x_np1,phi_np1,MuPhi,SigPhi);
    end
    if(keep==1)
       % True, accept
       phi_np1  = phi_p;
       x_np1  = x_p;
       % Increase the number of acceptance
       n_a = n_a + 1;
    end
    phi_np1_store(:,i)=phi_np1;
end
end
```

MCMC Posterior Distribution Code

```
function [Phi_np1_all,X_np1_all,Craz_np1_all,Crru_np1_all,f_a] =
POSTDIST(phi_np1_store,N_reps,x_obs,Craz_obs,Crru_obs,Frru,Craz0,t)
% Reset noise parameters
sig_obs   = 0.035; % Observational error, variance of plate reader, interpolation error,
PD = 0.5;
sig_v = PD*std(phi_np1_store(1,:));
sig_R = PD*std(phi_np1_store(2,:));
sig_alpha = PD*std(phi_np1_store(3,:));
sig_k1 = PD*std(phi_np1_store(4,:));
sig_k2 = PD*std(phi_np1_store(5,:));
sig_k12 = PD*std(phi_np1_store(6,:));
SigPhi = [sig_v; sig_R; sig_alpha; sig_k1; sig_k2; sig_k12]; %use the distributions from
the burn in to start the posterior distribution
%SigPhi = SigPhi_PD; %[sig_v sig_R sig_alpha sig_k1 sig_k2 sig_k12]';
MuPhi = [median(phi_np1_store(1,:)) median(phi_np1_store(2,:))
median(phi_np1_store(3,:)) median(phi_np1_store(4,:)) median(phi_np1_store(5,:))
median(phi_np1_store(6,:))]';
% Declare some empty containers
Phi_np1_all  = zeros(length(MuPhi),N_reps,'single');
X_np1_all    = zeros(length(x_obs),N_reps,'single');
Craz_np1_all = zeros(length(Craz_obs),N_reps,'single');
Crru_np1_all = zeros(length(Crru_obs),N_reps,'single');
```

```
%generate starting position for posterior distribution
Phi_np1_all(:,1)  = [randsample(phi_np1_store(1,:),1) randsample(phi_np1_store(2,:),1)
randsample(phi_np1_store(3,:),1) randsample(phi_np1_store(4,:),1)
randsample(phi_np1_store(5,:),1) randsample(phi_np1_store(6,:),1)]; %select a randomly
selected accepted run from burn in to start posterior distribution
[t,Craz_np1,Crru_np1] = RRADE_MCMC(Phi_np1_all(:,1),Frru,Craz0,t);
x_np1 = [Craz_np1; Crru_np1];
phi_np1 = Phi_np1_all(:,1);
% Reset counter
n_a = 0;
%3. Get a Markov Chain using the MCMC algorithm
for i=2:N_reps
   %MCMC_progress = i/N_reps
   % 3a. Generate a candidate parameter set using a random walk
   v_p     = Phi_np1_all(1,i-1) + sig_v*randn;
   while(v_p<=0)
      v_p     = Phi_np1_all(1,i-1) + sig_v*randn;
   end

   R_p     = Phi_np1_all(2,i-1) + sig_R*randn;
   while(R_p<=1)
      R_p     = Phi_np1_all(2,i-1) + sig_R*randn;
   end
```

```
alpha_p = Phi_np1_all(3,i-1) + sig_alpha*randn;
while((alpha_p<=0)||(alpha_p>5))
   alpha_p = Phi_np1_all(3,i-1) + sig_alpha*randn;
end
k1_p    = Phi_np1_all(4,i-1) + sig_k1*randn;
while(k1_p<=0)
   k1_p    = Phi_np1_all(4,i-1) + sig_k1*randn;
end
k2_p    = Phi_np1_all(5,i-1) + sig_k2*randn;
while(k2_p<k1_p) %set k2 > k1
   k2_p    = Phi_np1_all(5,i-1) + sig_k2*randn;
end
k12_p   = Phi_np1_all(6,i-1) + sig_k12*randn;
while(k12_p<=0)
   k12_p   = Phi_np1_all(6,i-1) + sig_k12*randn;
end
phi_p = [v_p R_p alpha_p k1_p k2_p k12_p]';
% 3b. Run the advection-dispersion model
[t,Craz_p,Crru_p] = RRADE_MCMC(phi_p,Frru,Craz0,t);
x_p = [Craz_p; Crru_p];
% 3c. Perform the Metropolis-Hastings decision
if(i==1)
   keep = 1;
```

```
    elseif(isnan(x_p))
        keep = 0;
    else
        [keep,x_p,phi_p,Craz_p,Crru_p] =
MH_Decision_PD_MAE(x_obs,sig_obs,x_p,phi_p,x_np1,phi_np1,MuPhi,SigPhi,Frru,Cr
az0,t,Craz_p,Crru_p);
    end
    if(keep==1)
        % True, accept
        x_np1    = x_p;
        phi_np1  = phi_p;
        Craz_np1 = Craz_p;
        Crru_np1 = Crru_p;
        % Store values
        Phi_np1_all(:,i)  = phi_np1;
        X_np1_all(:,i)    = x_np1;
        Craz_np1_all(:,i) = Craz_np1;
        Crru_np1_all(:,i) = Crru_np1;
        % Increase the number of acceptance
        n_a = n_a + 1;
    else
        % Store values: there is no change. The model predictions and
        % parameters from the previous step in the Markov chain will be
```

```
        % kept
        Phi_np1_all(:,i)  = phi_np1;
        X_np1_all(:,i)    = x_np1;
        Craz_np1_all(:,i) = Craz_np1;
        Crru_np1_all(:,i) = Crru_np1;

    end
end
%output acceptance
f_a = n_a./N_reps
end
```

MCMC Metropolis Hastings Burn in Decision Code

```
function [keep,phi_p] =
MH_Decision_Burn(x_obs,sig_obs,x_p,phi_p,x_np1,phi_np1,MuPhi,SigPhi)
    obs2assim = 1:10:length(x_obs);
    x_obs = x_obs(obs2assim);
    x_p   = x_p(obs2assim);
    x_np1 = x_np1(obs2assim);
    pi_p = exp(-(1/2)*sum((phi_p - MuPhi).^2./SigPhi.^2)); %this is model simulation
    pi_n = exp(-(1/2)*sum((phi_np1 - MuPhi).^2./SigPhi.^2)); %this is model simulation
    f_xp = exp(-(1/2)*sum((x_obs - x_p).^2./sig_obs.^2)); % this has the observed data
    f_xn = exp(-(1/2)*sum((x_obs - x_np1).^2./sig_obs.^2)); %this has the observed data
    r = rand;
```

```
    if(((pi_p*f_xp)/(pi_n*f_xn))>r)
        % Accept
        keep=1;
    else
        % Reject
        keep=0;
    end

end
```

MCMC Metropolis Hastings Posterior Distribution Decision Code

```
function keep =
MH_Decision_PD(x_obs,sig_obs,x_p,phi_p,x_np1,phi_np1,MuPhi,SigPhi)
obs2assim = 1:10:length(x_obs);
x_obs = x_obs(obs2assim);
x_p   = x_p(obs2assim);
x_np1 = x_np1(obs2assim);
pi_p = exp(-(1/2)*sum((phi_p - MuPhi).^2./SigPhi.^2)); %this is model simulation
pi_n = exp(-(1/2)*sum((phi_np1 - MuPhi).^2./SigPhi.^2)); %this is model simulation
f_xp = exp(-(1/2)*sum((x_obs - x_p).^2./sig_obs.^2)); % this has the observed data
f_xn = exp(-(1/2)*sum((x_obs - x_np1).^2./sig_obs.^2)); %this has the observed data
p = rand;
r = rand;
c = 0.995; %this is the threshold criteria for unconditional acceptance
ratio = ((pi_p*f_xp)/(pi_n*f_xn));
```

```
if(p>c)
    keep = 1;
elseif(ratio>r)
    keep = 1;
else
    % Reject
    keep=0;
end
end
```

APPENDIX D

Column Data

Table D.1 Bitterroot River Column 1

Discrete Time Point Sample Data

				Dissolved Oxygen (μmol L^{-1})		
Time (hr)	Raz Conc (μmol L^{-1})	Rru Conc (μmol L^{-1})	EC (μs cm^{-1})	Influent DO	Effluent DO	Change in DO
0.00	0.00	0.00	-	-	-	-
0.22	0.00	0.00	76.90	321.20	250.80	70.40
0.47	0.00	0.00	83.90	295.80	223.40	72.40
0.72	0.00	0.00	82.40	314.60	240.60	74.00
1.03	0.00	0.00	80.50	304.50	222.40	82.10
1.27	0.02	0.01	94.00	296.10	230.00	66.10
1.48	0.06	0.07	139.70	325.20	253.50	71.70
1.70	0.10	0.15	195.30	307.10	228.00	79.10
1.95	0.12	0.28	241.60	293.70	231.40	62.30
2.20	0.12	0.37	263.00	324.70	257.20	67.50
2.45	0.13	0.44	275.10	301.90	230.30	71.60
2.90	0.15	0.54	282.60	312.50	241.30	71.20
3.17	0.14	0.58	284.20	295.20	231.10	64.10
3.38	0.14	0.60	283.10	328.70	265.60	63.10
3.63	0.14	0.59	284.80	302.00	229.40	72.60
4.00	0.14	0.61	284.70	315.20	258.30	56.90

Column Average Data

		Effluent Metal Concentrations (μg L^{-1})					Sediment Association Metal Concentrations (mg g^{-1})						
OC (μg g^{-1})	pH	Copper	Zinc	Arsenic	Cadmium	Lead	Manganese	Iron	Copper	Zinc	Arsenic	Cadmium	Lead
0.45	6.72	1.53	45.31	20.58	0.12	0.00	108.56	2247.20	2.66	4.45	0.79	0.01	1.83

Table D.2 Bitterroot River Column 2

Discrete Time Point Sample Data

				Dissolved Oxygen (µmol L^{-1})		
Time (hr)	Raz Conc (µmol L^{-1})	Rru Conc (µmol L^{-1})	EC (µs cm^{-1})	Influent DO	Effluent DO	Change in DO
0.00	0.00	0.00	-	-	-	-
0.27	0.00	0.01	77.70	308.40	225.20	83.20
0.52	0.00	0.01	84.50	293.00	212.20	80.80
0.77	0.00	0.01	83.70	322.30	230.50	91.80
1.08	0.00	0.01	80.90	303.00	207.50	95.50
1.32	0.00	0.01	87.30	296.50	227.60	68.90
1.55	0.04	0.05	120.20	324.60	245.70	78.90
1.78	0.09	0.16	188.90	300.70	219.20	81.50
2.02	0.12	0.28	234.70	302.10	233.90	68.20
2.25	0.12	0.39	255.10	321.50	239.70	81.80
2.50	0.14	0.46	270.30	298.70	219.80	78.90
2.97	0.15	0.57	277.70	307.40	228.40	79.00
3.23	0.14	0.60	284.20	295.60	223.30	72.30
3.45	0.14	0.60	280.80	322.50	246.80	75.70
3.68	0.13	0.59	283.80	298.50	223.20	75.30
4.05	0.12	0.53	282.30	317.70	245.60	72.10

Column Average Data

		Effluent Metal Concentrations (µg L^{-1})					Sediment Association Metal Concentrations (mg g^{-1})						
OC (µg g^{-1})	pH	Copper	Zinc	Arsenic	Cadmium	Lead	Manganese	Iron	Copper	Zinc	Arsenic	Cadmium	Lead
0.36	6.72	1.69	29.30	17.99	0.10	0.00	108.56	2247.20	2.66	4.45	0.79	0.01	1.83

Table D.3 Bitterroot River Column 3

Discrete Time Point Sample Data

				Dissolved Oxygen (µmol L^{-1})		
Time (hr)	Raz Conc (µmol L^{-1})	Rru Conc (µmol L^{-1})	EC (µs cm^{-1})	Influent DO	Effluent DO	Change in DO
0.00	0.00	0.00	-	-	-	-
0.32	0.00	0.00	78.00	300.80	231.90	68.90
0.58	0.00	0.00	86.90	289.60	217.00	72.60
0.82	0.00	0.00	84.90	324.30	231.50	92.80
1.13	0.00	0.00	81.50	299.00	222.40	76.60
1.37	0.02	0.01	84.50	312.80	246.50	66.30
1.60	0.08	0.07	140.90	319.70	238.80	80.90
1.83	0.11	0.20	228.30	298.40	227.70	70.70
2.07	0.12	0.34	267.10	316.90	249.20	67.70
2.32	0.14	0.44	276.90	314.60	234.10	80.50
2.57	0.13	0.52	281.90	295.90	229.30	66.60
3.03	0.14	0.59	284.30	302.60	228.50	74.10
3.28	0.14	0.59	285.50	312.80	243.50	69.30
3.50	0.13	0.56	282.20	314.90	242.10	72.80
3.75	0.15	0.59	285.90	296.80	224.90	71.90
4.08	0.14	0.62	282.70	322.30	251.00	71.30

Column Average Data

		Effluent Metal Concentrations (µg L^{-1})					Sediment Association Metal Concentrations (mg g^{-1})						
OC (µg g^{-1})	pH	Copper	Zinc	Arsenic	Cadmium	Lead	Manganese	Iron	Copper	Zinc	Arsenic	Cadmium	Lead
0.26	6.72	0.85	36.52	20.18	0.17	0.00	108.56	2247.20	2.66	4.45	0.79	0.01	1.83

Table D.4 Bitterroot River Column 4

Discrete Time Point Sample Data

				Dissolved Oxygen (µmol L^{-1})		
Time (hr)	Raz Conc (µmol L^{-1})	Rru Conc (µmol L^{-1})	EC (µs cm^{-1})	Influent DO	Effluent DO	Change in DO
0.00	0.00	0.00	-	-	-	-
0.40	0.00	0.00	87.10	303.30	225.90	77.40
0.63	0.00	0.00	86.50	299.50	222.10	77.40
0.87	0.00	0.00	83.80	326.90	234.60	92.30
1.18	0.00	0.00	81.70	301.30	215.50	85.80
1.43	0.01	0.01	86.50	330.40	250.90	79.50
1.65	0.05	0.06	137.60	318.10	228.80	89.30
1.88	0.08	0.17	220.40	301.30	220.60	80.70
2.13	0.11	0.30	258.20	328.50	250.60	77.90
2.37	0.11	0.40	276.80	314.00	223.00	91.00
2.63	0.13	0.54	282.00	297.20	223.50	73.70
3.10	0.12	0.56	285.30	302.00	221.80	80.20
3.33	0.12	0.57	283.80	328.60	248.90	79.70
3.57	0.13	0.58	284.60	315.20	231.00	84.20
3.80	0.13	0.61	287.60	297.30	220.90	76.40
4.15	0.13	0.61	284.90	324.60	237.10	87.50

Column Average Data

		Effluent Metal Concentrations (µg L^{-1})					Sediment Association Metal Concentrations (mg g^{-1})						
OC (µg g^{-1})	pH	Copper	Zinc	Arsenic	Cadmium	Lead	Manganese	Iron	Copper	Zinc	Arsenic	Cadmium	Lead
0.26	6.72	4.58	66.76	24.43	0.11	0.02	108.56	2247.20	2.66	4.45	0.79	0.01	1.83

Table D.5 CF at Missoula Column 1

Discrete Time Point Sample Data

				Dissolved Oxygen (µmol L^{-1})		
Time (hr)	Raz Conc (µmol L^{-1})	Rru Conc (µmol L^{-1})	EC (µs cm^{-1})	Influent DO	Effluent DO	Change in DO
0.00	0.00	0.00	-	-	-	-
0.17	0.00	0.00	103.60	290.60	213.50	77.10
0.42	0.00	0.00	119.90	330.10	211.90	118.20
0.65	0.00	0.00	121.70	307.50	175.20	132.30
1.03	0.01	0.00	116.20	332.80	184.80	148.00
1.32	0.07	0.02	126.10	307.60	194.90	112.70
1.53	0.22	0.12	197.10	318.40	227.10	91.30
1.75	0.25	0.23	270.30	326.50	239.30	87.20
1.97	0.24	0.30	308.00	305.40	214.20	91.20
2.20	0.24	0.42	320.00	332.40	248.50	83.90
2.48	0.23	0.45	318.00	318.10	226.90	91.20
2.73	0.22	0.51	319.00	306.60	227.20	79.40
2.98	0.22	0.55	310.00	323.40	243.20	80.20
3.22	0.20	0.55	310.00	304.50	223.10	81.40
3.53	0.21	0.59	305.00	321.00	245.30	75.70
3.88	0.20	0.57	306.00	313.90	236.70	77.20

Column Average Data

		Effluent Metal Concentrations (µg L^{-1})					Sediment Association Metal Concentrations (mg g^{-1})						
OC (µg g^{-1})	pH	Copper	Zinc	Arsenic	Cadmium	Lead	Manganese	Iron	Copper	Zinc	Arsenic	Cadmium	Lead
7.45	6.75	38.23	64.47	237.19	0.36	0.42	313.36	3539.00	23.75	89.83	4.05	0.23	4.80

Table D.6 CF at Missoula Column 2

Discrete Time Point Sample Data

					Dissolved Oxygen (µmol L^{-1})		
Time (hr)	Raz Conc (µmol L^{-1})	Rru Conc (µmol L^{-1})	Effluent As (µg g^{-1})	EC (µs cm^{-1})	Influent DO	Effluent DO	Change in DO
0.00	0.00	0.00	-	-	-	-	-
0.23	0.00	0.00	5.62	110.40	275.70	165.00	110.70
0.48	0.00	0.00	5.57	126.00	325.70	195.30	130.40
0.72	0.00	0.00	-	126.10	296.20	159.70	136.50
1.08	0.00	0.00	32.44	118.00	331.60	193.10	138.50
1.37	0.12	0.04	118.87	131.50	298.90	206.70	92.20
1.58	0.27	0.17	152.36	213.50	331.80	244.20	87.60
1.80	0.29	0.29	140.16	284.30	307.70	225.70	82.00
2.02	0.27	0.37	137.76	315.00	296.90	215.10	81.80
2.25	0.26	0.45	120.68	317.00	339.70	256.90	82.80
2.53	0.24	0.49	-	314.00	309.60	223.20	86.40
2.80	0.21	0.53	105.55	315.00	323.70	244.90	78.80
3.05	0.23	0.57	-	309.00	311.80	228.90	82.90
3.27	0.23	0.60	91.29	309.00	299.70	221.10	78.60
3.58	0.24	0.63	84.06	306.00	315.20	232.70	82.50
3.93	0.22	0.63	-	304.00	321.70	246.40	75.30

Column Average Data

		Effluent Metal Concentrations (µg L^{-1})					Sediment Association Metal Concentrations (mg g^{-1})						
OC (µg g^{-1})	pH	Copper	Zinc	Arsenic	Cadmium	Lead	Manganese	Iron	Copper	Zinc	Arsenic	Cadmium	Lead
5.43	6.75	25.57	47.30	188.39	0.18	0.31	313.36	3539.00	23.75	89.83	4.05	0.23	4.80

Table D.7 CF at Missoula Column 3

Discrete Time Point Sample Data

				Dissolved Oxygen (µmol L^{-1})		
Time (hr)	Raz Conc (µmol L^{-1})	Rru Conc (µmol L^{-1})	EC (µs cm^{-1})	Influent DO	Effluent DO	Change in DO
0.00	0.00	0.00	-	-	-	-
0.22	0.01	0.00	108.70	298.40	186.10	112.30
0.47	0.00	0.00	124.30	320.20	179.40	140.80
0.70	0.00	0.00	127.30	293.70	151.20	142.50
1.13	0.01	0.00	119.40	304.00	164.60	139.40
1.35	0.12	0.05	140.80	293.70	185.00	108.70
1.57	0.29	0.18	216.60	335.40	226.70	108.70
1.78	0.34	0.32	285.30	303.40	205.50	97.90
2.00	0.27	0.37	312.00	293.80	197.80	96.00
2.23	0.26	0.44	316.00	347.40	244.50	102.90
2.52	0.25	0.52	318.00	305.90	209.30	96.60
2.80	0.23	0.55	313.00	331.70	237.30	94.40
3.03	0.24	0.57	310.00	305.70	213.20	92.50
3.25	0.23	0.58	308.00	305.50	212.40	93.10
3.57	0.21	0.61	307.00	310.50	219.40	91.10
3.90	0.23	0.64	303.00	333.30	238.90	94.40

Column Average Data

		Effluent Metal Concentrations (µg L^{-1})					Sediment Association Metal Concentrations (mg g^{-1})						
OC (µg g^{-1})	pH	Copper	Zinc	Arsenic	Cadmium	Lead	Manganese	Iron	Copper	Zinc	Arsenic	Cadmium	Lead
5.60	6.75	31.51	63.28	189.59	0.18	0.27	313.36	3539.00	23.75	89.83	4.05	0.23	4.80

Table D.8 CF at Missoula Column 4

Discrete Time Point Sample Data

				Dissolved Oxygen ($\mu mol\ L^{-1}$)		
Time (hr)	Raz Conc ($\mu mol\ L^{-1}$)	Rru Conc ($\mu mol\ L^{-1}$)	EC ($\mu s\ cm^{-1}$)	Influent DO	Effluent DO	Change in DO
0.00	0.00	0.00	-	-	-	-
0.35	0.00	0.00	114.10	322.00	198.50	123.50
0.58	0.00	0.00	122.40	310.60	162.10	148.50
0.83	0.01	0.00	120.60	296.20	135.60	160.60
1.22	0.03	0.01	121.00	300.10	173.70	126.40
1.48	0.18	0.10	184.00	302.00	198.10	103.90
1.70	0.29	0.24	267.80	353.50	236.00	117.50
1.90	0.30	0.36	310.00	310.60	202.70	107.90
2.12	0.27	0.42	321.00	302.50	204.50	98.00
2.35	0.25	0.47	315.00	337.40	227.70	109.70
2.65	0.24	0.53	317.00	310.70	211.60	99.10
2.92	0.22	0.56	312.00	345.40	237.10	108.30
3.15	0.22	0.59	310.00	311.30	211.30	100.00
3.37	0.22	0.60	308.00	327.20	230.30	96.90
3.70	0.21	0.62	306.00	310.70	215.30	95.40
4.02	0.24	0.67	300.00	342.20	241.80	100.40

Column Average Data

		Effluent Metal Concentrations ($\mu g\ L^{-1}$)					Sediment Association Metal Concentrations ($mg\ g^{-1}$)						
OC ($\mu g\ g^{-1}$)	pH	Copper	Zinc	Arsenic	Cadmium	Lead	Manganese	Iron	Copper	Zinc	Arsenic	Cadmium	Lead
10.51	6.75	45.46	61.41	172.69	0.22	0.68	313.36	3539.00	23.75	89.83	4.05	0.23	4.80

Table D.9 Rock Creek Column 1

Discrete Time Point Sample Data

				Dissolved Oxygen (µmol L^{-1})		
Time (hr)	Raz Conc (µmol L^{-1})	Rru Conc (µmol L^{-1})	EC (µs cm^{-1})	Influent DO	Effluent DO	Change in DO
0.00	0.00	0.00	-	-	-	-
0.18	0.00	0.00	84.00	295.80	199.30	96.50
0.47	0.00	0.00	87.10	326.90	189.30	137.60
0.83	0.00	0.00	87.60	324.70	167.30	157.40
1.08	0.00	0.00	89.00	317.10	182.00	135.10
1.37	0.00	0.01	93.00	340.20	258.10	82.10
1.62	0.07	0.05	158.90	319.20	260.00	59.20
1.87	0.15	0.15	236.50	349.60	304.10	45.50
2.15	0.21	0.29	267.90	333.80	269.50	64.30
2.45	0.22	0.37	279.00	324.90	281.30	43.60
2.72	0.23	0.43	278.80	340.90	285.00	55.90
3.08	0.26	0.48	285.20	320.80	274.20	46.60
3.35	0.25	0.53	279.50	358.80	304.20	54.60
3.60	0.24	0.53	282.50	320.80	264.90	55.90
3.83	0.25	0.54	284.20	337.70	292.30	45.40
4.12	0.25	0.55	282.80	336.80	275.20	61.60

Column Average Data

		Effluent Metal Concentrations (µg L^{-1})					Sediment Association Metal Concentrations (mg g^{-1})						
OC (µg g^{-1})	pH	Copper	Zinc	Arsenic	Cadmium	Lead	Manganese	Iron	Copper	Zinc	Arsenic	Cadmium	Lead
11.14	6.57	0.45	34.50	25.04	0.22	0.03	52.72	4458.50	2.48	3.57	3.43	0.01	1.96

Table D.10 Rock Creek Column 2

Discrete Time Point Sample Data

				Dissolved Oxygen (µmol L^{-1})		
Time (hr)	Raz Conc (µmol L^{-1})	Rru Conc (µmol L^{-1})	EC (µs cm^{-1})	Influent DO	Effluent DO	Change in DO
0.00	0.00	0.00	-	-	-	-
0.27	0.00	0.00	85.40	316.10	194.50	121.60
0.53	0.00	0.00	87.20	344.30	193.00	151.30
0.90	0.00	0.00	88.60	328.10	161.70	166.40
1.15	0.00	0.00	88.90	344.40	196.40	148.00
1.42	0.00	0.01	94.20	338.00	253.50	84.50
1.68	0.08	0.06	159.30	320.80	262.40	58.40
1.93	0.16	0.17	230.10	361.60	302.10	59.50
2.20	0.18	0.27	265.50	331.80	265.50	66.30
2.50	0.20	0.37	274.60	347.70	297.60	50.10
2.78	0.25	0.43	276.90	342.40	275.20	67.20
3.13	0.25	0.48	281.50	323.20	276.10	47.10
3.40	0.22	0.53	277.70	345.30	283.70	61.60
3.67	0.23	0.53	279.35	321.70	263.50	58.20
3.90	0.23	0.54	281.00	354.10	304.90	49.20
4.18	0.22	0.55	282.30	334.80	271.40	63.40

Column Average Data

		Effluent Metal Concentrations (µg L^{-1})					Sediment Association Metal Concentrations (mg g^{-1})						
OC (µg g^{-1})	pH	Copper	Zinc	Arsenic	Cadmium	Lead	Manganese	Iron	Copper	Zinc	Arsenic	Cadmium	Lead
5.54	6.57	0.42	31.14	25.36	0.61	0.04	52.72	4458.50	2.48	3.57	3.43	0.01	1.96

Table D.11 Rock Creek Column 3

Discrete Time Point Sample Data

				Dissolved Oxygen ($\mu mol\ L^{-1}$)		
Time (hr)	Raz Conc ($\mu mol\ L^{-1}$)	Rru Conc ($\mu mol\ L^{-1}$)	EC ($\mu s\ cm^{-1}$)	Influent DO	Effluent DO	Change in DO
0.00	0.00	0.00	-	-	-	-
0.32	0.00	0.00	86.60	295.30	191.90	103.40
0.60	0.00	0.00	87.10	350.10	196.20	153.90
0.95	0.00	0.00	88.40	321.50	166.70	154.80
1.22	0.00	0.00	88.10	354.60	234.90	119.70
1.48	0.04	0.02	116.20	333.20	263.70	69.50
1.73	0.15	0.11	201.10	324.00	274.30	49.70
2.00	0.20	0.23	250.40	364.70	297.10	67.60
2.30	0.23	0.33	273.90	328.50	272.10	56.40
2.57	0.22	0.37	277.70	366.10	308.10	58.00
2.85	0.24	0.42	279.30	337.70	275.10	62.60
3.20	0.29	0.52	283.00	354.70	303.40	51.30
3.47	0.25	0.52	280.70	345.40	282.00	63.40
3.70	0.27	0.54	283.90	321.20	272.60	48.60
3.95	0.26	0.53	281.20	376.30	312.60	63.70
4.22	0.25	0.53	283.10	333.50	274.00	59.50

Column Average Data

		Effluent Metal Concentrations ($\mu g\ L^{-1}$)					Sediment Association Metal Concentrations ($mg\ g^{-1}$)						
OC ($\mu g\ g^{-1}$)	pH	Copper	Zinc	Arsenic	Cadmium	Lead	Manganese	Iron	Copper	Zinc	Arsenic	Cadmium	Lead
5.85	6.57	0.74	49.29	23.61	0.18	0.07	52.72	4458.50	2.48	3.57	3.43	0.01	1.96

Table D.12 Rock Creek Column 4

Discrete Time Point Sample Data

					Dissolved Oxygen (µmol L^{-1})		
Time (hr)	Raz Conc (µmol L^{-1})	Rru Conc (µmol L^{-1})	Effluent As (µg g^{-1})	EC (µs cm^{-1})	Influent DO	Effluent DO	Change in DO
0.00	0.00	0.00	-	-	-	-	-
0.37	0.00	0.00	1.29	89.00	313.00	195.00	118.00
0.67	0.00	0.00	-	88.90	348.00	191.40	156.60
1.02	0.00	0.00	1.44	89.90	326.90	163.40	163.50
1.28	0.00	0.00	7.12	89.30	356.70	249.30	107.40
1.55	0.03	0.02	16.95	115.40	331.00	259.40	71.60
1.80	0.12	0.09	19.03	202.70	351.80	291.00	60.80
2.08	0.18	0.23	18.65	253.00	347.10	276.10	71.00
2.35	0.20	0.32	17.65	273.00	327.60	270.30	57.30
2.63	0.25	0.42	17.02	273.80	369.90	301.00	68.90
2.92	0.26	0.49	15.41	280.10	330.40	268.60	61.80
3.27	0.24	0.52	-	279.50	364.80	303.20	61.60
3.53	0.25	0.52	14.34	281.30	338.00	269.50	68.50
3.77	0.26	0.55	-	284.60	321.30	267.80	53.50
4.00	0.25	0.57	12.89	278.50	367.50	299.50	68.00
4.28	0.26	0.54	-	282.40	330.70	267.00	63.70

Column Average Data

		Effluent Metal Concentrations (µg L^{-1})					Sediment Association Metal Concentrations (mg g^{-1})						
OC (µg g^{-1})	pH	Copper	Zinc	Arsenic	Cadmium	Lead	Manganese	Iron	Copper	Zinc	Arsenic	admiur	Lead
6.28	6.57	0.52	38.56	26.26	0.16	0.09	52.72	4458.50	2.48	3.57	3.43	0.01	1.96

Table D.13 CF at Drummond Column 1

Discrete Time Point Sample Data

				Dissolved Oxygen ($\mu mol\ L^{-1}$)		
Time (hr)	Raz Conc ($\mu mol\ L^{-1}$)	Rru Conc ($\mu mol\ L^{-1}$)	EC ($\mu s\ cm^{-1}$)	Influent DO	Effluent DO	Change in DO
0.00	0.00	0.00	-	-	-	-
0.22	0.00	0.00	117.60	320.20	181.40	138.80
0.48	0.00	0.00	138.80	313.10	170.00	143.10
0.75	0.00	0.00	137.00	321.80	180.10	141.70
1.02	0.01	0.00	136.00	308.00	209.80	98.20
1.28	0.07	0.02	154.60	317.20	254.60	62.60
1.48	0.17	0.05	185.60	326.20	268.10	58.10
1.65	0.24	0.09	226.00	314.20	255.50	58.70
1.85	0.34	0.15	265.20	306.40	253.20	53.20
2.07	0.37	0.19	283.00	322.60	268.80	53.80
2.28	0.36	0.24	292.30	323.20	267.50	55.70
2.52	0.41	0.29	300.00	310.40	256.90	53.50
2.75	0.40	0.31	298.00	326.70	272.50	54.20
3.08	0.44	0.34	301.00	315.10	256.80	58.30
3.35	0.42	0.35	301.00	307.10	258.80	48.30
3.62	0.42	0.36	297.00	332.70	279.60	53.10
3.88	0.43	0.38	300.00	313.50	259.60	53.90

Column Average Data

		Effluent Metal Concentrations ($\mu g\ L^{-1}$)					Sediment Association Metal Concentrations ($mg\ g^{-1}$)						
OC ($\mu g\ g^{-1}$)	pH	Copper	Zinc	Arsenic	Cadmium	Lead	Manganese	Iron	Copper	Zinc	Arsenic	Cadmium	Lead
2.30	6.65	26.84	94.16	339.39	0.30	0.53	319.46	3857.20	41.88	121.17	6.82	0.29	12.18

Table D.14 CF at Drummond Column 2

Discrete Time Point Sample Data

				Dissolved Oxygen (µmol L^{-1})		
Time (hr)	Raz Conc (µmol L^{-1})	Rru Conc (µmol L^{-1})	EC (µs cm^{-1})	Influent DO	Effluent DO	Change in DO
0.00	0.00	0.00	-	-	-	-
0.28	0.00	0.00	124.90	293.60	173.70	119.90
0.53	0.00	0.00	135.20	306.80	172.70	134.10
0.80	0.00	0.00	131.20	312.30	164.50	147.80
1.07	0.00	0.00	125.70	298.40	176.10	122.30
1.33	0.05	0.01	128.30	311.50	240.80	70.70
1.52	0.17	0.04	177.40	314.70	247.70	67.00
1.70	0.27	0.10	236.40	303.40	243.30	60.10
1.90	0.32	0.15	278.50	294.90	245.20	49.70
2.12	0.34	0.21	293.80	312.70	256.50	56.20
2.33	0.39	0.27	300.00	309.20	247.60	61.60
2.57	0.39	0.31	305.00	299.00	246.50	52.50
2.80	0.38	0.33	300.00	315.50	260.60	54.90
3.13	0.38	0.35	305.00	301.70	242.40	59.30
3.40	0.36	0.36	302.00	304.40	255.20	49.20
3.67	0.34	0.36	298.00	317.50	261.40	56.10
3.93	0.38	0.38	300.00	298.80	246.60	52.20

Column Average Data

		Effluent Metal Concentrations (µg L^{-1})					Sediment Association Metal Concentrations (mg g^{-1})						
OC (µg g^{-1})	pH	Copper	Zinc	Arsenic	Cadmium	Lead	Manganese	Iron	Copper	Zinc	Arsenic	Cadmium	Lead
8.10	6.65	11.88	28.28	164.59	0.10	0.16	319.46	3857.20	41.88	121.17	6.82	0.29	12.18

Table D.15 CF at Drummond Column 3

Discrete Time Point Sample Data

				Dissolved Oxygen (µmol L^{-1})		
Time (hr)	Raz Conc (µmol L^{-1})	Rru Conc (µmol L^{-1})	EC (µs cm^{-1})	Influent DO	Effluent DO	Change in DO
0.00	0.00	0.00	-	-	-	-
0.35	0.00	0.00	137.30	287.60	177.00	110.60
0.58	0.00	0.00	139.90	311.00	178.50	132.50
0.87	0.00	0.00	128.90	313.40	162.70	150.70
1.12	0.00	0.00	128.20	300.20	184.40	115.80
1.38	0.07	0.01	141.50	321.50	237.10	84.40
1.57	0.20	0.06	201.20	321.80	245.70	76.10
1.75	0.32	0.12	259.50	308.50	246.90	61.60
1.95	0.36	0.18	288.50	303.80	248.30	55.50
2.17	0.38	0.23	296.00	325.70	266.30	59.40
2.38	0.38	0.26	300.00	317.30	252.60	64.70
2.63	0.41	0.31	301.00	320.20	260.80	59.40
2.87	0.40	0.32	298.00	331.50	269.90	61.60
3.18	0.41	0.35	303.00	309.10	252.20	56.90
3.45	0.42	0.37	300.00	325.60	271.00	54.60
3.72	0.42	0.37	297.00	326.60	267.50	59.10
3.97	0.42	0.38	300.00	310.90	252.40	58.50

Column Average Data

		Effluent Metal Concentrations (µg L^{-1})					Sediment Association Metal Concentrations (mg g^{-1})						
OC (µg g^{-1})	pH	Copper	Zinc	Arsenic	Cadmium	Lead	Manganese	Iron	Copper	Zinc	Arsenic	Cadmium	Lead
4.05	6.65	14.49	488.36	155.29	0.30	0.87	319.46	3857.20	41.88	121.17	6.82	0.29	12.18

Table D.16 CF at Drummond Column 4

Discrete Time Point Sample Data

					Dissolved Oxygen ($\mu mol\ L^{-1}$)		
Time (hr)	Raz Conc ($\mu mol\ L^{-1}$)	Rru Conc ($\mu mol\ L^{-1}$)	Effluent As ($\mu g\ g^{-1}$)	EC ($\mu s\ cm^{-1}$)	Influent DO	Effluent DO	Change in DO
0.00	0.00	0.00	-	-	-	-	-
0.40	0.00	0.00	14.45	121.70	289.30	176.80	112.50
0.63	0.00	0.00	-	133.00	318.20	179.40	138.80
0.92	0.00	0.00	28.71	131.40	306.30	173.70	132.60
1.17	0.01	0.00	-	132.30	299.20	220.90	78.30
1.43	0.14	0.03	235.98	173.90	323.10	257.90	65.20
1.60	0.29	0.10	266.46	243.00	312.10	250.50	61.60
1.80	0.35	0.16	-	286.30	300.70	248.90	51.80
2.02	0.39	0.22	230.06	301.00	309.60	258.40	51.20
2.23	0.37	0.27	-	301.00	323.30	264.30	59.00
2.45	0.44	0.33	193.52	305.00	304.30	250.60	53.70
2.68	0.42	0.35	171.24	303.00	318.60	263.40	55.20
2.90	0.39	0.35	158.17	299.00	317.60	252.00	65.60
3.22	0.41	0.36	148.86	305.00	299.50	251.30	48.20
3.48	0.42	0.40	-	302.00	324.70	267.80	56.90
3.75	0.39	0.40	128.64	298.00	315.90	255.80	60.10

Column Average Data

		Effluent Metal Concentrations ($\mu g\ L^{-1}$)					Sediment Association Metal Concentrations ($mg\ g^{-1}$)						
OC ($\mu g\ g^{-1}$)	pH	Copper	Zinc	Arsenic	Cadmium	Lead	Manganese	Iron	Copper	Zinc	Arsenic	Cadmium	Lead
4.95	6.65	14.83	64.68	156.39	0.17	0.21	319.46	3857.20	41.88	121.17	6.82	0.29	12.18

Table D.17 Little Blackfoot River Column 1

Discrete Time Point Sample Data

				Dissolved Oxygen (µmol L^{-1})		
Time (hr)	Raz Conc (µmol L^{-1})	Rru Conc (µmol L^{-1})	EC (µs cm^{-1})	Influent DO	Effluent DO	Change in DO
0.00	0.00	0.00	-	-	-	-
0.23	0.00	0.00	100.40	302.40	217.00	85.40
0.47	0.00	0.00	114.20	284.90	158.50	126.40
0.75	0.00	0.00	115.00	292.20	156.80	135.40
1.02	0.00	0.00	111.50	293.10	154.80	138.30
1.28	0.00	0.00	114.20	278.50	196.90	81.60
1.53	0.06	0.04	155.50	304.30	237.30	67.00
1.78	0.09	0.13	244.40	282.30	225.70	56.60
2.05	0.11	0.23	289.90	310.80	264.10	46.70
2.30	0.10	0.29	307.00	291.70	230.50	61.20
2.57	0.09	0.31	314.00	286.00	238.70	47.30
2.87	0.11	0.40	313.00	296.20	242.00	54.20
3.22	0.11	0.43	313.00	295.80	252.60	43.20
3.48	0.12	0.50	313.00	299.90	249.00	50.90
3.70	0.12	0.49	312.00	286.80	233.10	53.70
4.02	0.12	0.51	312.00	313.20	267.80	45.40

Column Average Data

		Effluent Metal Concentrations (µg L^{-1})					Sediment Association Metal Concentrations (mg g^{-1})						
OC (µg g^{-1})	pH	Copper	Zinc	Arsenic	Cadmium	Lead	Manganese	Iron	Copper	Zinc	Arsenic	Cadmium	Lead
4.71	6.64	0.68	65.12	159.59	9.55	0.10	280.60	6883.80	4.67	27.40	8.56	0.10	5.89

Table D.18 Little Blackfoot River Column 2

Discrete Time Point Sample Data

				Dissolved Oxygen (µmol L^{-1})		
Time (hr)	Raz Conc (µmol L^{-1})	Rru Conc (µmol L^{-1})	EC (µs cm^{-1})	Influent DO	Effluent DO	Change in DO
0.00	0.00	0.00	-	-	-	-
0.28	0.00	0.00	105.70	287.20	175.00	112.20
0.53	0.00	0.00	118.10	277.10	148.40	128.70
0.80	0.00	0.00	115.40	302.30	147.00	155.30
1.07	0.00	0.00	112.40	285.40	148.90	136.50
1.35	0.02	0.01	122.90	295.80	215.20	80.60
1.58	0.05	0.05	170.90	295.10	220.60	74.50
1.87	0.08	0.14	240.90	279.60	216.80	62.80
2.12	0.09	0.23	283.40	310.50	245.70	64.80
2.37	0.10	0.29	305.00	287.30	221.40	65.90
2.70	0.11	0.37	309.00	309.40	252.10	57.30
2.93	0.11	0.43	314.00	293.30	225.60	67.70
3.28	0.12	0.47	313.00	309.90	253.40	56.50
3.53	0.10	0.46	312.00	293.10	228.90	64.20
3.75	0.11	0.48	314.00	283.10	227.60	55.50
4.02	0.11	0.50	313.00	311.20	252.40	58.80

Column Average Data

		Effluent Metal Concentrations (µg L^{-1})					Sediment Association Metal Concentrations (mg g^{-1})						
OC (µg g^{-1})	pH	Copper	Zinc	Arsenic	Cadmium	Lead	Manganese	Iron	Copper	Zinc	Arsenic	Cadmium	Lead
2.60	6.64	1.13	44.90	149.39	9.54	0.08	280.60	6883.80	4.67	27.40	8.56	0.10	5.89

Table D.19 Little Blackfoot River Column 3

Discrete Time Point Sample Data

				Dissolved Oxygen ($\mu mol\ L^{-1}$)		
Time (hr)	Raz Conc ($\mu mol\ L^{-1}$)	Rru Conc ($\mu mol\ L^{-1}$)	EC ($\mu s\ cm^{-1}$)	Influent DO	Effluent DO	Change in DO
0.00	0.00	0.00	-	-	-	-
0.35	0.00	0.00	109.20	293.60	166.70	126.90
0.58	0.00	0.00	116.90	280.10	144.30	135.80
0.88	0.00	0.00	112.90	310.40	142.90	167.50
1.13	0.00	0.00	111.80	288.20	160.70	127.50
1.40	0.02	0.02	127.00	309.60	229.60	80.00
1.65	0.09	0.09	193.50	293.00	213.50	79.50
1.92	0.11	0.19	257.70	298.20	229.80	68.40
2.18	0.12	0.27	281.10	304.20	229.80	74.40
2.43	0.11	0.33	290.70	287.00	219.30	67.70
2.77	0.13	0.40	292.00	313.10	243.40	69.70
3.00	0.12	0.44	292.90	289.40	222.50	66.90
3.35	0.11	0.44	290.30	315.10	249.40	65.70
3.58	0.13	0.48	291.30	292.10	222.50	69.60
3.80	0.13	0.50	292.30	279.90	226.60	53.30
4.02	0.12	0.47	292.50	313.50	246.90	66.60

Column Average Data

		Effluent Metal Concentrations ($\mu g\ L^{-1}$)					Sediment Association Metal Concentrations ($mg\ g^{-1}$)						
OC ($\mu g\ g^{-1}$)	pH	Copper	Zinc	Arsenic	Cadmium	Lead	Manganese	Iron	Copper	Zinc	Arsenic	Cadmium	Lead
7.81	6.58	0.77	36.15	156.09	1.26	0.09	280.60	6883.80	4.67	27.40	8.56	0.10	5.89

Table D.20 Little Blackfoot River Column 4

Discrete Time Point Sample Data

				Dissolved Oxygen (μmol L^{-1})		
Time (hr)	Raz Conc (μmol L^{-1})	Rru Conc (μmol L^{-1})	EC (μs cm^{-1})	Influent DO	Effluent DO	Change in DO
0.00	0.00	0.00	-	-	-	-
0.40	0.00	0.00	112.40	286.00	152.90	133.10
0.67	0.00	0.00	119.50	275.50	135.20	140.30
0.90	0.00	0.00	115.90	304.00	131.80	172.20
1.22	0.00	0.00	117.50	283.10	184.50	98.60
1.47	0.05	0.04	149.00	319.20	232.30	86.90
1.72	0.09	0.12	215.30	288.20	209.00	79.20
1.98	0.09	0.21	257.40	313.70	239.00	74.70
2.23	0.11	0.29	277.10	300.40	219.10	81.30
2.50	0.11	0.36	289.80	285.00	218.50	66.50
2.82	0.13	0.43	291.00	309.20	228.80	80.40
3.05	0.11	0.44	294.80	287.30	222.30	65.00
3.42	0.12	0.46	291.70	318.30	239.20	79.10
3.63	0.11	0.47	294.30	292.20	220.70	71.50
3.87	0.12	0.50	295.00	299.90	239.00	60.90
4.02	0.13	0.50	292.80	319.30	241.70	77.60

Column Average Data

		Effluent Metal Concentrations (μg L^{-1})					Sediment Association Metal Concentrations (mg g^{-1})						
OC (μg g^{-1})	pH	Copper	Zinc	Arsenic	Cadmium	Lead	Manganese	Iron	Copper	Zinc	Arsenic	Cadmium	Lead
2.90	6.58	1.03	38.95	154.49	1.25	0.07	280.60	6883.80	4.67	27.40	8.56	0.10	5.89

Table D.21 CF at Kohr's Ranch Column 1

Discrete Time Point Sample Data

				Dissolved Oxygen (µmol L^{-1})		
Time (hr)	Raz Conc (µmol L^{-1})	Rru Conc (µmol L^{-1})	EC (µs cm^{-1})	Influent DO	Effluent DO	Change in DO
0.00	0.00	0.00	-	-	-	-
0.18	0.00	0.00	131.00	299.70	151.30	148.40
0.45	0.00	0.00	155.30	320.90	141.70	179.20
0.67	0.00	0.00	149.70	324.60	139.20	185.40
0.93	0.00	0.00	142.20	309.60	130.70	178.90
1.18	0.00	0.00	129.70	341.10	234.10	107.00
1.40	0.07	0.02	138.60	318.70	244.40	74.30
1.60	0.20	0.10	205.40	308.30	253.40	54.90
1.80	0.30	0.22	268.90	345.80	286.60	59.20
1.98	0.24	0.24	297.00	323.40	255.10	68.30
2.18	0.24	0.30	314.00	311.70	252.00	59.70
2.40	0.29	0.39	313.00	338.20	285.40	52.80
2.75	0.29	0.43	314.00	319.60	254.60	65.00
2.97	0.29	0.47	312.00	325.50	275.80	49.70
3.18	0.25	0.47	307.00	335.10	273.90	61.20
3.45	0.24	0.49	310.00	312.90	257.60	55.30
3.80	0.25	0.54	305.00	336.90	279.50	57.40

Column Average Data

		Effluent Metal Concentrations (µg L^{-1})					Sediment Association Metal Concentrations (mg g^{-1})						
OC (µg g^{-1})	pH	Copper	Zinc	Arsenic	Cadmium	Lead	Manganese	Iron	Copper	Zinc	Arsenic	Cadmium	Lead
1.44	6.65	18.07	46.88	205.79	0.12	0.19	294.26	2308.60	142.47	101.50	26.64	0.30	10.01

Table D.22 CF at Kohr's Ranch Column 2

Discrete Time Point Sample Data

					Dissolved Oxygen (µmol L^{-1})		
Time (hr)	Raz Conc (µmol L^{-1})	Rru Conc (µmol L^{-1})	Effluent As (µg g^{-1})	EC (µs cm^{-1})	Influent DO	Effluent DO	Change in DO
0.00	0.00	0.00	-	-	-	-	-
0.28	0.00	0.00	-	144.90	298.20	161.50	136.70
0.55	0.00	0.00	18.21	153.90	323.80	156.90	166.90
0.75	0.00	0.00	-	146.20	315.20	141.90	173.30
1.02	0.00	0.00	-	138.40	307.50	150.30	157.20
1.25	0.00	0.00	151.14	126.10	336.10	254.30	81.80
1.50	0.14	0.05	305.78	162.40	313.80	248.00	65.80
1.70	0.27	0.15	337.71	247.70	319.50	267.90	51.60
1.88	0.29	0.23	-	290.50	333.20	280.90	52.30
2.07	0.30	0.30	287.98	309.00	318.60	255.90	62.70
2.27	0.31	0.37	-	315.00	307.20	257.30	49.90
2.48	0.33	0.43	225.18	310.00	334.90	288.60	46.30
2.83	0.30	0.46	206.67	309.00	313.30	258.00	55.30
3.07	0.27	0.45	190.24	306.00	330.00	284.60	45.40
3.27	0.28	0.48	178.91	303.00	328.40	267.90	60.50
3.55	0.27	0.47	162.89	308.00	310.30	261.30	49.00

Column Average Data

		Effluent Metal Concentrations (µg L^{-1})					Sediment Association Metal Concentrations (mg g^{-1})						
OC (µg g^{-1})	pH	Copper	Zinc	Arsenic	Cadmium	Lead	Manganese	Iron	Copper	Zinc	Arsenic	Cadmium	Lead
1.64	6.65	22.53	55.88	186.59	0.13	0.21	294.26	2308.60	142.47	101.50	26.64	0.30	10.01

Table D.23 CF at Kohr's Ranch Column 3

Discrete Time Point Sample Data

				Dissolved Oxygen (µmol L^{-1})		
Time (hr)	Raz Conc (µmol L^{-1})	Rru Conc (µmol L^{-1})	EC (µs cm^{-1})	Influent DO	Effluent DO	Change in DO
0.00	0.00	0.00	-	-	-	-
0.35	0.00	0.00	127.80	311.00	164.40	146.60
0.62	0.00	0.00	147.30	337.60	166.40	171.20
0.82	0.00	0.00	148.00	326.40	136.70	189.70
1.08	0.00	0.00	139.90	320.30	136.30	184.00
1.33	0.00	0.00	131.20	336.90	207.90	129.00
1.57	0.12	0.04	156.60	322.50	230.50	92.00
1.77	0.24	0.15	234.90	339.50	259.20	80.30
1.95	0.28	0.22	284.80	337.80	267.60	70.20
2.13	0.28	0.28	309.00	326.60	250.40	76.20
2.33	0.26	0.33	313.00	328.40	260.90	67.50
2.55	0.29	0.39	310.00	344.50	278.20	66.30
2.90	0.24	0.39	312.00	321.00	251.70	69.30
3.13	0.25	0.42	308.00	346.50	286.10	60.40
3.35	0.25	0.44	304.00	333.70	261.10	72.60
3.63	0.26	0.47	307.00	320.00	256.00	64.00
3.97	0.24	0.47	303.00	336.40	264.90	71.50

Column Average Data

		Effluent Metal Concentrations (µg L^{-1})					Sediment Association Metal Concentrations (mg g^{-1})						
OC (µg g^{-1})	pH	Copper	Zinc	Arsenic	Cadmium	Lead	Manganese	Iron	Copper	Zinc	Arsenic	Cadmium	Lead
2.09	6.65	21.18	81.93	195.29	0.13	0.17	294.26	2308.60	142.47	101.50	26.64	0.30	10.01

Table D.24 CF at Kohr's Ranch Column 4

Discrete Time Point Sample Data

				Dissolved Oxygen (µmol L^{-1})		
Time (hr)	Raz Conc (µmol L^{-1})	Rru Conc (µmol L^{-1})	EC (µs cm^{-1})	Influent DO	Effluent DO	Change in DO
0.00	0.00	0.00	-	-	-	-
0.38	0.00	0.00	136.40	297.60	149.30	148.30
0.65	0.00	0.00	145.30	336.20	141.70	194.50
0.85	0.00	0.00	140.60	316.50	119.60	196.90
1.13	0.00	0.00	135.50	336.00	158.90	177.10
1.37	0.04	0.01	133.10	330.70	224.90	105.80
1.60	0.18	0.08	184.70	316.90	239.30	77.60
1.80	0.26	0.17	260.20	347.70	270.60	77.10
1.98	0.27	0.24	289.50	334.10	257.10	77.00
2.17	0.27	0.30	311.00	320.90	247.10	73.80
2.38	0.30	0.39	310.00	340.80	270.10	70.70
2.60	0.27	0.38	311.00	339.80	261.60	78.20
2.93	0.25	0.43	314.00	317.20	251.00	66.20
3.17	0.27	0.47	307.00	357.20	282.90	74.30
3.40	0.26	0.48	305.00	327.00	251.70	75.30
3.67	0.25	0.49	303.00	333.20	265.90	67.30
4.00	0.25	0.49	307.00	328.00	255.40	72.60

Column Average Data

		Effluent Metal Concentrations (µg L^{-1})					Sediment Association Metal Concentrations (mg g^{-1})						
OC (µg g^{-1})	pH	Copper	Zinc	Arsenic	Cadmium	Lead	Manganese	Iron	Copper	Zinc	Arsenic	Cadmium	Lead
1.57	6.65	17.65	30.41	191.49	0.10	0.21	294.26	2308.60	142.47	101.50	26.64	0.30	10.01

Table D.25 Metal Stress Little Blackfoot River Control Column 1

Discrete Time Point Sample Data

Time (hr)	Raz Conc (µmol L^{-1})	Rru Conc (µmol L^{-1})	EC (µs cm^{-1})
0.00	0.00	0.00	-
0.33	0.00	0.00	215.30
0.60	0.00	0.00	213.70
0.83	0.00	0.00	218.10
1.08	0.00	0.00	215.40
1.32	0.01	0.01	266.20
1.55	0.09	0.05	347.00
1.77	0.16	0.11	430.00
1.97	0.22	0.18	474.00
2.18	0.26	0.22	487.00
2.40	0.28	0.26	502.00
2.62	0.32	0.31	497.00
2.83	0.34	0.34	501.00
3.07	0.36	0.37	499.00
3.28	0.37	0.34	499.00
3.50	0.37	0.38	503.00
4.03	0.37	0.39	501.00

Column Average Data

		Effluent Metal Concentrations (µg L^{-1})					Sediment Association Metal Concentrations (mg g^{-1})						
OC (µg g^{-1})	pH	Copper	Zinc	Arsenic	Cadmium	Lead	Manganese	Iron	Copper	Zinc	Arsenic	Cadmium	Lead
3.76	6.70	0.27	5.45	2.19	3.33	0.01	209.76	7504.00	4.58	29.90	8.84	0.10	6.31

Table D.26 Metal Stress Little Blackfoot River Control Column 2

Discrete Time Point Sample Data

Time (hr)	Raz Conc (µmol L^{-1})	Rru Conc (µmol L^{-1})	EC (µs cm^{-1})
0.00	0.00	0.00	-
0.40	0.00	0.00	215.10
0.67	0.00	0.00	215.40
0.88	0.00	0.00	217.80
1.13	0.00	0.00	217.30
1.37	0.03	0.01	270.70
1.58	0.09	0.06	357.00
1.80	0.17	0.12	429.00
2.02	0.22	0.17	467.00
2.22	0.27	0.24	489.00
2.45	0.32	0.29	501.00
2.67	0.36	0.33	490.00
2.88	0.36	0.34	503.00
3.10	0.36	0.35	499.00
3.33	0.37	0.36	501.00
3.55	0.35	0.34	502.00
4.08	0.34	0.35	502.00

Column Average Data

		Effluent Metal Concentrations (µg L^{-1})					Sediment Association Metal Concentrations (mg g^{-1})						
OC (µg g^{-1})	pH	Copper	Zinc	Arsenic	Cadmium	Lead	Manganese	Iron	Copper	Zinc	Arsenic	Cadmium	Lead
2.03	6.70	0.37	8.58	2.05	0.75	0.02	209.76	7504.00	4.58	29.90	8.84	0.10	6.31

Table D.27 Metal Stress Little Blackfoot River Treatment Column 1

Discrete Time Point Sample Data

Time (hr)	Raz Conc (µmol L^{-1})	Rru Conc (µmol L^{-1})	EC (µs cm^{-1})
0.00	0.00	0.00	-
0.45	0.00	0.00	494.00
0.72	0.00	0.00	500.00
0.93	0.00	0.00	487.00
1.18	0.00	0.00	489.00
1.42	0.00	0.01	516.00
1.63	0.05	0.03	557.00
1.85	0.10	0.06	598.00
2.05	0.15	0.11	617.00
2.28	0.18	0.15	637.00
2.50	0.24	0.21	636.00
2.72	0.25	0.23	634.00
2.93	0.29	0.27	639.00
3.15	0.27	0.28	635.00
3.37	0.30	0.29	640.00
3.63	0.30	0.29	635.00
4.13	0.29	0.28	634.00

Column Average Data

		Effluent Metal Concentrations (µg L^{-1})					Sediment Association Metal Concentrations (mg g^{-1})						
OC (µg g^{-1})	pH	Copper	Zinc	Arsenic	Cadmium	Lead	Manganese	Iron	Copper	Zinc	Arsenic	Cadmium	Lead
1.60	6.75	1.88	82.34	1.44	191.00	0.02	209.76	7504.00	4.58	29.90	8.84	0.10	6.31

Table D.28 Metal Stress Little Blackfoot River Treatment Column 2

Discrete Time Point Sample Data

Time (hr)	Raz Conc (µmol L^{-1})	Rru Conc (µmol L^{-1})	EC (µs cm^{-1})
0.00	0.00	0.00	-
0.53	0.00	0.00	490.00
0.78	0.00	0.00	489.00
1.00	0.00	0.00	492.00
1.25	0.04	0.01	521.00
1.48	0.10	0.04	570.00
1.70	0.16	0.08	613.00
1.92	0.22	0.13	638.00
2.12	0.25	0.16	633.00
2.33	0.31	0.21	628.00
2.57	0.36	0.27	631.00
2.78	0.39	0.28	638.00
3.00	0.39	0.27	636.00
3.22	0.39	0.29	636.00
3.43	0.40	0.29	636.00
3.68	0.40	0.30	637.00
4.18	0.41	0.30	633.00

Column Average Data

		Effluent Metal Concentrations (µg L^{-1})					Sediment Association Metal Concentrations (mg g^{-1})						
OC (µg g^{-1})	pH	Copper	Zinc	Arsenic	Cadmium	Lead	Manganese	Iron	Copper	Zinc	Arsenic	Cadmium	Lead
2.94	6.75	0.72	17.78	0.90	1755.00	0.01	209.76	7504.00	4.58	29.90	8.84	0.10	6.31

Table D.29 Metal Stress CF at Kohr's Bend Control Column 1

Discrete Time Point Sample Data

Time (hr)	Raz Conc (µmol L^{-1})	Rru Conc (µmol L^{-1})	EC (µs cm^{-1})
0.00	0.00	0.00	-
0.30	0.00	0.00	221.50
0.55	0.01	0.00	222.20
0.78	0.01	0.00	220.10
1.02	0.00	0.00	220.10
1.25	0.01	0.01	264.80
1.45	0.02	0.04	345.00
1.65	0.04	0.10	439.00
1.87	0.06	0.19	503.00
2.05	0.07	0.30	521.00
2.28	0.08	0.38	534.00
2.50	0.09	0.46	533.00
2.70	0.09	0.49	531.00
2.95	0.10	0.54	538.00
3.20	0.12	0.58	532.00
3.55	0.11	0.60	537.00
4.00	0.10	0.56	528.00

Column Average Data

		Effluent Metal Concentrations (µg L^{-1})					Sediment Association Metal Concentrations (mg g^{-1})						
OC (µg g^{-1})	pH	Copper	Zinc	Arsenic	Cadmium	Lead	Manganese	Iron	Copper	Zinc	Arsenic	Cadmium	Lead
0.71	6.65	9.33	25.48	8.83	10.24	0.00	284.88	3204.20	66.72	97.99	7.30	0.23	12.08

Table D.30 Metal Stress CF at Kohr's Bend Control Column 2

Discrete Time Point Sample Data

Time (hr)	Raz Conc (µmol L^{-1})	Rru Conc (µmol L^{-1})	EC (µs cm^{-1})
0.00	0.00	0.00	-
0.35	0.01	0.00	220.70
0.60	0.00	0.00	219.95
0.83	0.00	0.00	219.20
1.07	0.01	0.00	219.70
1.30	0.01	0.00	251.30
1.50	0.02	0.03	356.00
1.70	0.03	0.10	443.00
1.90	0.04	0.18	499.00
2.10	0.07	0.32	515.00
2.32	0.07	0.37	534.00
2.53	0.08	0.41	529.00
2.73	0.09	0.47	533.00
3.00	0.10	0.57	536.00
3.25	0.11	0.58	532.00
3.60	0.10	0.58	536.00
4.03	0.09	0.56	534.00

Column Average Data

		Effluent Metal Concentrations (µg L^{-1})					Sediment Association Metal Concentrations (mg g^{-1})						
OC (µg g^{-1})	pH	Copper	Zinc	Arsenic	Cadmium	Lead	Manganese	Iron	Copper	Zinc	Arsenic	Cadmium	Lead
0.60	6.65	10.03	38.69	9.18	225.39	0.03	284.88	3204.20	66.72	97.99	7.30	0.23	12.08

Table D.31 Metal Stress CF at Kohr's Bend Treatment Column 1

Discrete Time Point Sample Data

Time (hr)	Raz Conc (µmol L^{-1})	Rru Conc (µmol L^{-1})	EC (µs cm^{-1})
0.00	0.00	0.00	-
0.40	0.00	0.00	485.00
0.65	0.00	0.00	490.00
0.88	0.00	0.00	481.00
1.12	0.01	0.00	486.00
1.35	0.01	0.01	526.00
1.55	0.02	0.04	604.00
1.75	0.05	0.11	650.00
1.95	0.07	0.20	665.00
2.13	0.11	0.28	667.00
2.37	0.10	0.35	677.00
2.58	0.11	0.41	664.00
2.80	0.13	0.46	676.00
3.05	0.14	0.50	675.00
3.30	0.16	0.55	673.00
3.65	0.16	0.57	676.00
4.07	0.16	0.52	667.00

Column Average Data

		Effluent Metal Concentrations (µg L^{-1})					Sediment Association Metal Concentrations (mg g^{-1})						
OC (µg g^{-1})	pH	Copper	Zinc	Arsenic	Cadmium	Lead	Manganese	Iron	Copper	Zinc	Arsenic	Cadmium	Lead
0.71	6.74	17.80	473.06	5.18	2791.99	0.03	284.88	3204.20	66.72	97.99	7.30	0.23	12.08

Table D.32 Metal Stress CF at Kohr's Bend Treatment Column 2

Discrete Time Point Sample Data

Time (hr)	Raz Conc (µmol L^{-1})	Rru Conc (µmol L^{-1})	EC (µs cm^{-1})
0.00	0.00	0.00	-
0.47	0.00	0.00	490.00
0.72	0.00	0.00	488.00
0.95	0.01	0.00	485.00
1.20	0.01	0.00	503.00
1.40	0.02	0.02	558.00
1.60	0.04	0.08	615.00
1.80	0.06	0.16	655.00
2.00	0.08	0.23	657.00
2.18	0.10	0.30	658.00
2.42	0.11	0.36	678.00
2.63	0.12	0.41	668.00
2.85	0.13	0.46	666.00
3.12	0.14	0.50	673.00
3.35	0.16	0.55	672.00
3.67	0.18	0.58	675.00
4.08	0.15	0.52	671.00

Column Average Data

		Effluent Metal Concentrations (µg L^{-1})					Sediment Association Metal Concentrations (mg g^{-1})						
OC (µg g^{-1})	pH	Copper	Zinc	Arsenic	Cadmium	Lead	Manganese	Iron	Copper	Zinc	Arsenic	Cadmium	Lead
1.17	6.74	18.80	536.76	5.20	4318.99	0.04	284.88	3204.20	66.72	97.99	7.30	0.23	12.08